



Review

## Design methods of high-entropy alloys: Current status and prospects



Lingxin Li <sup>a</sup>, Zhengdi Liu <sup>b,\*</sup>, Xulong An <sup>c,\*</sup>, Wenwen Sun <sup>a,\*</sup>

<sup>a</sup> School of Materials Science and Engineering, Southeast University, Nanjing 211189, China

<sup>b</sup> Department of Materials Science and Engineering, Monash University, Clayton, VIC 3800, Australia

<sup>c</sup> School of Materials Science and Engineering, Changzhou University, Changzhou 213164, China

### ARTICLE INFO

**Keywords:**

High-entropy alloys  
Alloy design  
Machine learning  
High-throughput experiments  
Computational materials science

### ABSTRACT

High-entropy alloys (HEAs), with their outstanding comprehensive properties, hold significant potential for applications in aerospace, energy, and military fields. However, due to the vast compositional space of HEAs, the traditional trial-and-error approach not only consumes considerable resources but also suffers from low efficiency, severely hindering the development of these alloys. In recent years, the rapid advancements in high-throughput experiments, computational materials science, and machine learning have offered new opportunities for the design of HEAs. This paper aims to explore the design methods for HEAs, including those based on high-throughput experiments, computational materials science, materials science, and machine learning. It discusses the current state of research on these four design methods, analyzing the advantages and limitations of each. Finally, the paper addresses the future trends in the development of design methods for HEAs.

### 1. Introduction

Since antiquity, the evolutionary trajectory of human society has been inextricably tied to the advancement of materials [1]. During the Stone Age, humans fashioned stones into cutting and hunting tools, significantly enhancing their survival capabilities and expanding their activity range. In the Bronze Age, the mastery of bronze smelting technology enabled the creation of more intricate and refined tools, thereby improving production efficiency and quality of life. With the advent of the Iron Age, the development of smelting techniques allowed iron, more abundant and economical than bronze, to become the primary material for tools and weapons. In contemporary society, metal materials such as titanium alloys, magnesium alloys, and superalloys play a pivotal role in production and daily life, driving the progress of human civilization. For an extended period, most metal materials have been designed using one or two alloying elements as the primary constituents, following the traditional alloying strategy. The swift advancement of technology imposes greater demands on the performance of metal materials. Metal materials produced through the traditional alloying strategy often encounter the strength-ductility trade-off dilemma [2], whereby an enhancement in the strength of metal materials is typically accompanied by a reduction in their ductility. The introduction of high-entropy alloys (HEAs), also known as multi-principal-element alloys or compositionally-complex alloys, revolutionizes the traditional

alloying strategy [3,4], broadening the principal elements in alloy design to encompass more than three components and shifting the range of alloy composition design from the peripheral regions to the core areas of the phase diagram, which remain relatively unexplored by the traditional alloying strategy. The alloying approach of HEAs offers a novel solution to overcoming the strength-ductility trade-off dilemma in metal materials. Recent research has demonstrated that HEAs exhibit remarkable strength [5–8], ductility [9–12], wear resistance [13–15], corrosion resistance [16–18], oxidation resistance [19–21], and thermal stability [22–24], presenting extensive application potential in aerospace, energy, military, and other domains. Nevertheless, given the vast compositional space of HEAs, the traditional trial-and-error method proves to be time-consuming and resource-intensive, hindering the advancement of HEAs. Since its proposal in 2011, the Materials Genome Initiative has provided a theoretical framework for the transformation of materials research and development paradigms [25,26]. The key technologies it promotes, including high-throughput experiments, computational modeling, and materials databases, are profoundly reshaping multiple aspects of HEA research, such as deformation behavior, performance prediction, and property optimization. These advances are driving a transition in HEA design from traditional trial-and-error approaches to precise and efficient rational design methodologies. It is worth noting that, although numerous excellent reviews have addressed fabrication processes [27–29], microstructural evolution [30,31], and

\* Corresponding authors.

E-mail addresses: zhengdi.liu@monash.edu (Z. Liu), 781483770@qq.com (X. An), swwcsu@live.cn (W. Sun).

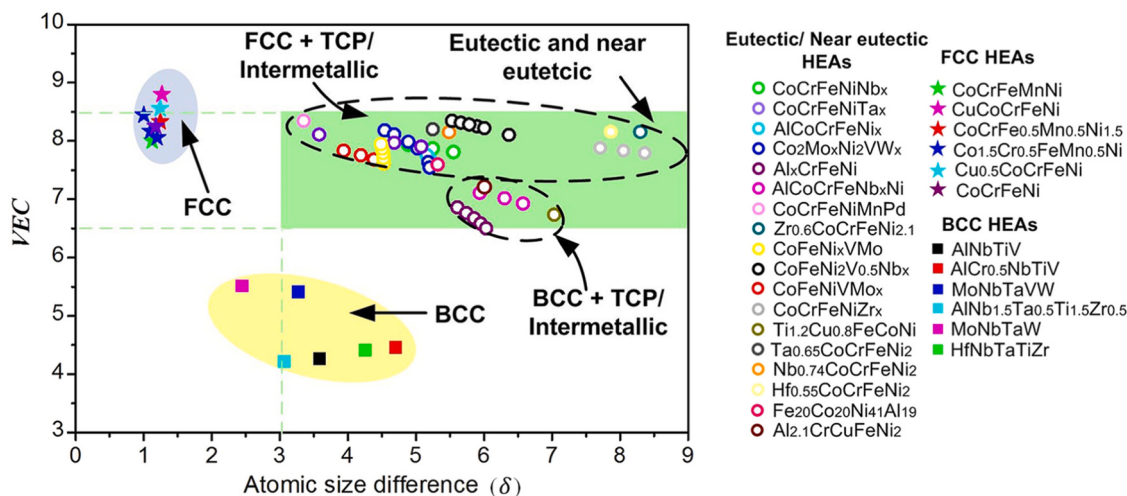


Fig. 1. The relationship between VEC and  $\delta$  in some HEAs [40–62].

performance optimization [32–35] of HEAs, systematic and comprehensive reviews focusing specifically on design strategies remain scarce. This paper focuses on the design methodologies of HEAs, systematically outlining the design principles based on four core approaches: materials science, computational materials science, machine learning, and high-throughput experiments. It further provides an in-depth analysis of the advantages and limitations of various HEA design methods and explores future directions for their development.

## 2. Design methods for HEAs based on materials science

The concept of HEAs was first proposed in 2004 [3,4], and its development history spans only twenty years. HEAs design methods based on materials science have been crucial in the early stages, aiming to design HEAs with targeted approaches grounded in materials science principles. This methodology primarily includes empirical criterion methods and the application of classical alloy design concepts.

### 2.1. Empirical criterion methods

A profound relationship exists between the phase structure and the properties of HEAs. For instance, HEAs with a face-centered cubic (FCC) structure typically exhibit superior plasticity, whereas those with a body-centered cubic (BCC) structure often demonstrate elevated strength and hardness [36]. Thus, the design of alloys with the desired phase structure is a pivotal consideration in the development of HEAs. In recent years, a diverse array of empirical criteria has been developed to anticipate the phase structure of HEAs, utilizing parameters such as mixing enthalpy, mixing entropy ( $\Delta S_{mix}$ ), atomic size difference, and valence electron concentration (VEC).

#### (1) Mixing enthalpy & atomic size difference criterion

Zhang et al. [37] extended the Hume-Rothery criterion to HEAs, proposing parameters affecting the formation of high-entropy alloy (HEA) phases, namely atomic size difference ( $\delta$ ) and mixing enthalpy ( $\Delta H_{mix}$ ). The calculation formula is as follows:

$$\Delta H_{mix} = \sum_{i=1, i \neq j}^n 4\Delta H_{ij}^{mix} c_i c_j \quad (1)$$

$$\delta = \sqrt{\sum_{i=1}^n c_i \left(1 - \frac{r_i}{\bar{r}}\right)^2} \quad (2)$$

In Eq. (1) and Eq. (2),  $c_i$  and  $c_j$  represent the atomic percentages

of the  $i$ th and  $j$ th principal elements, respectively;  $n$  is the number of principal elements; and  $\Delta H_{ij}^{mix}$  is the mixing enthalpy between the  $i$ th and  $j$ th principal elements.  $\bar{r}$  represents the average atomic radius of the principal elements, and  $r_i$  is the atomic radius of the  $i$ th principal element. According to the  $\Delta H_{mix}$ - $\delta$  criterion, HEAs tend to form a solid solution phase when  $\delta < 5\%$  and  $-15 \text{ kJ/mol} < \Delta H_{mix} < 5 \text{ kJ/mol}$ .

#### (2) VEC criterion

Guo et al. [38] studied the effect of VEC on the phase structure of HEAs. The formula for calculating the VEC of the alloy is as follows:

$$\text{VEC} = \sum_{i=1}^n c_i (\text{VEC})_i \quad (3)$$

In Eq. (3),  $(\text{VEC})_i$  represents the VEC of the  $i$ th principal element. When  $\text{VEC} \geq 8$ , the alloy tends to form a single-phase FCC solid solution; when  $\text{VEC} < 6.8$ , it tends to form a single-phase BCC solid solution [38].

#### (3) VEC- $\Delta H_{mix}$ - $\delta$ criterion

Jiang et al. [39] proposed the VEC- $\Delta H_{mix}$ - $\delta$  criterion by combining the parameters VEC,  $\Delta H_{mix}$ , and  $\delta$ . According to this criterion, when  $\delta < 4.27\%$ ,  $-7.27 \text{ kJ/mol} < \Delta H_{mix} < 4 \text{ kJ/mol}$ , and  $\text{VEC} > 8$ , the alloy tends to form a single-phase FCC solid solution; when  $\delta < 4.27\%$ ,  $-7.27 \text{ kJ/mol} < \Delta H_{mix} < 4 \text{ kJ/mol}$ , and  $\text{VEC} < 6.87$ , it tends to form a single-phase BCC solid solution. Chanda et al. [40] pointed out that the  $\Delta H_{mix}$ - $\delta$  criterion cannot effectively predict the stability of the eutectic phase in eutectic HEAs. By incorporating the VEC parameter, the stability of the eutectic phase can be better predicted. As shown in Fig. 1, when  $-18 \leq \Delta H_{mix} \leq -6$ ,  $6 \leq \text{VEC} \leq 8.5$ , and  $\delta > 3\%$ , the eutectic phase can stably exist.

#### (4) $\Omega$ parameter & $\delta$ criterion

Yang et al. [63], considering the effects of mixing entropy and mixing enthalpy on phase formation, proposed the  $\Omega$  parameter, which is calculated as follows:

$$\Omega = \frac{T_m \Delta S_{mix}}{|\Delta H_{mix}|} \quad (4)$$

In Eq. (4),  $\Delta S_{mix}$  and  $\Delta H_{mix}$  represent the mixing entropy and mixing enthalpy of the alloy, respectively;  $T_m$  is the theoretical melting point of the alloy. Combining the  $\Omega$  parameter with the  $\delta$ , HEAs tend to form a solid solution structure when  $\Omega \geq 1.1$  and

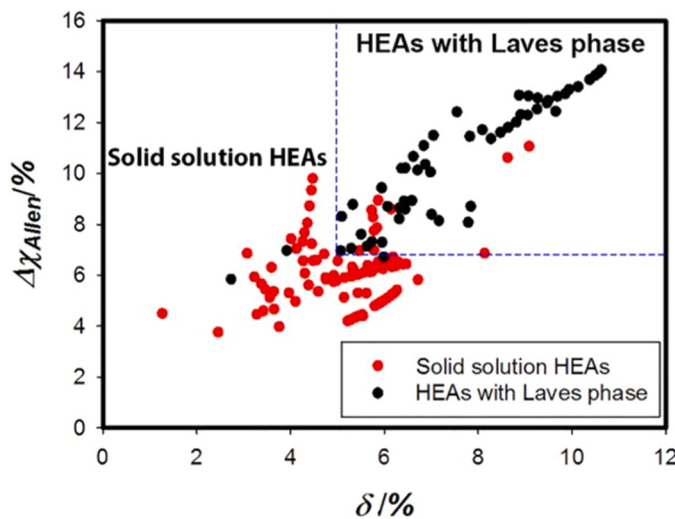


Fig. 2. The relationship between  $\Delta\chi_{\text{Allen}}$  and  $\delta$  in some HEAs [67].

$$\delta \leq 6.6\%.$$

#### (5) $\phi$ parameter criterion

Ye et al. [64] used the  $\phi$  parameter to determine the phase structure of HEAs. The specific calculation method for the  $\phi$  parameter is shown in Eqs. (2–5). When  $\phi > 20$ , the alloy tends to form a single-phase disordered solid solution; whereas when  $\phi < 20$ , it tends to form a multiphase structure.

$$\phi = \frac{S_C - |\Delta H_{\text{mix}}|/T_m}{|S_E|} \quad (5)$$

In Eq. (5),  $S_C$  represents the mixing entropy in the ideal gas state, and  $S_E$  represents the residual mixing entropy resulting from atomic arrangement and atomic radius.

#### (6) $\gamma$ parameter criterion

Wang et al. [65] proposed the atomic size difference parameter, namely the  $\gamma$  parameter, to predict the formation of solid solution structures. The calculation method for the  $\gamma$  parameter is shown in Eq. (6). When  $\gamma < 1.175$ , the alloy tends to form a solid solution structure.

$$\gamma = \left[ 1 - \sqrt{\frac{(r_s + \bar{r})^2 - \bar{r}^2}{(r_s + \bar{r})^2}} \right] \left[ 1 - \sqrt{\frac{(r_L + \bar{r})^2 - \bar{r}^2}{(r_L + \bar{r})^2}} \right]^{-1} \quad (6)$$

Where  $r_s$  and  $r_L$  are the minimum and maximum atomic radii, respectively, and  $\bar{r}$  is the average atomic radius.

#### (7) Pauling electro-negativity difference criterion

Dong et al. [66] utilized the Pauling electro-negativity difference ( $\Delta\chi_{\text{Pauling}}$ ) to predict the stability of the topologically close-packed (TCP) phase in HEAs. The calculation method for the Pauling electro-negativity difference is shown in Eq. (7) and Eq. (8). The study indicates that when  $\Delta\chi_{\text{Pauling}} > 0.133$ , the TCP phase can stably exist.

$$\Delta\chi_{\text{Pauling}} = \sqrt{\sum_{i=1}^n c_i (\chi_i^{\text{Pauling}} - \bar{\chi})^2} \quad (7)$$

$$\bar{\chi} = \sum_{i=1}^n c_i \chi_i^{\text{Pauling}} \quad (8)$$

Where  $\Delta\chi_{\text{Pauling}}$  is the Pauling electro-negativity difference,  $\chi_i^{\text{Pauling}}$  is the Pauling electro-negativity of the  $i$ th principal element, and  $\bar{\chi}$  is the average Pauling electro-negativity of the principal elements in the alloy.

#### (8) Allen electro-negativity difference & $\delta$ criterion

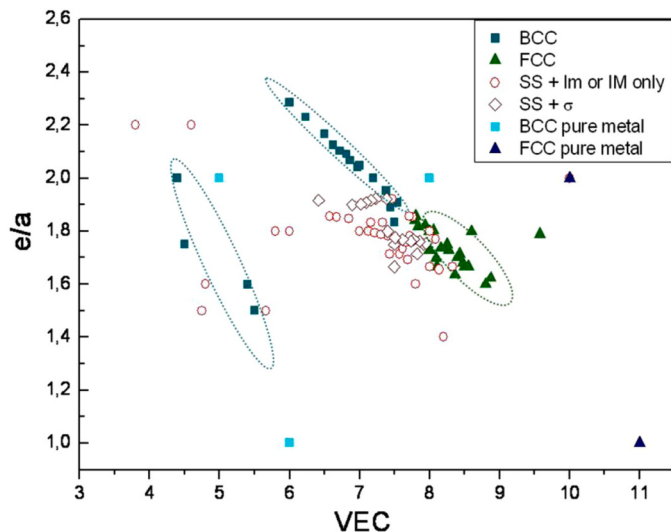


Fig. 3. The relationship between VEC and  $e/a$  in some HEAs [70].

Yurchenko et al. [67] combined the Allen electro-negativity difference ( $\Delta\chi_{\text{Allen}}$ ) with the  $\delta$  to predict the formation of Laves phases in HEAs. The calculation formula for the Allen electro-negativity difference is as follows:

$$\Delta\chi_{\text{Allen}} = \sqrt{\sum_{i=1}^n c_i \left( 1 - \frac{\chi_i^{\text{Allen}}}{\chi_a} \right)^2} \quad (9)$$

$$\chi_a = \sum_{i=1}^n c_i \chi_i^{\text{Allen}} \quad (10)$$

In Eq. (9) and Eq. (10),  $\Delta\chi_{\text{Allen}}$  is the Allen electro-negativity difference of the alloy,  $\chi_i^{\text{Allen}}$  is the Allen electro-negativity of the  $i$ th principal element, and  $\chi_a$  is the average Allen electro-negativity of the principal elements in the alloy. The study [67] indicates that when  $\delta > 5.0\%$  and  $\Delta\chi_{\text{Allen}} > 7.0\%$ , HEAs tend to form Laves phases, as shown in Fig. 2.

#### (9) $\Lambda$ parameter criterion

Singh et al. [68] introduced the  $\Lambda$  parameter to predict the formation of disordered solid solutions in HEA systems. The specific calculation formula for the  $\Lambda$  parameter is as follows:

$$\Lambda = \frac{\Delta S_{\text{mix}}}{\delta^2} \quad (11)$$

When  $\Lambda > 0.96$ , the alloy tends to form a disordered solid solution; when  $0.24 < \Lambda < 0.96$ , the alloy tends to form a mixture of disordered solid solution and compounds; when  $\Lambda < 0.24$ , the alloy tends to form compounds [68].

#### (10) $\overline{Md}$ parameter criterion

The d-orbital energy level ( $Md$ ) is related to the electro-negativity and atomic radius of the elements and is also associated with the stability of the alloy. Lu et al. [69] used the  $\overline{Md}$  parameter criterion to predict the formation of TCP phases in HEAs. When  $Md > 1.09$ , the alloy tends to form TCP phases. The calculation formula for the average value of the d-orbital energy level ( $\overline{Md}$ ) is as follows:

$$\overline{Md} = \sum_{i=1}^n c_i (Md)_i \quad (12)$$

In Eq. (12),  $(Md)_i$  is the d-orbital energy level value of the  $i$ th principal element, and  $c_i$  is the atomic percentage of the  $i$ th principal element.

#### (11) Itinerant electron concentration & VEC criterion

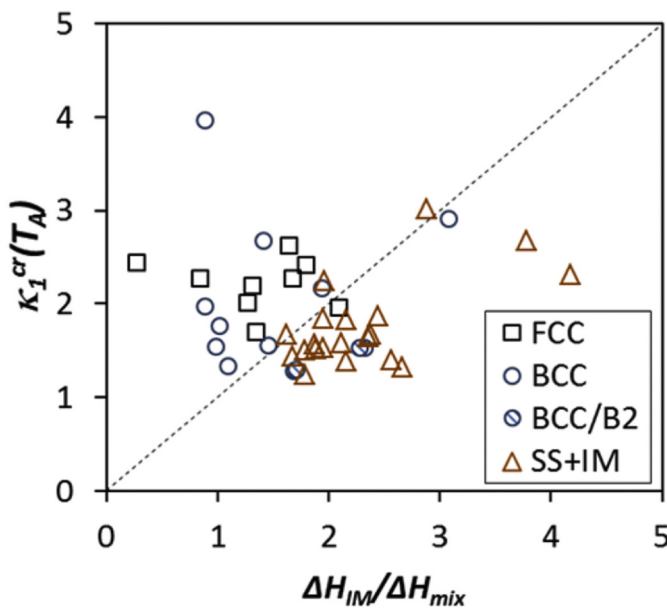


Fig. 4. Relationship between  $\kappa_1^{cr}$  and  $\Delta H_{IM}/\Delta H_{mix}$  in HEAs [72].

Poletti et al. [70] combined the itinerant electron concentration ( $e/a$ ) with the VEC to predict the type of solid solution phase in HEAs. As shown in Fig. 3, when VEC > 7.5 and  $1.6 < e/a < 1.8$ , the alloy tends to form an FCC phase; when VEC < 7.5 and  $1.8 < e/a < 2.3$ , the alloy tends to form a BCC phase.

#### (12) $\Delta H_{mix}$ - $\delta$ - $\Delta S_{mix}$ criterion

Guo et al. [71] used the  $\Delta S_{mix}$ ,  $\delta$ , and  $\Delta H_{mix}$  to jointly predict the formation of solid solution phases. When  $-22 \text{ kJ/mol} \leq \Delta H_{mix} \leq 7 \text{ kJ/mol}$ ,  $0 \leq \delta \leq 8.5\%$ , and  $11 \text{ J/(K·mol)} \leq \Delta S_{mix} \leq 19.5 \text{ J/(K·mol)}$ , the alloy tends to form a solid solution phase.

#### (13) $\kappa_1^{cr}$ parameter criterion

Senkov et al. [72] proposed the  $\kappa_1^{cr}$  parameter to predict the phase structure of HEAs at a given annealing temperature. The calculation formula for the  $\kappa_1^{cr}$  parameter is as follows:

$$\kappa_1^{cr} = 1 + \frac{T\Delta S_{mix}}{|\Delta H_{mix}|}(1 - \kappa_2) \quad (13)$$

In Eq. (13),  $T$  represents the annealing temperature, and  $\kappa_2$  is a constant ranging from 0 to 1. As depicted in Fig. 4, when  $\kappa_1^{cr} > \Delta H_{IM}/\Delta H_{mix}$  (where  $\Delta H_{IM}$  is the formation enthalpy of intermetallic compounds), the formation of intermetallic (IM) phases is suppressed.

#### (14) VEC & Paired sigma-forming element (PSFE) criterion

The research by Tsai et al. [57] shows that when the VEC is between 6.88 and 7.84, HEAs containing Cr and V elements tend to form  $\sigma$  phase. Subsequently, Tsai et al. [73] introduced a restrictive parameter called the PSFE content. They pointed out that when the PSFE content is below a certain threshold, HEAs generally do not form  $\sigma$  phase even if the VEC is between 6.88 and 7.84.

#### (15) Summary of empirical criterion methods

There are three types of empirical criteria for predicting the phase structure of HEAs: 1) Determining whether the alloy is a solid solution, primarily used to distinguish solid solutions, intermetallic compounds, and amorphous structures. 2) Assessing the phase structure of the solid solution, such as FCC and BCC phases. 3) Evaluating whether the alloy forms a secondary phase, such as Laves and  $\sigma$  phases. The empirical parameters for phase formation in HEAs are based on the fundamental properties of the constituent elements, such as thermodynamic parameters and atomic size parameters, offering advantages like convenient parameter acquisition and rapid calculation speed. Additionally, the qualitative relationships between some empirical parameters and phase structures can guide the design of HEAs. However, the empirical parameters for phase formation in HEAs are derived from extensive experimental data that do not encompass all HEA systems and treatment conditions, thus limiting the applicability of these criteria. The phase structure of HEAs is typically influenced by numerous factors, and the current phase formation criteria consider only a limited number of influencing parameters, thereby reducing their predictive accuracy to

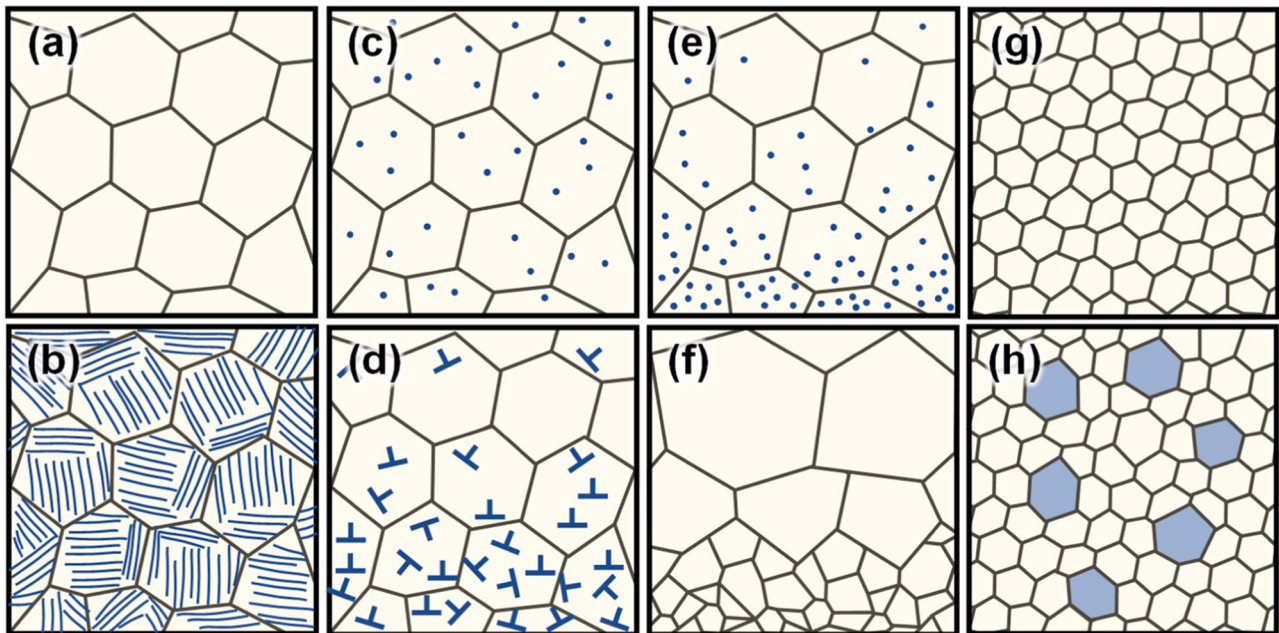


Fig. 5. The schematic diagram of classical alloy design concepts: (a) single phase; (b) lamellae; (c) dispersed precipitation phase; (d) gradient dislocation cell; (e) gradient precipitate volume fraction; (f) gradient grain size; (g) nanocrystalline grains; (h) bimodal grains.

some extent.

## 2.2. The application of classical alloy design concepts

After years of development in traditional metal materials, numerous classical alloy design concepts have emerged. In recent years, leveraging these classical alloy design concepts, a variety of HEAs have been conceived and developed. Fig. 5(a) illustrates the schematic of single-phase structural alloys. Presently, developed single-phase HEAs include the CoCrFeMnNi alloy with an FCC structure [4], the WMoNbTa alloy with a BCC structure [74], and among others. The alloying strategy of HEAs allows researchers to transcend the limitation of restricting the principal element in material design to one or two elements. Therefore, in accordance with the aforementioned alloying strategy, the design of HEAs should similarly not be confined to single-phase structures.

The lamellar structure depicted in Fig. 5(b) is extensively utilized in conventional alloys [75–77]. Inspired by the design principles of the lamellar structure, scholars both domestically and internationally have developed and engineered numerous HEAs exhibiting remarkable properties. For instance, Lu et al. [42], employing the concept of eutectic alloys, designed the AlCoCrFeNi<sub>2.1</sub> HEA in 2014, which comprises a mixed FCC phase and B2 phase. And this alloy exhibited exceptional casting performance, with excellent strength and ductility. In 2020, Fan et al. [78] introduced a coherent nanolamellar structure into multi-principal element alloys. The Ni<sub>32.8</sub>Fe<sub>21.9</sub>Co<sub>21.9</sub>Cr<sub>10.9</sub>Al<sub>7.5</sub>Ti<sub>5.0</sub> alloy they developed comprises FCC and L<sub>1</sub><sub>2</sub> phase nanolamellae, displaying a yield strength exceeding 2 GPa and an elongation of 16 %. In 2021, Shi et al. [79] further regulated the microstructure of eutectic HEAs. Through directional solidification, they designed the eutectic lamellar structure of the Al<sub>19</sub>Fe<sub>20</sub>Co<sub>20</sub>Ni<sub>41</sub> HEA into a hierarchically organized herringbone structure. The results demonstrated that this alloy maintained excellent fracture toughness and elongation without sacrificing strength. In 2022, An et al. [80] incorporated the pearlite structure from steel materials into multi-principal element alloys. The engineered Fe<sub>44.5</sub>Co<sub>25.4</sub>Ni<sub>24.4</sub>Ti<sub>5.7</sub> alloy experienced eutectoid transformation, resulting in a pearlite structure of alternating BCC and Ni<sub>3</sub>Ti lamellae, demonstrating exceptional hardness and outstanding wear resistance.

As depicted in Fig. 5(c), the dispersive precipitation phase structure is a pivotal strengthening mechanism in traditional alloys such as aluminum and copper alloys [81–84]. In 2016, He et al. [85], with the objective of designing alloys with a nano-precipitation phase structure, successfully introduced L<sub>1</sub><sub>2</sub>-Ni<sub>3</sub>(Ti,Al) nano-precipitates into an FCC matrix by incorporating a small amount of Ti and Al into the FeCoNiCr HEA. The resultant (FeCoNiCr)<sub>94</sub>Ti<sub>2</sub>Al<sub>4</sub> HEA exhibited an exceptional combination of yield strength and elongation. In 2018, Yang et al. [86] engineered high-density metallic nanoparticles within a complex alloy system to enhance the mechanical properties of alloys. The resultant (FeCoNi)<sub>86</sub>Al<sub>7</sub>Ti<sub>7</sub> HEA achieved a tensile strength of approximately 1.5 GPa and an elongation of 50 %. Similarly, in 2018, Lei et al. [87] utilized TiZrHfNb as the base alloy, adding an appropriate amount of interstitial atom O to form an ordered interstitial complex structure in the HEA. The experimental results indicated that the (TiZrHfNb)<sub>98</sub>O<sub>2</sub> HEA, prepared based on this design concept, possessed outstanding strength and ductility.

Fig. 5(d), (e), and (f) respectively depict the gradient dislocation cell structure, gradient precipitate volume fraction structure, and gradient grain size structure. The design concept of gradient structures has demonstrated significant advantages in traditional metallic materials [88,89]. According to this design concept, Pan et al. [90] in 2021 employed cyclic torsion deformation techniques to successfully introduce a gradient dislocation cell structure into the Al<sub>0.1</sub>CoCrFeNi HEA. Experimental results indicated that the gradient dislocation cell structure significantly enhances the strength-ductility product of HEAs. In 2022, Qin et al. [91] utilized surface mechanical attrition treatment (SMAT) and heat treatment techniques to create a structure in

Al<sub>0.5</sub>Cr<sub>0.9</sub>FeNi<sub>2.5</sub>V<sub>0.2</sub> HEA that features both grain size and precipitate volume fraction gradients. The results showed that this combined gradient structure provides superior synergistic effects in terms of strength and ductility.

Relevant studies have shown that reducing the grain size of traditional alloys to the nanoscale (Fig. 5(g)) can improve their mechanical properties to some extent [92]. Based on this, Fu et al. [93] in 2016 successfully prepared a nanocrystalline Co<sub>25</sub>Ni<sub>25</sub>Fe<sub>25</sub>Al<sub>7.5</sub>Cu<sub>17.5</sub> HEA using mechanical alloying and spark plasma sintering (SPS) methods. The nanocrystalline microstructure further enhanced the yield strength and hardness of the Co<sub>25</sub>Ni<sub>25</sub>Fe<sub>25</sub>Al<sub>7.5</sub>Cu<sub>17.5</sub> alloy.

The study by Yinmin Wang et al. [94] elucidated that Cu with a bimodal grain structure (Fig. 5(h)) combines both high strength and excellent ductility. The design principle of the bimodal grain structure primarily employs fine grains to ensure high material strength while utilizing coarse grains to inhibit crack initiation and propagation. In 2023, Wang et al. [95] successfully employed the strategy of constructing a bimodal grain and nano-precipitate structure in an alloy, resulting in the fabrication of an Al<sub>7.3</sub>Co<sub>21.3</sub>Cr<sub>10.7</sub>Ti<sub>4.9</sub>Fe<sub>21.3</sub>Ni<sub>32.0</sub>Cu<sub>2.5</sub> HEA with a tensile strength of 1.68 GPa and an elongation of 13.5 %.

Furthermore, the design principles of metastability engineering [96, 97] and grain boundary engineering [98] in conventional metallic materials are also pertinent to HEAs. For instance, in 2015, Deng et al. [99] incorporated the twinning-induced plasticity (TWIP) effect into HEAs, specifically by designing and synthesizing Fe<sub>40</sub>Mn<sub>40</sub>Co<sub>10</sub>Cr<sub>10</sub> HEAs. This innovation resulted in a proliferation of deformation twins during room-temperature deformation, thereby enhancing the plasticity of these alloys. In 2016, Li et al. [100] applied the transformation-induced plasticity (TRIP) effect to HEAs, adhering to the principles of metastability engineering, and successfully developed the Fe<sub>50</sub>Mn<sub>30</sub>Co<sub>10</sub>Cr<sub>10</sub> dual-phase HEA. During deformation of this alloy, the FCC phase transitions to the HCP phase, thus improving its mechanical properties. In 2018, Seol et al. [101] utilized the concept of interstitial atoms to enhance the grain boundary cohesion in HEAs, specifically investigating Fe<sub>20</sub>Mn<sub>20</sub>Cr<sub>20</sub>Co<sub>20</sub>Ni<sub>20</sub> and Fe<sub>40</sub>Mn<sub>40</sub>Cr<sub>10</sub>Co<sub>10</sub> alloys with 30 ppm of interstitial boron atoms. The findings revealed that even a small quantity of interstitial boron significantly enhances the mechanical properties of HEAs.

The aforementioned microstructural configurations, including bimodal, gradient, and lamellar structures, exhibit distinct spatial morphologies. However, they all fundamentally display non-uniform structural characteristics, namely heterogeneous structures. Compared with conventional homogeneous materials, heterogeneous structured materials are composed of regions with significant differences in mechanical or physical properties. The interactions among these heterogeneous regions can induce synergistic effects, enabling the overall properties of the material to exceed the predictions of the rule of mixtures [102–104]. Heterogeneous structures are widely found in nature, such as the layered structure of shells and the fibrous structure of bamboo. These naturally evolved heterogeneous structures are the result of natural selection, indirectly demonstrating the unique advantages of heterogeneity in optimizing material performance. In particular, for refractory HEAs, the design strategy based on heterogeneous structures provides an innovative approach to improving plasticity and achieving an outstanding combination of strength and ductility [105]. For example, Zhang et al. [106] designed a complex multi-scale heterogeneous structure in the Al<sub>0.3</sub>NbTi<sub>3</sub>VZr<sub>1.5</sub> lightweight refractory HEA, which included bimodal grains, submicron spherical C14 Laves phase, nanoscale local chemical fluctuations, and atomic clusters smaller than 1 nm, achieving a combination of high strength and excellent uniform tensile ductility.

## 2.3. Section summary

In recent years, researchers have endeavored to investigate the microscopic mechanisms linking phase structure to the properties of

HEAs. They have developed numerous HEAs and HEA-based composite materials that fulfill performance criteria such as strength, wear resistance, oxidation resistance, and corrosion resistance [107–111]. Nevertheless, the relationship between phase structure and performance in HEAs remains intricate. To fortify the direct correlation between the design of HEAs and their performance, researchers aim to assess the contributions of various strengthening mechanisms from the standpoint of material science principles, including solid-solution strengthening, dislocation strengthening, precipitation strengthening, and grain boundary strengthening. These studies seek to formulate empirical equations for alloy properties, such as hardness and strength, thereby providing valuable insights for the design of HEAs. For instance, the research by Liu et al. [112] indicated that the Hall-Petch relationship remains applicable in FCC-structured CoCrFeMnNi HEAs. Gwalani et al. [113] demonstrated that the strength versus grain size of  $\text{Al}_{0.3}\text{CrCoFeNi}$  HEAs also conforms to the Hall-Petch relationship. Senkov et al. [61] proposed a solid solution strengthening formula for  $\text{TaNbHfZrTi}$  refractory HEAs, considering the contributions of atomic size mismatch and modulus mismatch to the strength. He et al. [85], Guo et al. [114], and Song et al. [115] applied the Bailey-Hirsch relationship to calculate the strength contribution from dislocation strengthening in HEAs. As for the strength contribution from precipitation strengthening, it can be quantitatively calculated by distinguishing between the dislocation shearing mechanism and the dislocation bypass mechanism based on the size and type of the precipitated phase. For example, Shim et al. [116] quantified the strength contributions of both dislocation shearing and bypass mechanisms in the as-cast  $\text{CoCrCu}_{1.5}\text{MnNi}$  HEA with micro-/nanoscale precipitation. Additionally, related studies [117,118] have indicated that the strength contributions of different strengthening mechanisms can be combined using either linear superposition or root-mean-square superposition to estimate the total strength of HEAs. There is a notable correlation between the hardness and strength of HEAs. Fan et al. [119] examined the relationship between the strength and Vickers hardness across hundreds of HEA compositions at room temperature, finding that the Vickers hardness is approximately three times the strength. Currently, the empirical formulas for predicting the properties of HEAs have considerable room for improvement.

In general, HEA design methods based on materials science mainly encompass empirical criterion methods and the application of classical alloy design concepts. These methods have played a significant role in the preliminary design phase of alloys. Although they are more targeted than traditional trial-and-error approaches, they primarily rely on existing materials science experience and data. For unknown HEA systems and multi-objective alloy design requirements, their applicability and guidance may be insufficient.

### 3. Design methods for HEAs based on computational materials science

With the significant advancement of computer processing power, computational materials science has developed rapidly, demonstrating unique advantages in the study of materials such as two-dimensional materials and metallic glasses [120–122]. The compositional complexity of HEAs presents a significant challenge to traditional trial-and-error methods, while computational materials science offers multiscale insights for the precise and efficient design of HEAs. This paper provides a detailed discussion on the design of HEAs based on first-principles, calculation of phase diagrams, finite element method, and molecular dynamics.

#### 3.1. First-principles

First-principles, a computational simulation method based on quantum mechanics theory, primarily involves solving the Schrödinger equation using approximate methods from the perspective of the microscopic electronic structure. This approach allows for the prediction

of material properties and behavior [123]. In recent years, first-principles has been extensively applied in the design and development of HEAs, focusing on four main areas: phase stability, mechanical properties, hydrogen storage capabilities, and corrosion resistance.

Phase stability significantly influences the performance of HEAs (HEAs). The phase stability of HEAs can be predicted through thermodynamic and microscopic physical parameters calculated by first-principles methods, indirectly guiding the design of these alloys. For instance, Qiu et al. [124] utilized first-principles calculations to study the thermodynamic properties of the lightweight  $\text{AlTiVCr}$  HEA. The results showed that the enthalpy of formation for the B2 phase is lower than that of the BCC phase at low temperatures, indicating that the B2 phase is more stable under these conditions, consistent with experimental results from XRD, HRTEM, and APT. Similarly, Ma et al. [125] investigated the thermodynamic properties and phase stability of the  $\text{CoCrFeMnNi}$  HEA using first-principles methods. Their calculations indicated that the paramagnetic FCC structure is most stable above room temperature, aligning with experimental observations. Chen et al. [126] treated the  $\text{HfNbTaTiZr}$  HEA as a pseudo-binary system. They first used first-principles methods to calculate parameters such as the mixing enthalpy, mixing entropy, and mixing Gibbs free energy of the HEA. By combining these calculations with a constructed pseudo-binary phase diagram, they predicted that the equiatomic  $\text{HfNbTaTiZr}$  HEA would undergo phase decomposition below a critical temperature of 1298 K, preferentially decomposing into NbTa-rich and HfZr-rich phases. This prediction is consistent with experimental results. Avula et al. [127] investigated the phase stability of the refractory  $\text{Ti}_x\text{Ta}_{2-x}\text{NbZrMo}$  HEA using parameters calculated from density functional theory (DFT), including the Wigner-Seitz radius, bulk modulus, enthalpy of formation, and phonon dispersion curve. Their findings indicated that the stability of the BCC phase increases with increasing Ta concentration. The oxide stability of HEAs can also be predicted using first-principles calculations. For example, Hong et al. [128] used first-principles methods to study the oxidation behavior of the  $\text{Al}_{0.3}\text{CoCrCuFeNi}$  HEA. The calculated cohesive energies of the oxides indicated that Al forms the thermodynamically most stable oxide (i.e.,  $\text{Al}_2\text{O}_3$ ), followed by Cr, which forms the second most stable oxide (i.e.,  $\text{Cr}_2\text{O}_3$ ). Similarly, Roy et al. [129] used formation energies derived from first-principles calculations to predict the oxide stability of the  $\text{AlCoCrFeNi}$  HEA. Their results showed that Cr and Al form the most stable oxides, specifically  $\text{Cr}_2\text{O}_3$  and  $\text{Al}_2\text{O}_3$ , which is consistent with the experimental results reported in the literature.

First-principles studies explore the mechanical properties of HEAs at the atomic scale, allowing for the calculation of crucial parameters such as elastic properties, electronic structure, and stacking fault energy. These studies provide a foundational data basis and theoretical support for the design of HEAs. For instance, Wu et al. [130] employed density functional theory to investigate the temperature-dependent variation of the elastic properties of  $\text{CoCrFeNi}$  multi-principal element alloy, highlighting the significance of spin fluctuations in predicting elastic properties. Hu et al. [131] examined the influence of the vanadium (V) element on the phase structure, elastic properties, and electronic structure of Nb-Mo-Ta-W refractory HEAs using first-principles methods. Their findings demonstrated that V can shorten the pseudo-energy gap and strengthen the interaction force between Mo and W atoms, thus guiding the design of high-hardness refractory HEAs. Chang et al. [132] calculated the mean square atomic displacement (MSAD) of  $\text{CoCrNiMo}$  multi-principal element alloys using first-principles methods. The MSAD and yield strength of the  $(\text{CoCr-Ni})_{97}\text{Mo}_3$  alloy were found to be higher than those of the  $\text{CoCrNi}$  alloy, indicating that the addition of Mo increases local lattice distortion, thereby allowing the prediction of yield strength trends based on MSAD. The stacking fault energy (SFE) plays a crucial role in the deformation mechanisms and mechanical properties of HEAs. Kies et al. [133] calculated the SFE of  $\text{Al}_x\text{C}_y\text{CoFeMnNi}$  multi-principal element alloys using density functional theory. For  $\text{CoFeMnNi}$  alloys, the addition of the carbon (C) element increases SFE, whereas for  $\text{Al}_{0.5}\text{CoFeMnNi}$  alloys

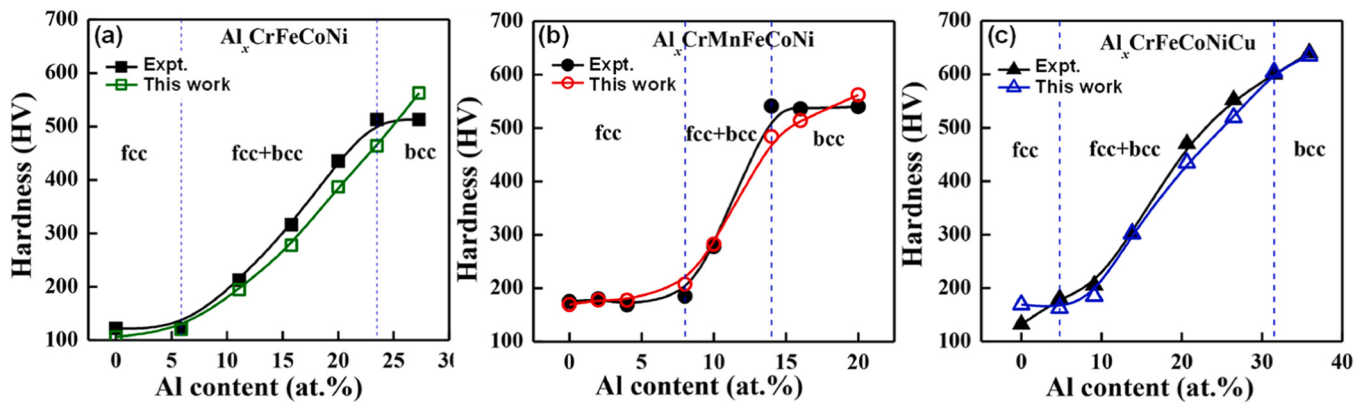


Fig. 6. Comparison of predicted and experimental hardness values of HEAs: (a)  $\text{Al}_x\text{CrFeCoNi}$ ; (b)  $\text{Al}_x\text{CrMnFeCoNi}$ ; (c)  $\text{Al}_x\text{CrFeCoNiCu}$  [134].

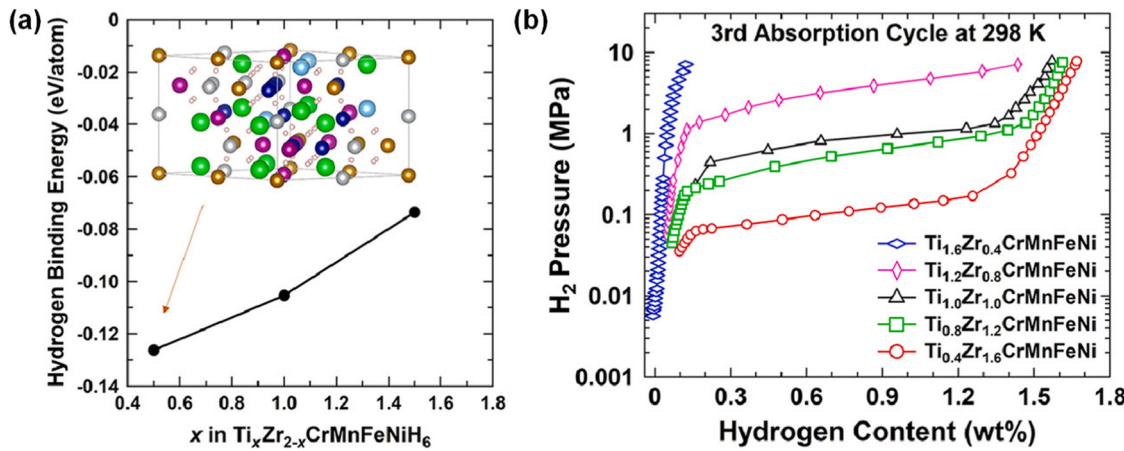


Fig. 7. Hydrogen binding energies of  $\text{Ti}_x\text{Zr}_{2-x}\text{CrMnFeNi}$  HEAs (a) and PCT absorption isotherms for the 3rd cycle (b) [138].

containing the Al element, it decreases SFE. Tensile and EBSD experiments revealed that the twinning-induced plasticity (TWIP) effect in the  $\text{Al}_{0.26}\text{C}_y\text{CoFeMnNi}$  alloy intensifies with the increasing C content, thus validating the accuracy of DFT calculations. Furthermore, combining first-principles calculations with strengthening models enables the prediction of macroscopic mechanical properties such as hardness and yield strength of HEAs. For example, Zhang et al. [134] employed first-principles calculations to determine the lattice constants and shear moduli of  $\text{Al}_x\text{CrFeCoNi}$ ,  $\text{Al}_x\text{CrMnFeCoNi}$ , and  $\text{Al}_x\text{CrFeCoNiCu}$  HEAs. They derived the size misfit parameters and shear modulus misfit parameters of these alloys and, by integrating them with the extended Labusch-Nabarro solid solution strengthening model, predicted the hardness of the HEAs. As shown in Fig. 6, the predicted hardness values of all three HEA systems increase with the increasing Al content, corresponding well with the experimental hardness values.

Kumar et al. [135] investigated the effect of adding 0.25–5 at% Al on the solid solution strengthening in CrCoFeMnNi alloys using density functional theory. The results indicated that the addition of Al caused significant local and global lattice distortions, which more effectively suppressed plastic deformation, thereby increasing the yield strength of the alloy. Based on the Varvenne model and the parameters calculated using density functional theory, the yield strength of the alloy was predicted with reasonable accuracy. Zhang et al. [136] employed first-principles methods to predict parameters such as the elastic constants, Young's modulus, shear modulus, and stacking fault energy of face-centered cubic HEAs. They proposed a method for predicting the yield strength of face-centered cubic HEAs based on generalized stacking fault energy curves, and the predicted yield strengths for CoFeNi, CoCrFeNi, CoCrFeCuNi, and RhIrPdPtNiCu alloys were in good

agreement with experimental values. Yan et al. [137] studied the effects of Mo elements on the phase stability, stacking fault energy, deformation mechanisms, and mechanical properties of  $(\text{CoCrNi})_{100-x}\text{Mo}_x$  multi-principal-element alloys using first-principles methods. They proposed composition design criteria for strong and ductile face-centered cubic  $(\text{CoCrNi})_{100-x}\text{Mo}_x$  multi-principal-element alloys, i.e., simultaneously satisfying negative free energy differences between FCC phase and other possible phases, lower stacking fault energy, and higher solid solution strengthening. According to these criteria, the designed  $(\text{CoCrNi})_{93}\text{Mo}_7$  alloy exhibited excellent strength and ductility combination.

First-principles calculations have significant applications in the design of HEAs for hydrogen storage. Mohammadi et al. [138] studied the Ti-Zr-Cr-Mn-Fe-Ni system as a hydrogen storage material, designing  $\text{Ti}_x\text{Zr}_{2-x}\text{CrMnFeNi}$  HEAs with varying Ti and Zr content. They calculated hydrogen binding energies of these HEAs using first-principles methods. As shown in Fig. 7(a), the hydrogen binding energies of the  $\text{Ti}_{0.5}\text{Zr}_{1.5}\text{CrMnFeNiH}_6$  and  $\text{Ti}_{1.0}\text{Zr}_{1.0}\text{CrMnFeNiH}_6$  alloys are slightly less than -0.1 eV, specifically -0.126 eV and -0.105 eV, respectively. The calculation results indicate that these two alloys have the potential for hydrogen storage at room temperature, which is consistent with the experimental characterization results in Fig. 7(b).

Gong et al. [139], based on first-principles calculations of the phonon spectra of NbTiVZr hydrides, predicted that the maximum hydrogen storage capacity of the NbTiVZr HEA is 2.94 wt%. This indicates that the NbTiVZr alloy has potential applications as a hydrogen storage material.

First-principles can also be used to understand and investigate the corrosion behavior of HEAs, guiding the design of corrosion-resistant HEAs. Yen et al. [140] studied the corrosion mechanism of the

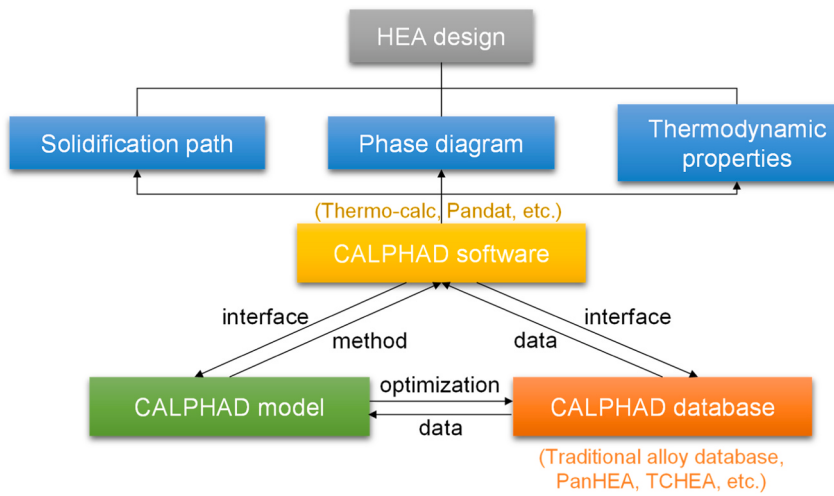


Fig. 8. Design of HEAs based on the CALPHAD method.

AlCoCrFeNi HEA in aerated aqueous solution using density functional theory. They calculated the average bonding energy per bond and per area for monolayer hydroxyl ions adsorbed on the (001) planes of FCC, BCC, and B2 phases in the AlCoCrFeNi alloy, respectively. The results showed that the B2 phase had the lowest average bonding energy per bond and per area, indicating that the B2 phase is more prone to corrosion in the aerated aqueous solution, which is consistent with experimental results.

First-principles methods serve as a vital research instrument for the design of HEAs. They eschew reliance on empirical parameters, instead deriving from fundamental physical principles to precisely predict properties such as electronic structure, band structure, elastic constants, and stacking fault energy of HEAs, thereby elucidating their microscopic mechanisms. Nevertheless, first-principles calculations encounter significant challenges due to extensive computational demands and high costs, particularly for intricate alloy systems and conditions. Moreover, the spatial scale accessible to first-principles studies is limited by these computational constraints.

### 3.2. Calculation of phase diagrams

Phase diagrams are fundamental for elucidating the relationships among composition, microstructure, and properties of materials. The calculation of phase diagrams (CALPHAD) method, introduced by

Kaufman and Bernstein in 1970 [141], is predicated on utilizing thermodynamic data acquired from experimental measurements or theoretical calculations, coupled with observed phase equilibrium information, to develop thermodynamic descriptions of binary and ternary systems, which are subsequently extrapolated to predict the phase behavior of higher-order systems [142]. As illustrated in Fig. 8, the three principal components of the CALPHAD method are the CALPHAD model, the CALPHAD database, and the CALPHAD software. An accurate CALPHAD database is essential for materials design, and the development and optimization of databases specifically for HEAs are vital for enhancing the calculation accuracy of the CALPHAD method [143]. Presently, two CALPHAD databases have been developed for HEAs: the TCHEA database by Thermo-Calc Software AB and the PanHEA database by CompuTherm LLC. The CALPHAD software integrates the CALPHAD database with the CALPHAD model, facilitating an intuitive interface for users. Commercial CALPHAD software mainly includes Thermo-Calc [144], Pandat [145], Matcalc [146], CaTCalc [147], MTDATA [148], and FactSage [149], while several open-source CALPHAD software options have also emerged, such as OpenCalphad [150] and PyCalphad [151].

The CALPHAD method can calculate the phase transformation behavior and thermodynamic properties of alloy systems, providing guidance for material design. Consequently, in recent years, many researchers have used the CALPHAD method to design HEAs with specific

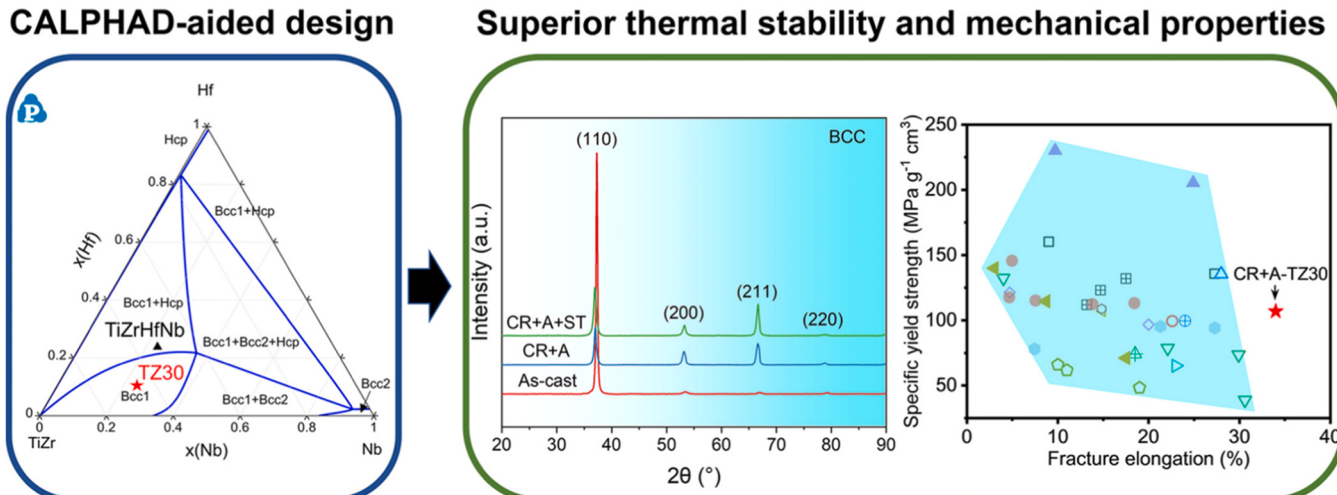
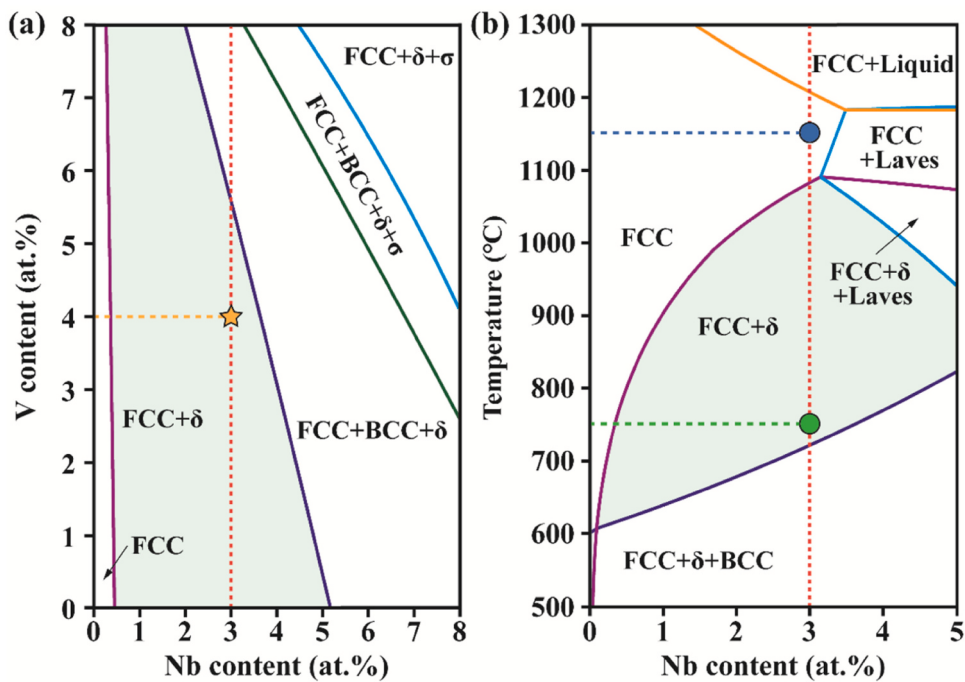
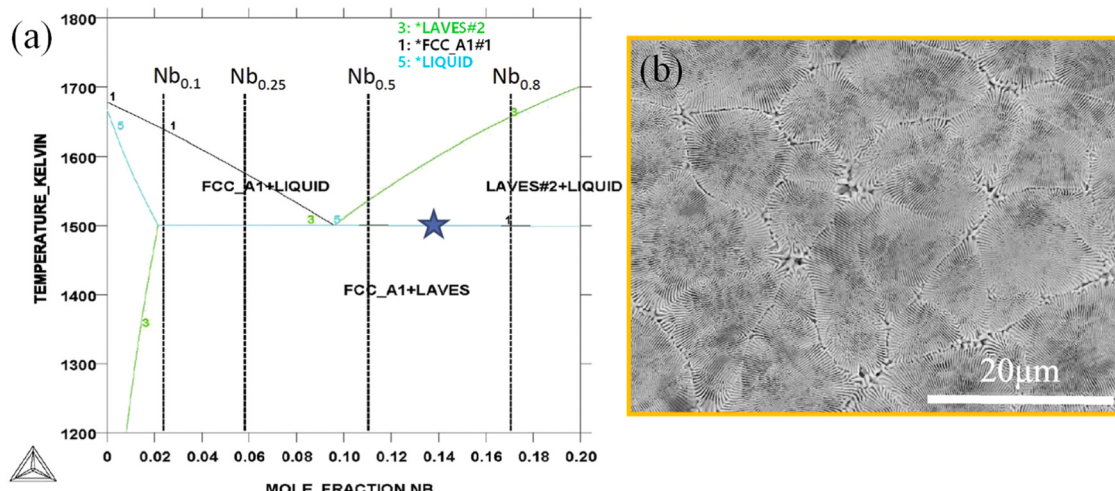


Fig. 9. Design of TiZrHfNb refractory HEAs using the CALPHAD method [152].



**Fig. 10.** Equilibrium phase diagram of the Ni-Fe-Cr-V-Nb-Mo system. (a) Evolution of phase component with different Nb/V ratios at 750°C. (b) Pseudo-binary phase diagram of  $\text{Ni}_{49-x}\text{Fe}_{23}\text{Cr}_{23}\text{V}_4\text{Nb}_x\text{Mo}_1$  alloys ( $0 < x < 5$  at%) [153].



**Fig. 11.** (a) Pseudo-binary phase diagram of the CoCrFeNiNb<sub>x</sub> alloy. (b) SEM image of the CoCrFeNiNb<sub>0.65</sub> alloy [156].

phase structures. As shown in Fig. 9, Li et al. [152] employed the CALPHAD method to calculate the pseudo-binary phase diagrams of the  $M_x(\text{TiZrHfNb})_{100-x}$  system (where M represents Ti, Zr, Hf, V, Nb, Ta, Cr, Mo, or W elements). The results indicated that the Ta element is detrimental to the phase stability of the Ti-Zr-Hf-Nb-Ta refractory HEA. By combining the calculated pseudo-ternary phase diagrams of the Ti-Zr-Hf-Nb system at 600°C, 900°C, and 1200°C, the  $\text{Ti}_{30}\text{Zr}_{30}\text{Hf}_{16}\text{Nb}_{24}$  (TZ30) refractory HEA was successfully designed. This alloy maintained a single-phase BCC structure after annealing at 600°C for 200 hours, exhibiting excellent thermal stability and mechanical properties.

Gan et al. [153] designed a D0<sub>22</sub> phase-strengthened  $\text{Ni}_{45.9}\text{Fe}_{23}\text{Cr}_{23}\text{V}_4\text{Nb}_3\text{Mo}_1\text{B}_{0.1}$  multi-principal-element alloy based on the CALPHAD method. According to the equilibrium phase diagram of the Ni-Fe-Cr-V-Nb-Mo system shown in Fig. 10, 1150 °C was chosen as the homogenization temperature and 750 °C as the aging temperature, resulting in the precipitation of the metastable D0<sub>22</sub> phase in the alloy.

Experimental results indicated that the tensile strengths of the alloy at 700 °C and 800 °C were 845 MPa and 589 MPa, respectively, with fracture elongation exceeding 24 % at both temperatures.

Do et al. [154] proposed a stepwise design strategy for HEAs based on the CALPHAD method, using the  $\text{Co}_{25}\text{Cr}_{15}\text{Fe}_{40}\text{Mn}_{10}\text{Ni}_{10}$  alloy as the base alloy. The CALPHAD method was employed to predict the equilibrium phase diagrams and phase fractions after adding Mo, V, C, and Si to the base alloy. These predictions were then verified using XRD, SEM, and other characterization techniques, gradually introducing precipitation strengthening, the TRIP effect, and other strengthening mechanisms into the alloy. The results demonstrated that the final  $\text{Co}_{21}\text{Cr}_{11}\text{Fe}_{49}\text{Mn}_4\text{Ni}_4\text{V}_2\text{C}_1\text{Mo}_3\text{Si}_5$  HEA exhibited an excellent combination of yield strength (732 MPa), tensile strength (1100 MPa), and elongation (47.5 %).

Eutectic HEAs possess excellent casting properties [155] and can also be designed using the CALPHAD method. He et al. [156] proposed a

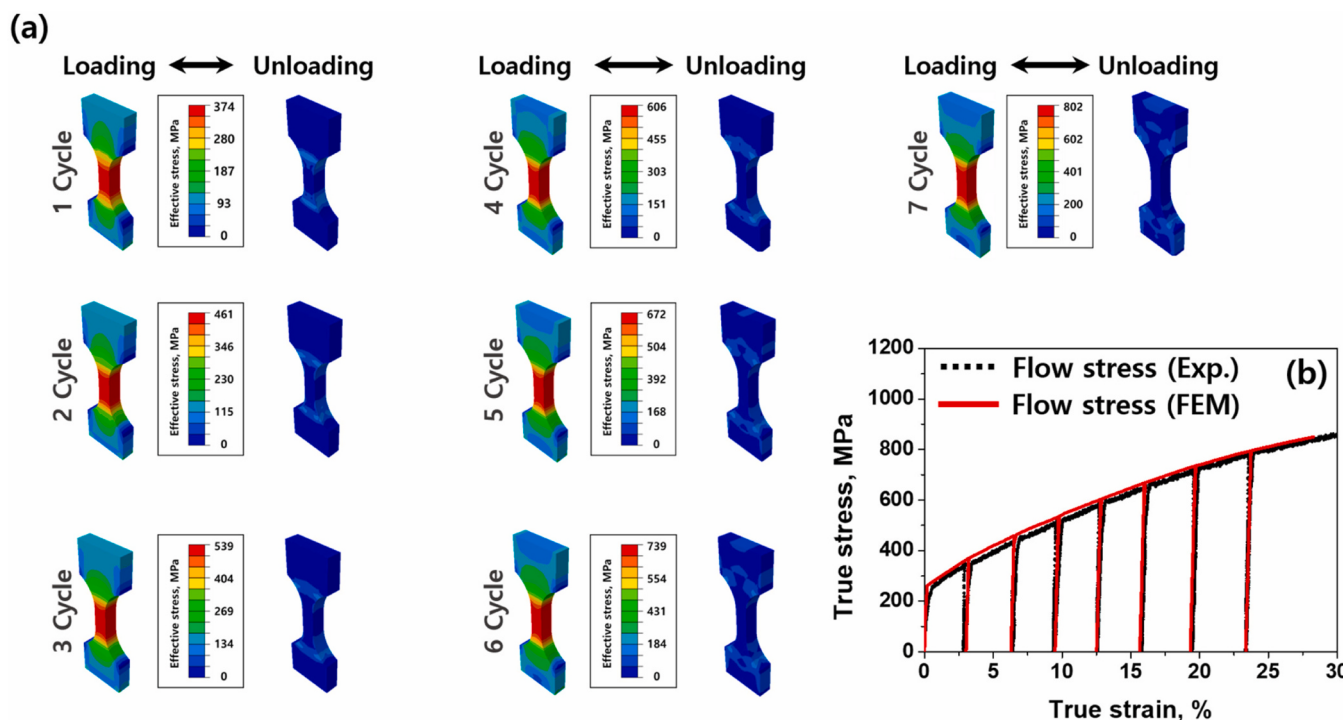


**Fig. 12.** (a) Stress distribution of the tensile specimen simulated by finite element method. (b) Comparison of the simulated and experimental results of the flow stress-strain curves [172].

design strategy for eutectic HEAs based on the CALPHAD method. As shown in Fig. 11(a), the pseudo-binary phase diagram of CoCrFeNiNb<sub>x</sub> alloys was calculated using the CALPHAD method. According to the predicted eutectic point, four CoCrFeNiNb<sub>x</sub> alloys with different Nb contents ( $x = 0.1, 0.25, 0.5, 0.8$ ) were designed. The predicted eutectic compositions were then fine-tuned using SEM experiments, ultimately leading to the design of the CoCrFeNiNb<sub>0.65</sub> alloy with a eutectic structure, as illustrated in Fig. 11(b).

Wu et al. [157] proposed a strategy for designing eutectic HEAs using the CALPHAD method. This strategy primarily involves constructing pseudo-binary phase diagrams of CoCrNi-NiAl or CoCrNi-CoAl to guide the design of eutectic HEAs with FCC and B2 dual phases, successfully producing Al<sub>17.4</sub>Co<sub>21.7</sub>Cr<sub>21.7</sub>Ni<sub>39.2</sub> and Al<sub>16.0</sub>Co<sub>38.6</sub>Cr<sub>22.7</sub>Ni<sub>22.7</sub> eutectic HEAs. Gasan et al. [158] utilized the TCHEA2 thermodynamic database in Thermo-calc software to calculate equilibrium phase diagrams of 324 Co-Cr-Fe-Mo-Ni-Al systems and selected 10 alloy compositions inclined to form eutectic structures. Based on alloy solidification curves calculated by the Scheil non-equilibrium solidification model and property diagrams, they chose alloys with a low tendency for  $\sigma$  phase formation during solidification for experimental preparation and study. Ultimately, based on SEM experimental results, the alloy compositions were fine-tuned, resulting in the (Co<sub>40</sub>Cr<sub>10</sub>Fe<sub>5</sub>Mo<sub>5</sub>Ni<sub>40</sub>)<sub>82.2</sub>Al<sub>17.8</sub> eutectic HEA with FCC and B2 dual phases.

Considering the vast compositional space of HEAs, a design strategy that combines the CALPHAD method with empirical criterion methods has been proposed. The empirical criterion methods primarily serve to narrow down the compositional space of HEAs, thereby improving the efficiency of alloy design. For example, Wang et al. [159] proposed a multi-principal-element alloy design strategy that integrates the CALPHAD method with the principle of overall valence electron concentration (OVEC). The main design concept is to strengthen the alloy by introducing the D0<sub>22</sub> phase. Therefore, it is first necessary to ensure that the alloy has a single-phase FCC structure at high temperatures and precipitates the D0<sub>22</sub> phase at low temperatures. With the restriction that the OVEC is above 8.4, the Ni element was used as a variable, and the CALPHAD method was employed to calculate the pseudo-binary

phase diagram of Ni<sub>x</sub>CoCrNb<sub>0.2</sub>, ultimately designing the D0<sub>22</sub> phase-strengthened Ni<sub>2</sub>CoCrNb<sub>0.2</sub> multi-principal-element alloy. Studies have shown that the C14\_Laves phase affects the hydrogen storage properties of alloys [160,161]. Ponsoni et al. [162] employed a combination of empirical formulas and the CALPHAD method to design multi-principal element alloys for hydrogen storage. Initially, 1208 candidate alloys were screened using empirical parameters such as the VEC, atomic radius ratio, and  $\delta$ . The phase stability of these candidate alloys was then assessed using the CALPHAD method, leading to the selection of 440 multi-principal-element alloys with a tendency to form the C14\_Laves phase. Lu et al. [163] employed an empirical approach to design two initial corrosion-resistant HEAs and utilized the TCHEA2 thermodynamic database to predict their phase compositions at 1100 °C. Subsequently, the CALPHAD method was used to assess the single-phase formation ability of the Ni<sub>38</sub>Cr<sub>21</sub>Fe<sub>20</sub>Ru<sub>13</sub>Mo<sub>6</sub>W<sub>2</sub> alloy. The findings revealed that this alloy possesses a broad single-phase region. Consequently, the Ni<sub>38</sub>Cr<sub>21</sub>Fe<sub>20</sub>Ru<sub>13</sub>Mo<sub>6</sub>W<sub>2</sub> alloy was selected as the final candidate for corrosion-resistant HEAs. Electrochemical testing further validated its exceptional corrosion resistance. Tazuddin et al. [164] used empirical parameters and the CALPHAD method to screen 10 compositions inclined to form single-phase HEAs from 1287 equiatomic quinary HEA systems. Experimental verification showed that 6 out of the 10 selected HEAs were single-phase HEAs, demonstrating the effectiveness of this design method in reducing the number of experiments.

Moreover, with the development of high-throughput computing technology [165], the high-throughput CALPHAD method has demonstrated substantial advantages in the design of HEAs. Yen et al. [166], based on the PanHEA2021 thermodynamic database, employed the high-throughput CALPHAD method to design Al-Co-Cr-Mo-Ti refractory HEAs with a B2 precipitation phase and a BCC matrix. From 211876 alloy composition combinations, the alloy composition that met the design requirements, namely the Al<sub>16</sub>Co<sub>20</sub>Cr<sub>58</sub>Mo<sub>4</sub>Ti<sub>2</sub> alloy, was successfully selected. Following solid solution and aging treatments, the alloy exhibited a microstructure with a uniformly precipitated B2 phase within the BCC matrix, demonstrating high hardness and exceptional thermal stability.

In summary, the CALPHAD method offers the following advantages: 1) HEAs involve numerous components, and the formation and transformation of phases are complex. The CALPHAD method provides a novel approach for designing HEAs, capable of not only predicting the specific phase composition and content of HEAs but also rapidly supplying parameters for guiding alloy design, such as atomic mobility data, which serve as input for phase-field simulations, diffusion simulations, and other computational analyses [167]. 2) Compared to experimental methods for determining alloy phase diagrams, the CALPHAD method can circumvent certain experimental challenges to predict phase diagrams and offers high computational efficiency. However, the CALPHAD method also has limitations: the accuracy of its predictions is heavily dependent on the thermodynamic database. The complexity of HEA systems limits the applicability of traditional alloy databases. Although thermodynamic databases specifically for HEAs have been developed in recent years, there is still room for improvement in their quality and applicability. Additionally, the accuracy and efficiency of CALPHAD calculations can be enhanced by refining the CALPHAD models, such as incorporating machine learning algorithms to improve the computational efficiency of the CALPHAD method [168]. For the CALPHAD software, continuous improvement in user interface friendliness and expandability remains a persistent goal.

### 3.3. Finite element method

The finite element method, as a macroscopic-scale numerical calculation method, primarily operates by discretizing the continuous solution domain into a combination of a finite number of small elements. Through the analysis of each element and the incorporation of boundary conditions, an approximate solution for the entire domain is obtained [169]. The finite element method process includes several steps: geometric model construction, mesh generation, material property definition, mathematical model building, equation solving, and post-processing. Among these, constructing the constitutive model of the material is crucial for accurately describing material deformation. The finite element method can simulate the stress-strain and temperature fields of HEAs during complex deformation processes, revealing their deformation and fracture behavior, thus providing guidance for the design of HEAs. For instance, Rahul et al. [170] utilized the finite element method to investigate the strain distribution and material flow of the AlCoCrFeNi<sub>2.1</sub> eutectic HEA during the forging process. Sinha et al. [171] employed the finite element method to study the notch-tensile behavior of the Al<sub>0.1</sub>CrFeCoNi HEA, finding that the simulated strain and stress distributions around the notch of the alloy specimens were consistent with the results from digital image correlation (DIC) experiments. Kim et al. [172] used Abaqus software to simulate the loading-unloading-reloading (LUR) tensile tests of the Cr<sub>12</sub>Fe<sub>42</sub>Mn<sub>24</sub>Ni<sub>22</sub> multi-principal-element alloy. As shown in Fig. 12, during each loading-unloading cycle, the flow stress was repeatedly concentrated and released in the central region of the tensile specimen. The flow stress curves obtained through finite element simulations closely matched the experimental measurements. These studies demonstrate the powerful capability of the finite element method in describing the stress-strain distribution of HEAs.

In addition to simulating relatively simple deformation processes of HEAs, the finite element method can also simulate complex processing procedures. For instance, Gao et al. [173] employed the finite element method to simulate the stress field distribution of the FeCoCrNi HEA coating deposited on TC4 titanium alloy substrate via laser cladding, investigating the mechanisms by which powder layer thickness and laser processing parameters influence crack formation. Similarly, Li et al. [174] developed a laser melting deposition (LMD) model for CoCr-FeMnNi HEAs using the finite element method and simulated the residual stress distribution in this alloy. The results indicated that, during the LMD process, the residual compressive stress in CoCrFeMnNi HEAs decreases along the building direction, which is consistent with neutron

diffraction results.

Furthermore, the finite element method offers a refined approach to accurately delineate the temperature distribution during the deformation of HEAs. For instance, Song et al. [175] utilized the finite element method to simulate the temperature field of a Co<sub>47.5</sub>Fe<sub>28.5</sub>Ni<sub>19</sub>Si<sub>3.4</sub>Al<sub>1.6</sub> HEA fabricated via laser powder bed fusion (LPBF), with a laser power of 200 W and a scanning speed of 800 mm/s. The simulations revealed that the alloy underwent thermal cycling during the LPBF process, exhibiting a temperature gradient of approximately  $5.6 \times 10^7$  K/m and a cooling rate of about  $1.07 \times 10^6$  K/s. Li et al. [176] employed a finite element model to compute the solidification parameters G and R of the CoCr-FeMnNi HEA during the LMD process. Combined with experimental characterization, they quantitatively elucidated the correlation between the G and R parameters and the columnar to equiaxed transition (CET) behavior, thus providing valuable guidance for the preparation of high-performance HEAs via the LMD. Similarly, Rui et al. [177] utilized a finite element model to simulate the temperature field distribution of FeCrNiMnAl HEA coatings on stainless steel substrates by laser cladding (LC) and investigated the CET behavior of FeCrNiMnAl HEA coatings under various solidification parameters.

The finite element method employs the concept of discretization, enabling it to analyze complex linear and nonlinear problems. It can simulate and analyze the stress-strain distribution, temperature distribution, and deformation behavior of HEAs under complex conditions, thereby optimizing the processing techniques of HEAs and providing macro-scale guidance for their design. However, the computational cost of the finite element method escalates with increasing model complexity. Addressing intricate problems often necessitates the construction of elaborate and detailed models, such as finely meshed grids. Reliable finite element analysis results depend on precise material properties and constitutive models, and currently, there are limited studies on the constitutive models of HEAs.

### 3.4. Molecular dynamics

Molecular dynamics simulation is a computational method for studying the physical motion of molecules and atoms within a system. It is based on solving Newton's equations of motion to determine the coordinates and velocities of atoms, thereby obtaining the relevant properties of the system [178]. Molecular dynamics simulation can explore the mechanical behavior and deformation mechanisms of HEAs at the atomic scale, thereby providing guidance for their design. For instance, Zhang et al. [179] utilized molecular dynamics to simulate the stress-strain curves of FeNiCrCoCu HEAs with different grain sizes, noting that the critical grain size for the inverse Hall-Petch effect increases as the temperature rises from 10 K to 600 K. Hsieh et al. [180] investigated the uniaxial compression deformation behavior of CoCr-FeMnNi HEAs along the [001], [110], and [111] directions using molecular dynamics simulations. The results indicated that stress-induced phase transformations in CoCrFeMnNi HEAs exhibit strong crystal orientation dependence. Molecular dynamics simulations also elucidate the friction and wear mechanisms of HEAs by constructing nano-scratching models. For example, Huang et al. [181] developed a nano-scratching model for AlCoCrFeNi HEA using molecular dynamics, exploring its tribological behavior. Wang et al. [182] studied the scratching force, friction coefficient, surface morphology, and dislocation density evolution of AlCrCuFeNi HEAs during nanoscratching via molecular dynamics, unveiling their deformation mechanisms at the atomic scale. Furthermore, molecular dynamics simulations have provided insights into the microscopic mechanisms of shock compression and nanoindentation processes in HEAs. Xie et al. [183] used nonequilibrium molecular dynamics to examine the dynamic deformation behavior of equiatomic FeNiCrCoCu HEAs under shock compression, finding that dislocation slip mechanisms dominate at lower shock velocities, while at higher velocities, the plasticity mechanisms of the

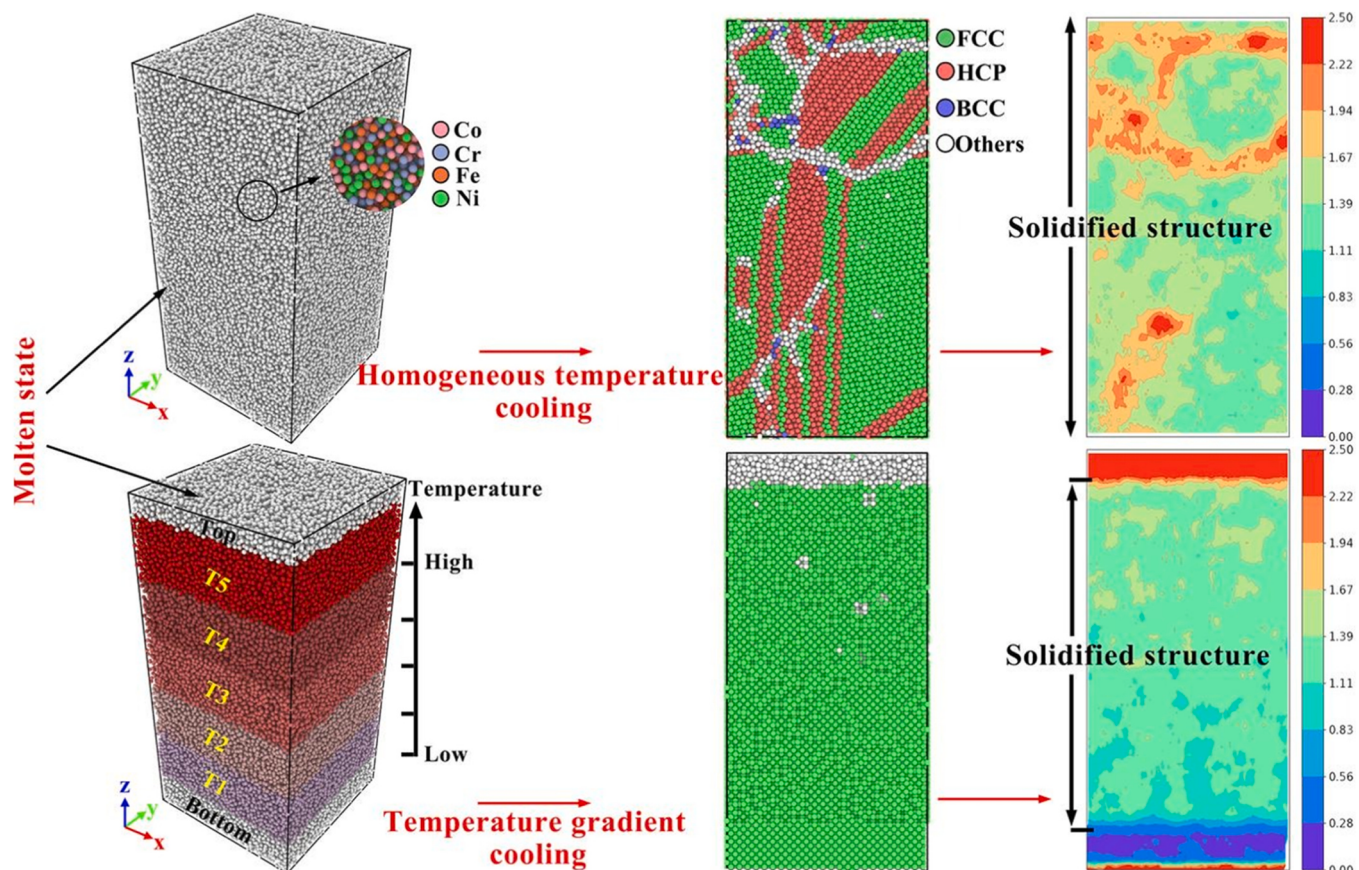


Fig. 13. The effect of temperature gradients on the solidification process of CoCrFeNi HEAs [186].

alloys are primarily governed by amorphization. Hua et al. [184] simulated the nanoindentation process of CoCrNi multi-principal-element alloys using molecular dynamics, highlighting

that Cr-rich clusters promote heterogeneous dislocation nucleation (HDN). Guo et al. [185] used molecular dynamics to simulate the nanoindentation process of Al<sub>0.3</sub>CoCrFeNi HEAs, studying the effects of

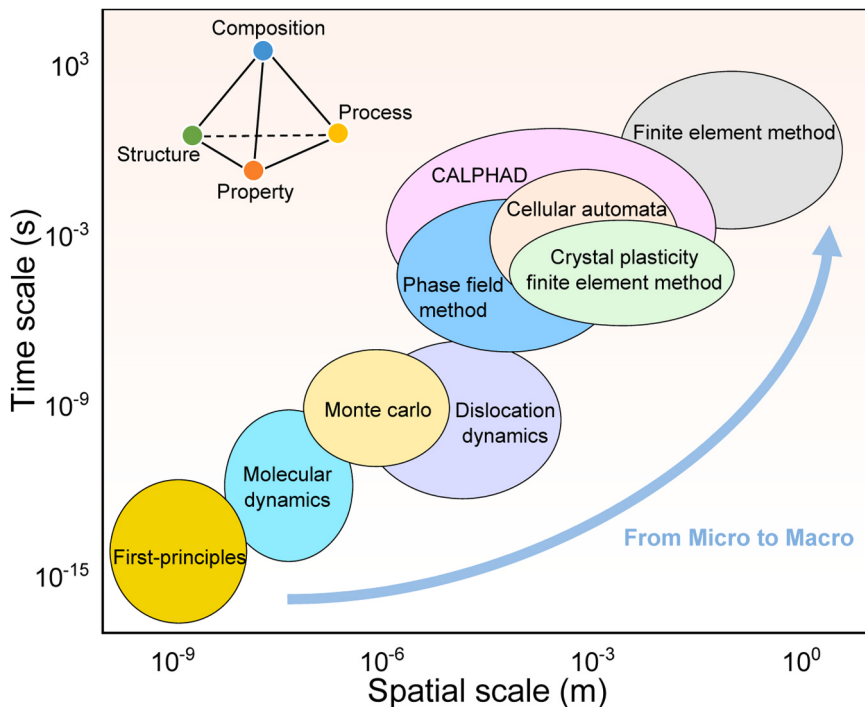
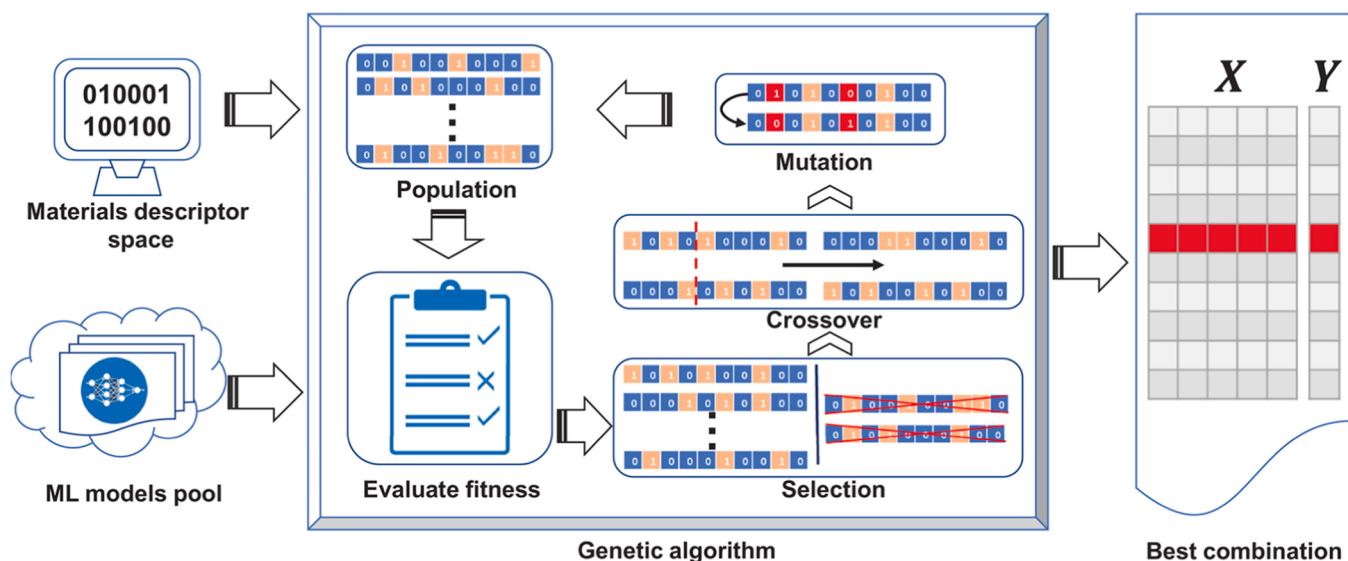


Fig. 14. Applicable time and spatial scales of computational materials science methods.



**Fig. 15.** Flowchart for searching the optimal combination of material descriptors and machine learning models [195].

crystal orientations [001], [101], and [111] on nanoindentation. The simulation results showed that with increasing indentation depth, independent nucleation of prismatic dislocation loops was observed in the [111] direction, while stacking fault tetrahedra without the participation of Frank dislocation loops were observed in the [101] direction.

Additionally, the molecular dynamics method has applications in the solidification behavior and irradiation damage of HEAs. Xie et al. [186] used molecular dynamics to study the effect of temperature gradients on the solidification process of CoCrFeNi HEAs. As shown in Fig. 13, under uniform temperature solidification conditions, the CoCrFeNi HEA forms FCC, HCP, and a small amount of BCC phases. However, under a temperature gradient of 50 K, the HEA not only forms a single and homogeneous FCC phase but also exhibits a better residual stress distribution, providing atomic-scale insights for designing single-phase HEAs. He et al. [187] investigated the generation and evolution of irradiation-induced defects in Ni, NiCr, NiCoCr, NiCoFeCr, and FeCoCrNiCu alloys using molecular dynamics. The simulation results indicated that as the complexity of the alloy system increases, the irradiation resistance of the alloys gradually improves.

Molecular dynamics simulations can investigate the solidification behavior, irradiation defects, mechanical behavior, and deformation mechanisms of HEAs, revealing quantitative relationships between composition, microstructure, and performance, thereby guiding the design of HEAs. However, the accuracy of molecular dynamics simulations depends on the potential functions, necessitating the development of more reliable potential functions for HEAs to enhance the computational precision. Additionally, the molecular dynamics method typically simulates systems containing tens of thousands to hundreds of thousands of atoms, with simulation times usually in the tens of nanoseconds, resulting in relatively small computational scales.

### 3.5. Section summary

In addition to utilizing molecular dynamics, first-principles calculations, the finite element method, and the CALPHAD method for designing HEAs, other computational materials science approaches such as the phase field method, cellular automata, crystal plasticity finite element method, Monte Carlo simulations, and dislocation dynamics can also be employed to establish quantitative relationships between the composition, processing, structure, and properties of HEAs, thereby guiding their design. For instance, Li et al. [188] simulated the evolution of coherent BCC/B2 microstructures in Al-Ni-Co-Fe-Cr HEAs using the phase field method. Roy et al. [189] employed cellular automata to

simulate the oxidation behavior of AlCoCrFeNi HEAs under specific rules. Lu et al. [190] developed a crystal plasticity finite element model incorporating a damage factor to investigate the damage distribution and texture characteristics of CoCrFeNi HEA shear-tension specimens under quasi-static deformation. Ye et al. [191] predicted the stability of AlCoCrFeMo<sub>0.05</sub>Ni<sub>2</sub> HEAs using kinetic Monte Carlo methods. Chen et al. [192] examined the irradiation hardening behavior of FeCoCrNi HEAs through discrete dislocation dynamics. However, due to the limited research on the application of the phase field method, cellular automata, crystal plasticity finite element method, Monte Carlo simulations, and dislocation dynamics in HEA design, this paper does not provide a detailed discussion. Fig. 14 summarizes the applicable time and spatial scales of commonly used computational materials science methods. It can be observed that from the micro to the macro scale, there are corresponding computational materials science methods. The core idea of designing HEAs using these methods is to establish quantitative relationships between composition, processing, structure, and properties. Each computational materials science method has its merits and drawbacks; thus, coupling multi-scale computational materials science methods to enhance alloy design efficiency is a promising future trend. The key to coupling multiscale computational methods lies in data transfer, whereby a stepwise simulation strategy is employed to use the computational results from one scale (such as the atomic scale) as input data for another scale (such as the mesoscale or macroscale). For instance, Liu et al. [193] utilized atomic-scale parameters of multi-principal element alloys obtained from molecular dynamics simulations as input for a crystal plasticity model. This stepwise simulation strategy offers distinct advantages, particularly in acquiring critical parameters that are difficult to obtain through experimental characterization. It should be emphasized that the accuracy of this approach is highly dependent on the effectiveness of data transfer across different scales. The innovative framework of the Materials Genome Initiative provides a systematic solution to the coupling challenges of multiscale computational methods. By integrating multiscale computational data through database technologies and employing machine learning as a connecting bridge, quantitative relationships among composition, microstructure, and properties in HEAs can be established. These aspects will be discussed in detail in Chapter 4.

### 4. Design methods for HEAs based on machine learning

The vast compositional space of HEAs, along with the complex nonlinear relationships between composition, structure, and properties,

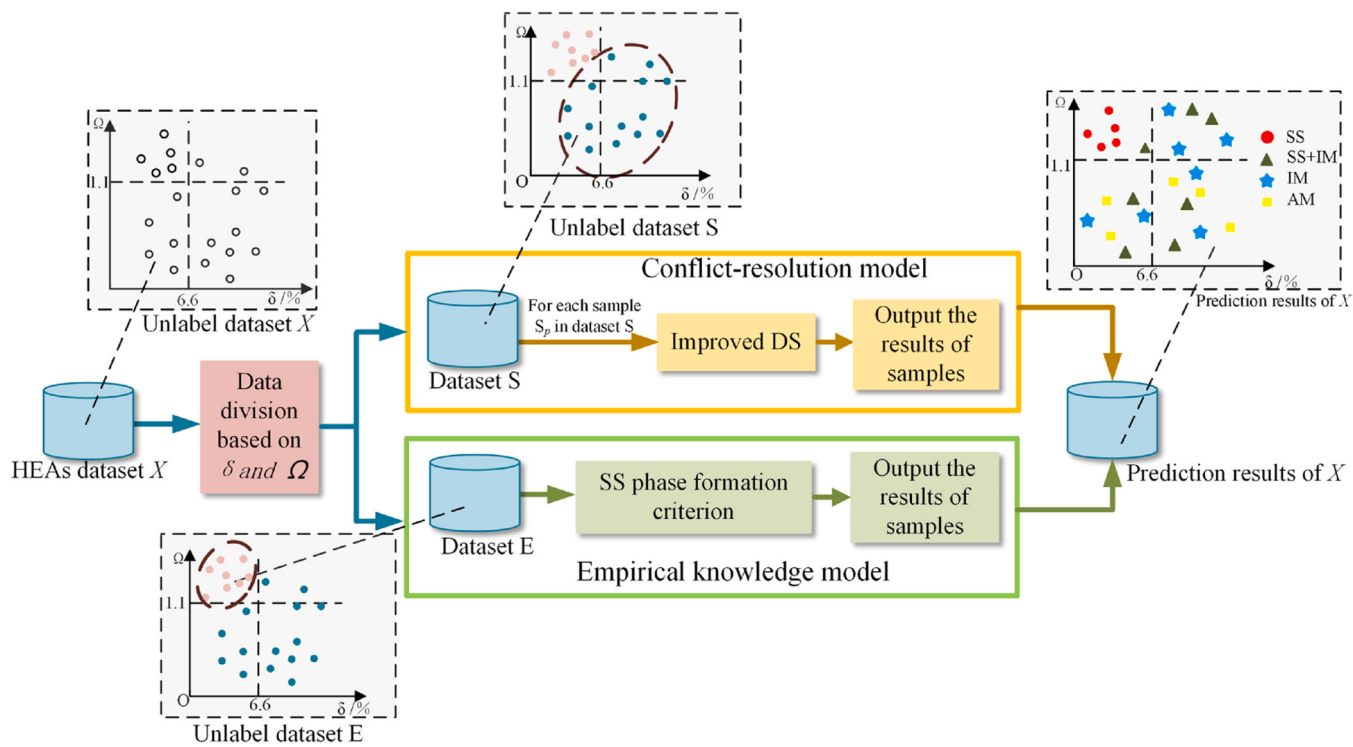


**Fig. 16.** HEA phase structure prediction model based on empirical knowledge and machine learning [203].

presents numerous challenges for alloy design. Over years of development, a substantial amount of data on the composition, phase structures, and properties of HEAs has been accumulated. The powerful data processing capabilities of machine learning methods offer new perspectives for HEA design. This paper will elaborate on two aspects: the prediction of phase structures and phase stability of HEAs, and the prediction of their properties.

#### 4.1. Prediction of phase structures and phase stability in HEAs

Phase structures and phase stability significantly influence the performance of HEAs [194]. Therefore, establishing predictive models for phase structures and phase stability in HEAs is crucial for guiding alloy design and accelerating the research and development process. Zhang et al. [195] constructed a material descriptor space and a pool of machine learning models, as shown in Fig. 15, and used genetic algorithms to search for the optimal combination of material descriptors and machine learning models. The HEA phase classification model developed

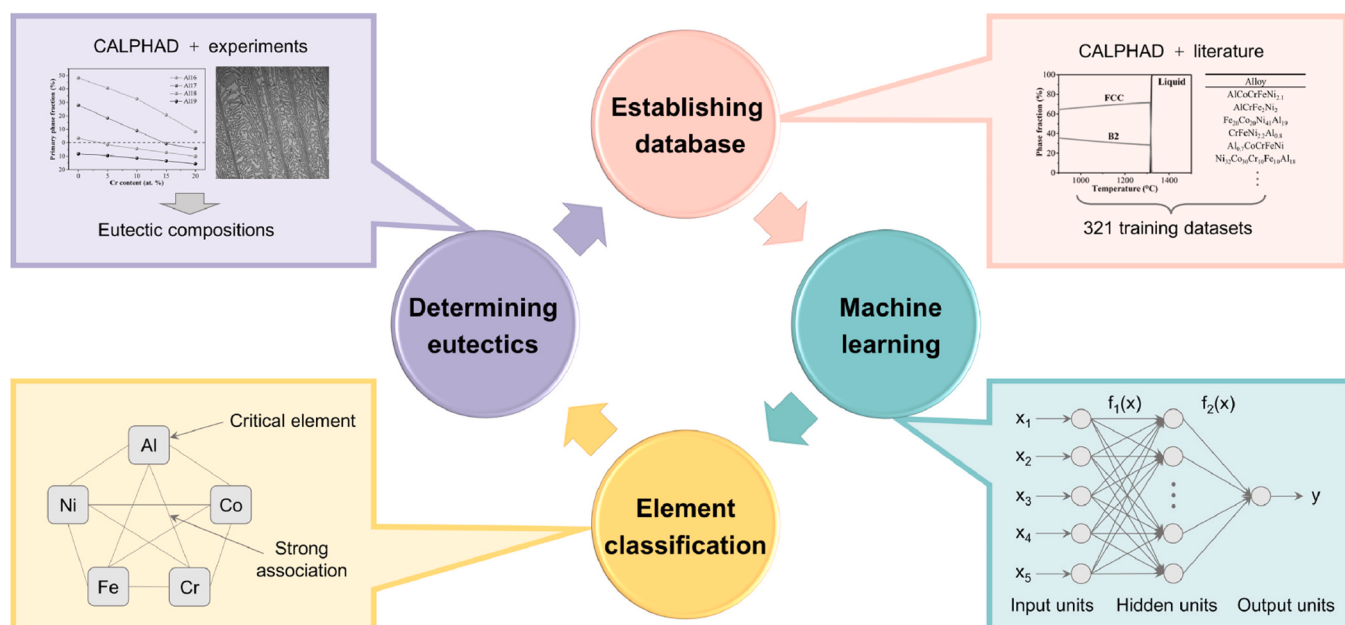


**Fig. 17.** Schematic diagram of designing Eutectic HEAs using machine learning [204].

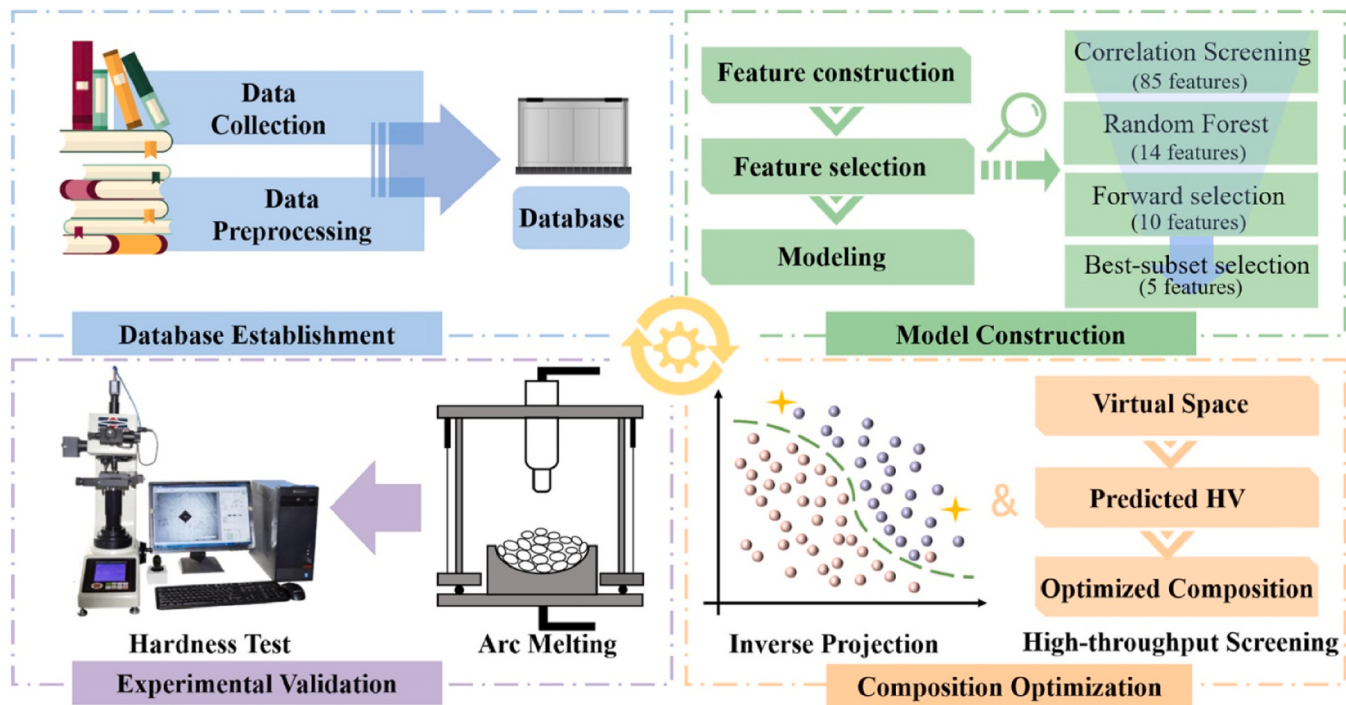


**Fig. 18.** The schematic diagram of the machine learning-based HEA design framework [213].

within this framework achieved high prediction accuracy. Huang et al. [196] employed K-nearest neighbors, support vector machines, and artificial neural networks to predict whether HEAs form single-phase solid solutions, intermetallic compounds, or mixed solid solutions and intermetallic compounds. Qu et al. [197] used support vector machines to establish a phase classification model for HEAs, achieving a prediction accuracy of over 85 %. Kaufmann et al. [198] coupled thermodynamic and chemical features with a random forest model to develop a high-precision predictive model for the solid solution forming ability in HEAs. As the HEA space continues to be explored, this model can be progressively refined through the systematic incorporation of new data.

He et al. [199], based on a collected dataset of 399 HEA samples, used support vector machines, decision trees, random forests, logistic regression, and K-nearest neighbors algorithms to predict the phase structures of HEAs. The results showed that the random forest algorithm effectively predicted BCC phases, FCC phases, dual phases (FCC + BCC), and amorphous phases, with a prediction accuracy of 87 %. Yan et al. [200] collected 1807 HEA samples from the literature and developed a gradient boosting model, which demonstrated an advantage in distinguishing whether refractory HEAs form single-phase solid solutions, achieving a prediction accuracy of 96.41 %. XRD technology was used to validate the predicted 10 single-phase refractory HEAs, and the prediction results were consistent with the experimental results. Zhu et al. [201] proposed a deep neural network based on a residual network for predicting the phase structures of HEAs, with an overall accuracy of 81.9 %. The prediction accuracy of single machine learning algorithms is limited. Nazir et al. [202] improved the prediction accuracy of HEA phase structures by combining multiple machine learning models using a voting ensemble method. Hou et al. [203] proposed a HEA phase structure prediction model based on empirical knowledge and machine learning. As shown in Fig. 16, this model consists of phase formation theories based on solid solution phases and a conflict resolution model, combining the strong generalization of empirical knowledge with the powerful learning capabilities of machine learning algorithms. The results indicated that this model achieved higher accuracy than traditional machine learning models.

Additionally, machine learning has applications in the design of

eutectic HEAs. As shown in Fig. 17, Wu et al. [204] used 321 sets of thermodynamic calculation data to establish a neural network prediction model, with alloy composition and primary phase molar fraction as inputs and outputs, respectively, to guide the design of eutectic HEAs in the AlCoCrFeNi system. The results showed that the screened Ni<sub>40</sub>C<sub>o<sub>20</sub></sub>Fe<sub>10</sub>Cr<sub>10</sub>Al<sub>18</sub>W<sub>2</sub> eutectic HEA achieved a tensile strength of approximately 1300 MPa and an elongation of about 20 %.

Liu et al. [205] developed a Ni-Co-Cr-Al alloy database grounded in literature research and the CALPHAD method. They assessed the significance of alloy compositions on eutectic phase formation using a machine learning model, identifying the range of key alloying elements. Ultimately, they simulated the alloy solidification process via the CALPHAD method and successfully selected two eutectic HEAs.

#### 4.2. Properties prediction of HEAs

Designing HEAs based on phase structure and phase stability is indirect, whereas the ultimate goal of alloy design is often to produce HEAs that meet specific performance requirements. Machine learning demonstrates significant advantages in developing performance prediction models for HEAs. For instance, Vazquez et al. [206] utilized an elasticity property database for Nb-Mo-Ta-W-V refractory alloys determined by density functional theory, developing a descriptor-based machine learning framework to predict the elastic properties of HEAs. Gao et al. [207] collected 261 sets of hardness data for single-phase HEAs from the literature. For HEA data containing only yield strength information, the yield strengths were converted to corresponding hardness values using a formula that relates hardness to yield strength [208]. After evaluating the performance of five different machine learning algorithms, it was concluded that the random forest algorithm was more advantageous in predicting the hardness of solid solution HEAs. Zhang et al. [209] employed machine learning algorithms to predict the stacking fault energy of the Co-Cr-Fe-Mn-Ni-V-Al HEA system. Support vector machines and random forest algorithms were employed to construct the classification model, while deep learning algorithms were used to construct the regression model. In recent years, numerous HEAs with exceptional performance have been efficiently designed based on

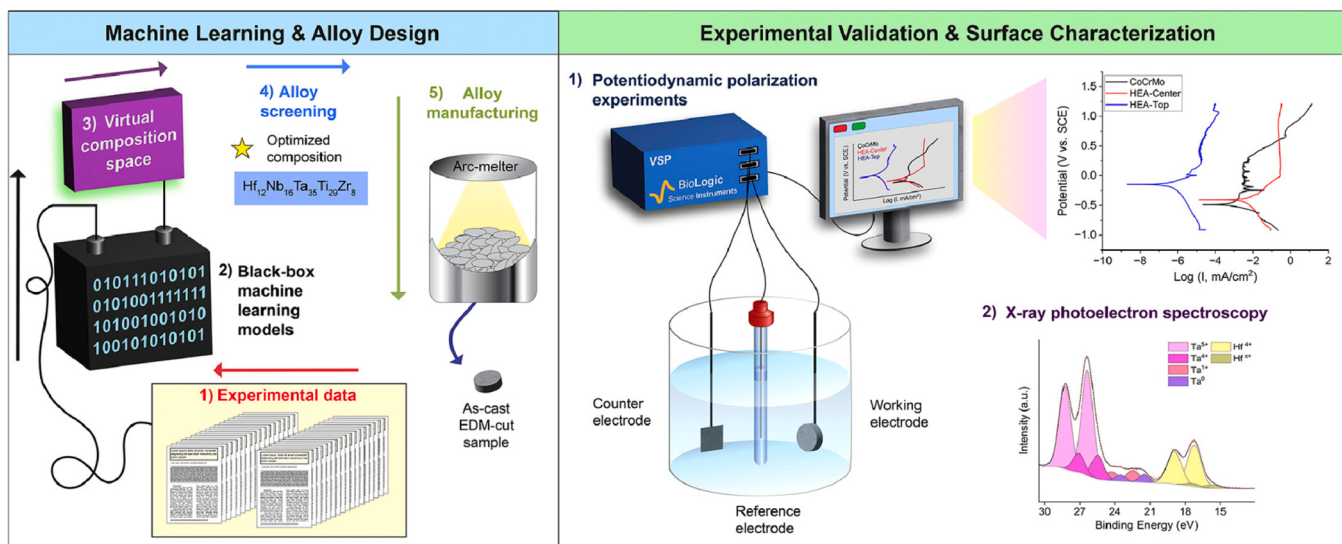


Fig. 19. Schematic diagram of designing corrosion-resistant HEAs using machine learning methods [215].

machine learning performance prediction models. For example, Wen et al. [210] established a relational model between composition/properties and hardness using HEA composition-hardness data. They employed a global optimization algorithm to search for alloys within the complex compositional space and continuously iterated and enhanced the model through experiments to expedite the design of high-hardness AlCoCrCuFeNi alloys. Chen et al. [211] collected hardness data from 305 sets of the AlCoCrCuFeNi HEA system, including 12 descriptors such as alloying element content, the VEC, and the  $\delta$ . By combining a machine learning model with a particle swarm algorithm, they designed a HEA with an average hardness value of 966 HV within a search space containing nearly 65,000 data points of the AlCoCrCuFeNi HEA system. Guo et al. [212] used the composition of HEAs as features to establish a

machine learning model for predicting hardness, identifying  $\text{Al}_{1.2}\text{Cr}_{17.42}\text{Fe}_{25.42}\text{Ni}_{28.32}\text{Ti}_{27.62}$  HEAs with a hardness of 869.88 HV. Yang et al. [213] developed a HEA hardness prediction model using a support vector machine algorithm and proposed a machine learning-based HEA design framework, as shown in Fig. 18. This framework primarily includes four modules: database construction, machine learning model development, composition optimization, and experimental validation. The  $\text{Co}_{18}\text{Cr}_7\text{Fe}_{35}\text{Ni}_5\text{V}_{35}$  HEA designed according to this framework exhibits superior hardness, exceeding the highest hardness in the original dataset by 24.8 %.

Dong et al. [214] utilized machine learning methods to guide the design of HEAs with exceptional high-temperature oxidation resistance, focusing on weight gain of the alloys after high-temperature exposure as

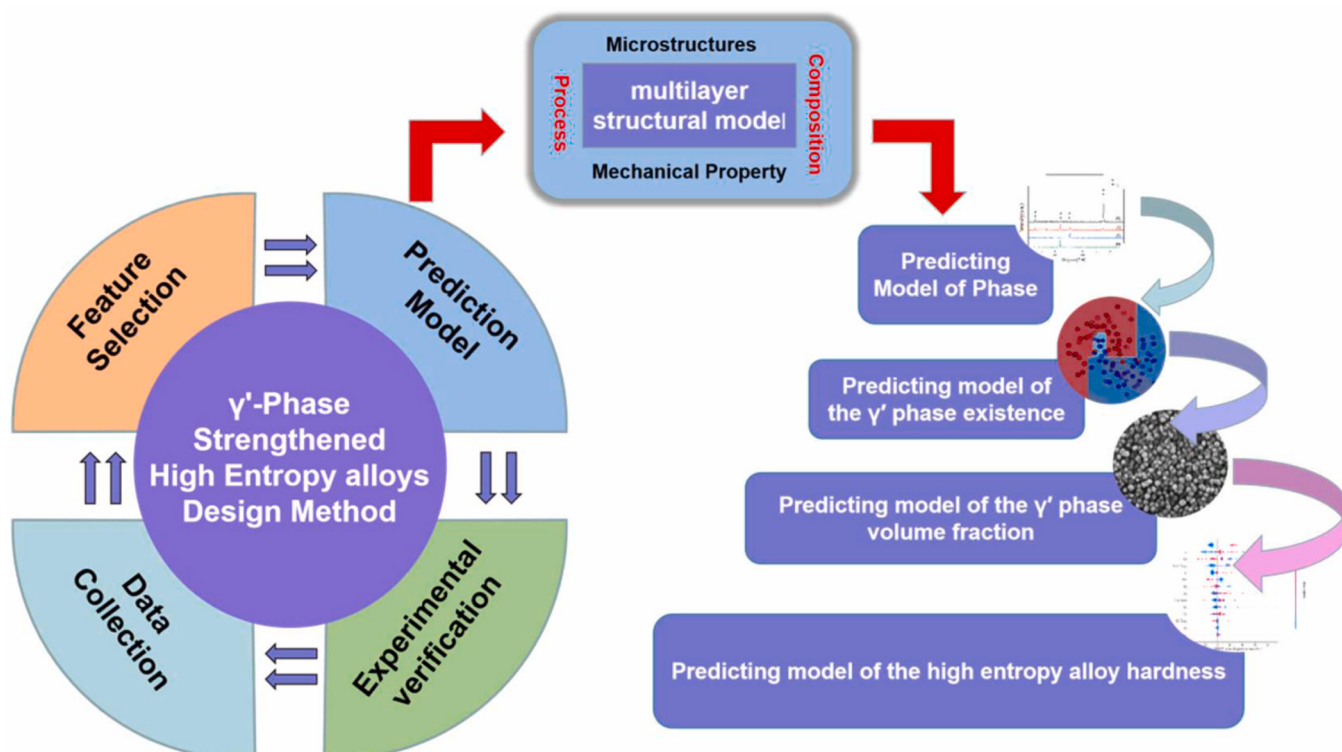


Fig. 20. Machine learning-based design strategy for multilayer structural models [216].

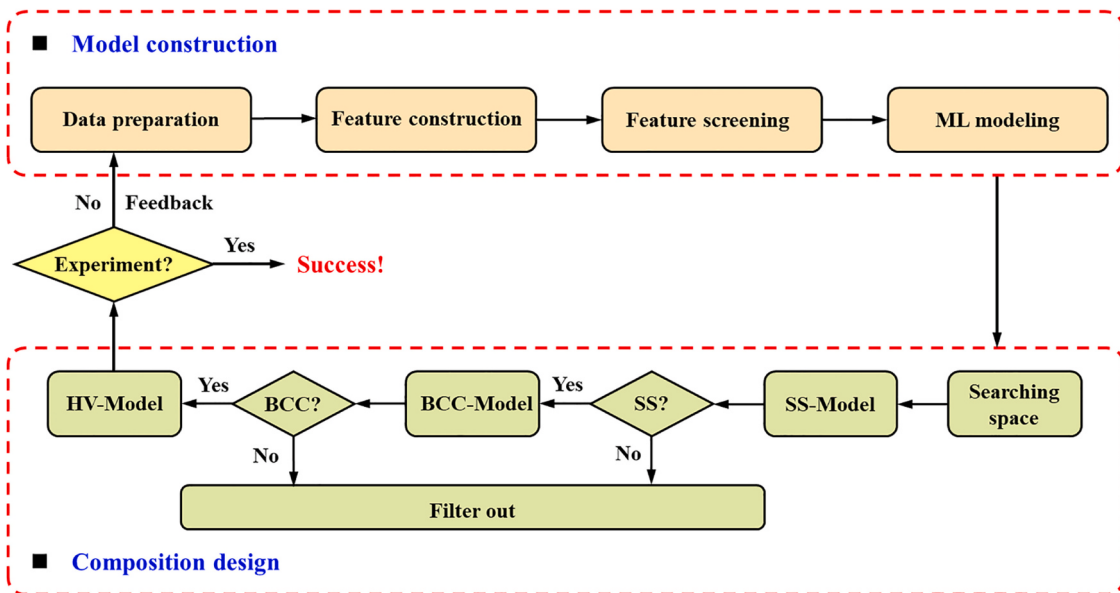


Fig. 21. Integrated design strategy for low-activation HEAs based on machine learning methods [217].

the target performance criterion. Ozdemir et al. [215] developed a machine learning-based framework for designing HEAs with superior corrosion resistance, with the detailed design process depicted in Fig. 19. Initially, a dataset for the HfNbTaTiZr alloy system was established through literature research. Subsequently, a machine learning algorithm was employed to develop a predictive model for the corrosion potential of the HfNbTaTiZr alloy system, creating a virtual space containing over 500,000 distinct alloy compositions, with Ti, Ta, Hf, Nb, and Zr contents varying between 5 at% and 35 at%. Finally, the established corrosion potential model was used to predict and select the optimal candidate alloys. Experimental results indicated that the designed Hf<sub>12</sub>Nb<sub>16</sub>Ta<sub>35</sub>Ti<sub>29</sub>Zr<sub>8</sub> HEA exhibits high corrosion resistance, with the predicted corrosion potential values aligning well with the experimental results.

Moreover, machine learning methods can address multi-objective HEA design problems. For instance, Liu et al. [216] introduced a machine learning-based design strategy for multilayer structural models. As depicted in Fig. 20, the process commenced with the establishment of

the HEA phase classification model, the binary classification model for  $\gamma'$  phase, the volume fraction prediction model for  $\gamma'$  phase, and the HEA hardness prediction model. Subsequently, 84 groups of HEA compositions and their corresponding treatment processes, which satisfied the design criteria, were selected from 800,000 candidate alloys through a meticulous layer-by-layer screening. Four of these groups were experimentally verified, demonstrating that they consisted of FCC phase and  $\gamma'$  phase, with the predicted  $\gamma'$ -phase volume fraction and hardness values of the HEAs consistent with the experimental results.

Li et al. [217] proposed an integrated design strategy for low-activation HEAs based on machine learning methods, successfully producing Fe<sub>35</sub>Cr<sub>30</sub>V<sub>20</sub>Mn<sub>10</sub>Ti<sub>5</sub> HEAs with a single-phase BCC structure and high hardness through only two experimental iterations. The specific design strategy, as illustrated in Fig. 21, begins with using a phase classification model to exclude non-solid solution HEAs from the search space. Another phase classification model is then employed to screen for HEAs with a single-phase BCC structure among the remaining candidates. Finally, a hardness prediction model is used to predict the

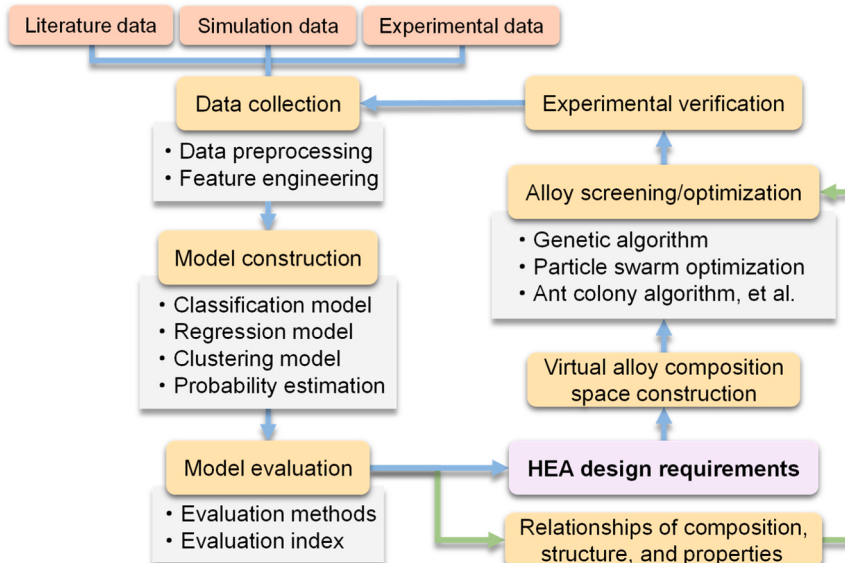


Fig. 22. Machine learning-based design flowchart for HEAs.

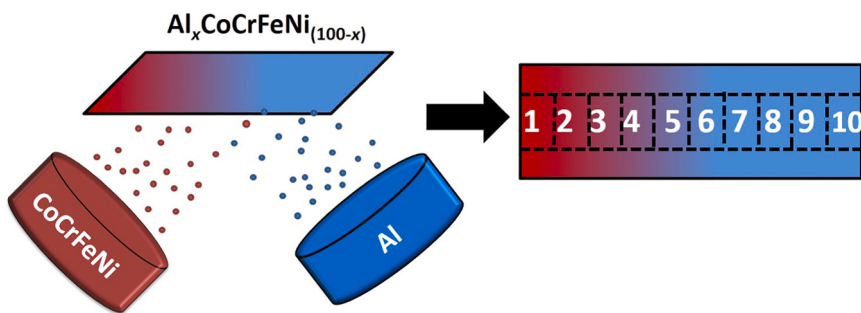


Fig. 23. Schematic diagram of the magnetron sputtering process [223].

hardness of the HEAs with a single-phase BCC structure.

Khan et al. [218] amalgamated density functional theory, machine learning, and CALPHAD methods to devise a stacking fault energy prediction model for CoCrFeMnNiVAL HEAs and proposed a design framework that considers both stacking fault energy and strength. The core concept entails using the CALPHAD method to screen alloy compositions that meet phase stability and solidification conditions from the initial composition space, calculating the stacking fault energy of the selected alloys using density functional theory, and employing machine learning methods to establish a stacking fault energy prediction model from a data perspective. Ultimately, by integrating this model with the HEA strength prediction model, candidate HEAs with potential application value are identified.

#### 4.3. Section summary

The overarching process for designing HEAs using machine learning is depicted in Fig. 22. Initially, a comprehensive database encompassing HEA composition, structure, and performance is constructed through literature research, experimental characterization, or simulation calculations. Driven by the Materials Genome Initiative, the data acquisition approach has gradually evolved toward a standardized and large-scale database construction model, leading to the emergence of numerous multiscale and integrated materials databases, such as AFLOWlib [219] and COD'HEM [220]. Subsequently, a suitable machine learning algorithm is selected to develop the predictive model for HEAs. Guided by specific requirements and based on this predictive model, the desired HEAs are then designed. Ultimately, the designed HEAs undergo experimental synthesis to verify if they fulfill the design criteria. This design method can significantly shorten the development process of HEAs and accelerate their innovation. Furthermore, integrating machine learning methods with intelligent optimization algorithms can expedite the search for optimal alloy compositions. The established prediction model can also be used to analyze the impact of input parameters on the structure and performance of HEAs, further elucidating the relationship between composition, structure, and performance. This approach facilitates the derivation of material science principles to guide the design of HEAs.

Machine learning exhibits unique advantages in the design of HEAs. It can efficiently analyze and process large volumes of data to establish quantitative relationships between the composition, structure, and properties of HEAs, thereby accelerating their design. Additionally, machine learning provides a new perspective on multi-scale and multi-method coupling, as demonstrated by the research of Khan et al. [218]. However, machine learning-based design methods for HEAs still face challenges. The primary challenge is the poor interpretability of machine learning models. These models make predictions based on data without focusing on the underlying physical mechanisms, but understanding these mechanisms is essential for HEA design. Furthermore, data quality significantly affects the accuracy of machine learning models, and in most cases, HEA data is characterized by small sample

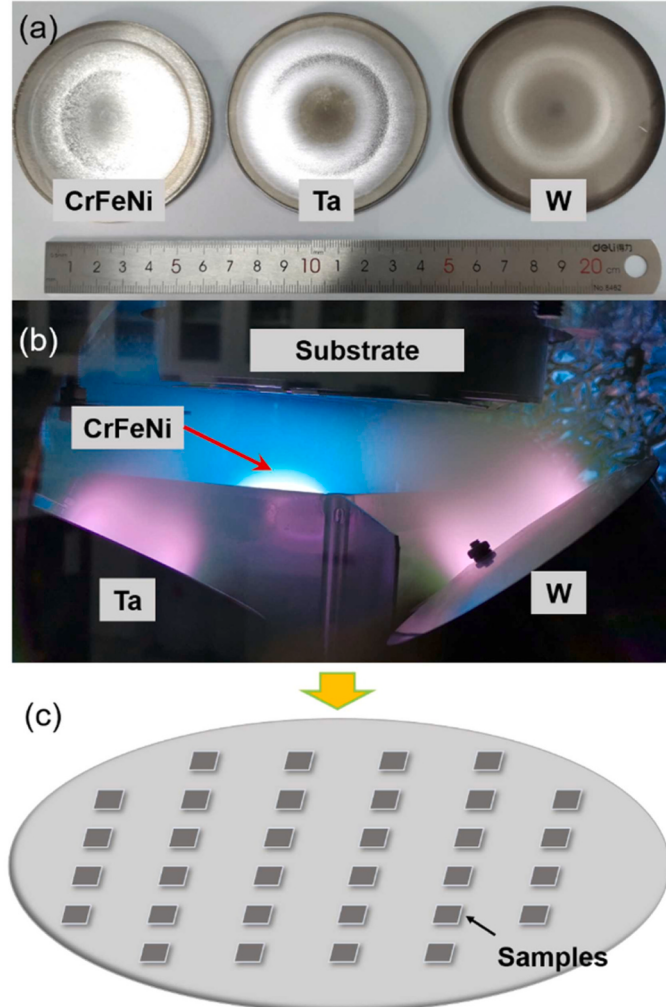


Fig. 24. (a) Alloy targets for magnetron sputtering. (b) Magnetron sputtering process. (c) W-Ta-CrFeNi film samples [225].

sizes and complexity.

#### 5. Design methods for HEAs based on high-throughput experiments

In 1970, to enhance the efficiency of material development, Hanak introduced the concept of “multiple-sample experiments” [221]. This concept was further developed into what is now known as high-throughput experiments. At present, high-throughput experiments have become one of the core technologies of materials genome

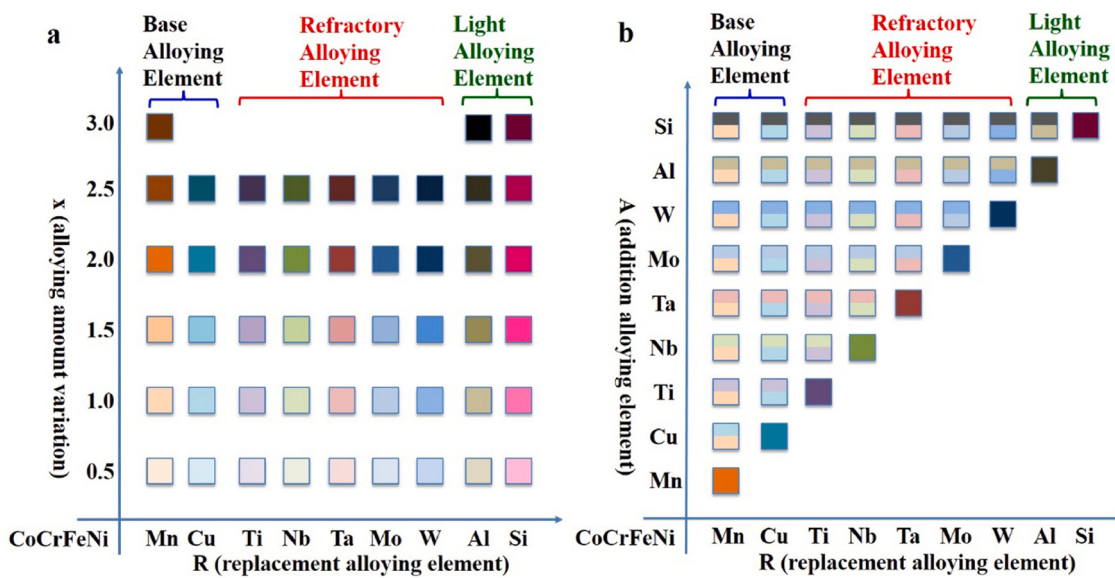


Fig. 25. Design strategies for CoCrFeNi-based HEAs: (a) CoCrFeNi-R<sub>x</sub> alloys; (b) CoCrFeNi-R-A alloys [227].

engineering and play an irreplaceable role in the efficient design of HEAs. High-throughput experiments encompass two main components: high-throughput preparation and high-throughput characterization, which will be discussed separately in this paper.

### 5.1. High-throughput preparation

The main idea of high-throughput preparation is to produce a large number of samples in a short time. Currently, the more mature high-throughput preparation techniques include magnetron sputtering, high-throughput powder metallurgy, diffusion multiples, additive manufacturing, and gradient heat treatment technologies.

#### 5.1.1. Magnetron sputtering

Magnetron sputtering, a type of physical vapor deposition, primarily utilizes sputtering to vaporize target materials, forming a thin film upon deposition [222]. By controlling process parameters, the composition gradient of the thin film can be achieved, enabling the study of the influence of film composition on performance and realizing high-throughput material preparation. For instance, Zhang et al. [223] prepared Ti-Al-(Cr, Fe, Ni) alloy systems with compositional gradients using magnetron sputtering, providing a data foundation for the high-throughput screening of multi-principal-element alloys. As shown in Fig. 23, Shi et al. [224] used pure aluminum and equiatomic CoCrFeNi as targets and achieved high-throughput synthesis and screening of Al<sub>x</sub>(CoCrFeNi)<sub>100-x</sub> HEAs through magnetron sputtering, studying the effect of aluminum content on microstructure and corrosion behavior. With increasing aluminum content, the crystal structure of the Al<sub>x</sub>(CoCrFeNi)<sub>100-x</sub> HEA films transitioned from face-centered cubic to body-centered cubic, and their corrosion resistance decreased.

Li et al. [225] prepared gradient composition films of W-Ta-(Cr, Fe, Ni) HEAs using a three-target magnetron sputtering technique. Fig. 24 shows a schematic diagram of the magnetron sputtering process. Screening of the HEA films revealed that the W<sub>15.39</sub>Ta<sub>38.81</sub>Cr<sub>14.58</sub>-Fe<sub>15.45</sub>Ni<sub>15.77</sub> high-entropy film exhibited a maximum hardness of approximately 20.6 GPa, providing guidance for the design of advanced ultra-hard materials.

#### 5.1.2. High-throughput powder metallurgy

Powder metallurgy, as an efficient material preparation technique [226], enables precise adjustment of material composition ratios and is one of the key methods for high-throughput sample preparation. For

example, Zhao et al. [227] systematically and efficiently prepared 85 types of CoCrFeNi-based HEAs, as shown in Fig. 25, using the high-throughput hot isostatic pressing micro-synthesis approach (HT-HIP-MSA), accelerating the establishment of the relationships among composition, microstructure, and properties of HEAs. This method first involves filling 85 different proportional mixtures of spherical powders into the corresponding cells of a honeycomb structure mold, followed by hot isostatic pressing to obtain a honeycomb structure HEA sample with 85 discrete compositions. Moreover, this method is also applicable for the high-throughput preparation of nickel-based superalloys and Co-Fe-Ni system alloys [228,229].

#### 5.1.3. Diffusion multiples

The diffusion multiple approach achieves gradient variations in alloy composition through the high-temperature long-term diffusion of single or multiple elements between different diffusion couples, obtaining extensive composition-structure-property data from limited samples [230], thus enabling high-throughput design of HEAs. For example, Hilhorst et al. [231] designed four different diffusion multiples to evaluate the Cr-Fe-Mn-Co-Ni HEA system. The study showed that the diffusion multiple approach has significant implications for alloy design in terms of phase prediction, diffusion, and mechanical properties. As shown in Fig. 26, Coury et al. [232] used the diffusion multiple approach to prepare compositional gradient samples of the Cr-Mn-Fe-Co-Ni HEA system, and combined with nanoindentation techniques, they quickly estimated the yield strength of single-phase HEAs. This method can reduce the number of experiments needed to find HEAs with the desired strength across a broad compositional space. Wilson et al. [233] prepared diffusion multiples for the Co-Cr-Fe-Mn-Ni system, studied the phase stability of HEAs, and pointed out that elastic modulus mismatch is a more accurate predictor of hardness.

Notably, due to the vast compositional space of HEAs, the prediction accuracy of the CALPHAD method is limited, and the diffusion multiple approach serves as a complement to the CALPHAD method. The diffusion multiple approach can be used to determine phase diagrams, laying the foundation for the construction of thermodynamic databases for materials. For instance, Zhao et al. [234,235] determined the phase diagrams of ternary systems such as Nb-Cr-Si and Nb-Ti-Si based on the diffusion multiple approach. This method can also be used to collect numerous binary system diffusion composition distribution curves, from which the diffusion coefficients of alloying elements in various phases can be extracted, facilitating the construction of atomic mobility

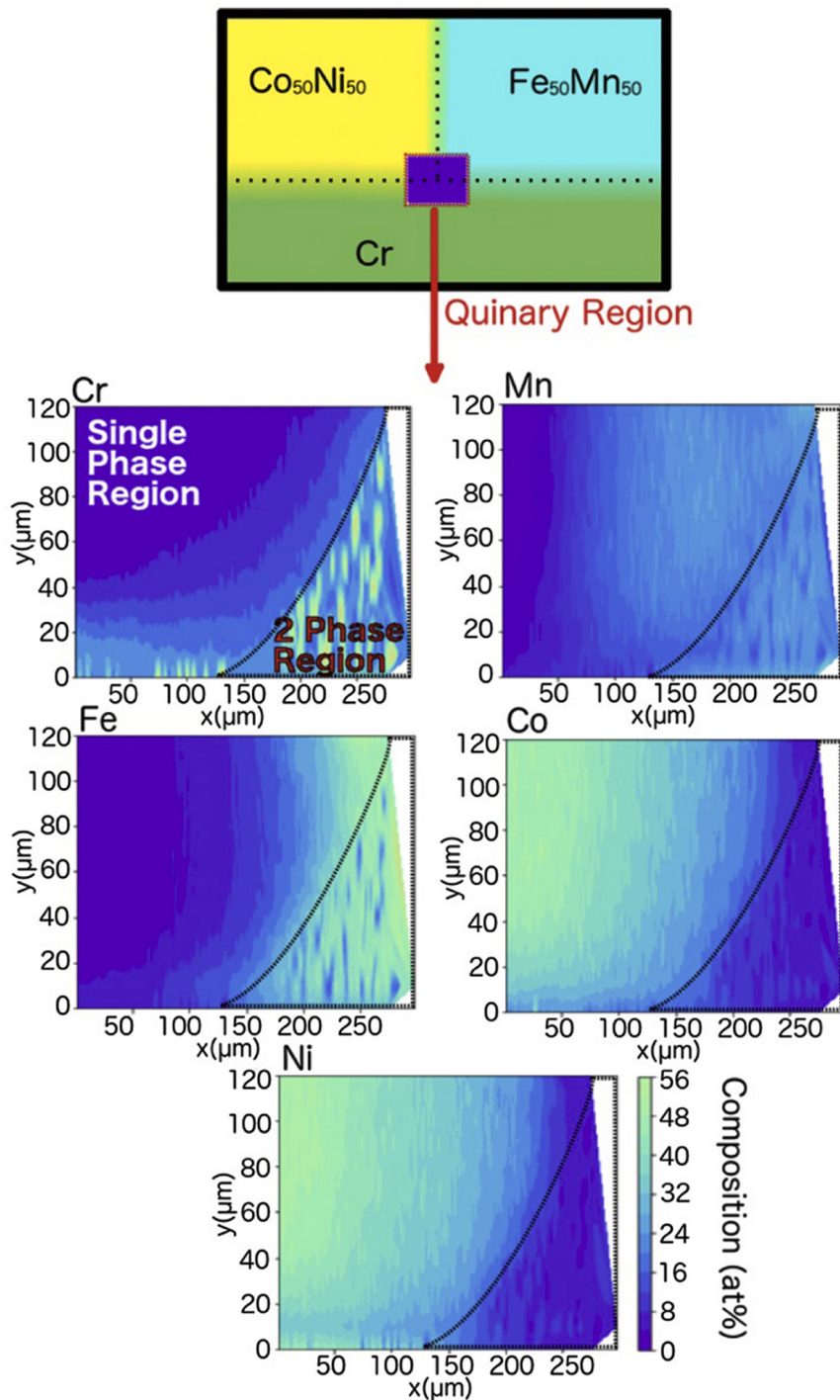


**Fig. 26.** Schematic diagram of the diffusion multiple and EDS measured composition distribution map of the quinary region [232].

databases for alloy elements. These databases are essential for kinetic simulations of material precipitation, growth, and interfacial reactions. For example, Li et al. [236] used the diffusion multiple approach to evaluate the composition-dependent interdiffusion coefficients of Al-Co-Cr-Fe-Ni HEAs at 1273 K, 1323 K, and 1373 K.

At present, the diffusion multiple approach faces several challenges: a) Contact issues between multiple interfaces, which can be resolved through high-precision machining and surface treatment of the samples. b) Oxidation of the samples, which can be addressed by heat treatment under high vacuum or reducing conditions. c) Avoidance of contamination from other non-designed elements.

#### 5.1.4. Additive manufacturing

Additive manufacturing (AM) constructs three-dimensional objects by layer-by-layer deposition of materials [237], offering high material utilization and the ability to fabricate complex-shaped parts. Additive manufacturing is widely used for preparing high-throughput samples. Currently, there are two main strategies for high-throughput preparation of HEA samples based on additive manufacturing: the powder-feeding strategy and the powder-bed strategy. The powder-feeding strategy introduces powder into the heat source of the printing head, with sample composition altered by controlling the feeding speed of multiple powder hoppers, exemplified by directed

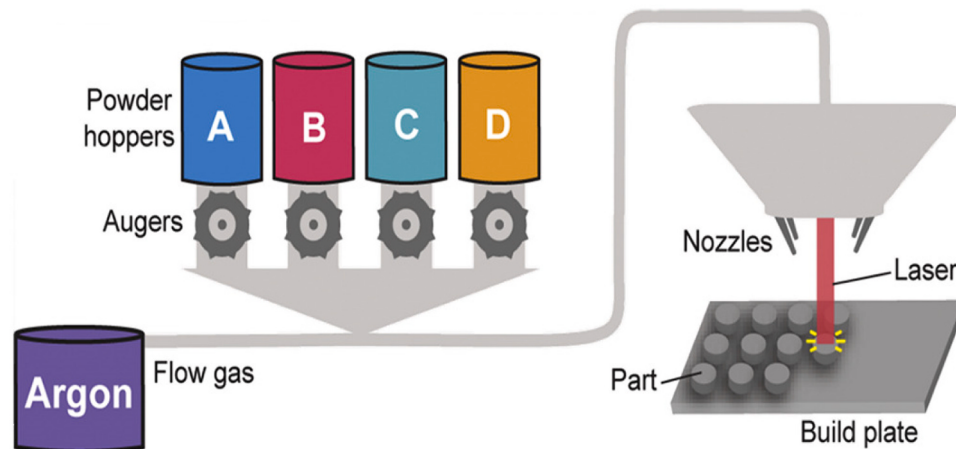


Fig. 27. Schematic diagram of preparing HEA composition arrays using AM technology [238].

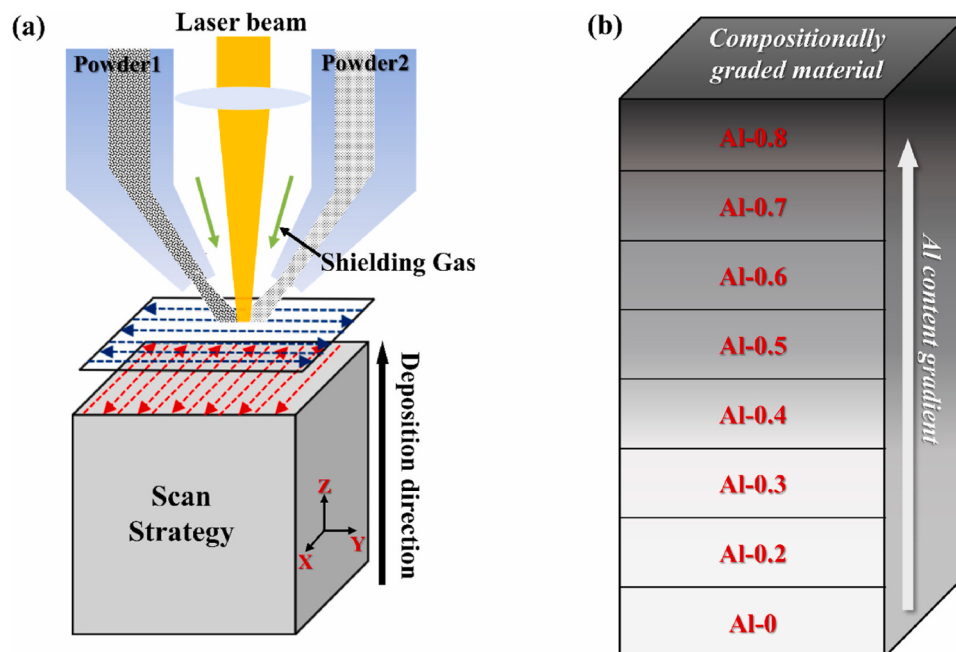


Fig. 28. (a) and (b) are the schematic diagrams of the DED process and the CoCrNiAl<sub>x</sub> composition gradient alloy, respectively [241].

energy deposition (DED) technology. The powder-bed strategy spreads a gradient powder layer according to the designed mixing ratio and uses a high-energy laser beam to sinter the powder to prepare compositional gradient samples, represented by laser powder bed fusion (LPBF) technology. The powder-feeding strategy is more advantageous for high-throughput preparation of HEA samples, capable of creating arrays of different HEA compositions. For instance, in 2020, Moorehead et al. [238] used directed energy deposition (DED) to prepare sample arrays of Mo-Nb-Ta-W HEAs. As shown in Fig. 27, there are four independently controlled powder hoppers containing Mo, Nb, Ta, and W metal powders. The laser beam sinters the metal powders delivered to the substrate, allowing the preparation of Mo-Nb-Ta-W HEA samples with different compositions through various combinations of metal powders. In 2021, Moorehead et al. [239] further applied directed energy deposition technology to prepare compositional arrays of Cr-Fe-Mn-Ni multi-principal-element alloys.

Moreover, the powder-feeding strategy can produce compositional gradients within a single sample. For instance, Borkar et al. [240] employed laser engineered net shaping (LENS) to establish a

compositional gradient in a single HEA specimen. The fundamental principle involves layer-by-layer adjustment of the feed rates of hoppers containing CrCuFeNi<sub>2</sub> powder and Al<sub>2</sub>CrCuFeNi<sub>2</sub> powder to achieve an Al compositional gradient, ranging from Al<sub>0</sub>CrCuFeNi<sub>2</sub> to Al<sub>1.5</sub>CrCuFeNi<sub>2</sub>. As shown in Fig. 28, Zheng et al. [241] used directed energy deposition to prepare CoCrNiAl<sub>x</sub> compositional gradient multi-principal-element alloys. The Al compositional gradient was achieved by keeping a constant feed rate for the hopper containing CoCrNi powder while varying the feed rate for the hopper containing Al powder. Similar work has also been conducted by Pegues [242], Yang [243], and Gwalani [244,245].

The powder-bed strategy can also be employed to prepare HEA samples with compositional gradients. For example, in 2023, Guo et al. [246] used the laser powder-bed fusion (LPBF) method to fabricate Al<sub>x</sub>CoCrFeNi HEA samples with compositional gradients. In the same year, Sun et al. [247] utilized the same method to produce aluminum alloy samples with Mg and Mn compositional gradients. As illustrated in Fig. 29, this method primarily relies on a newly designed powder mixing device to spread gradient powder layers, followed by high-energy laser

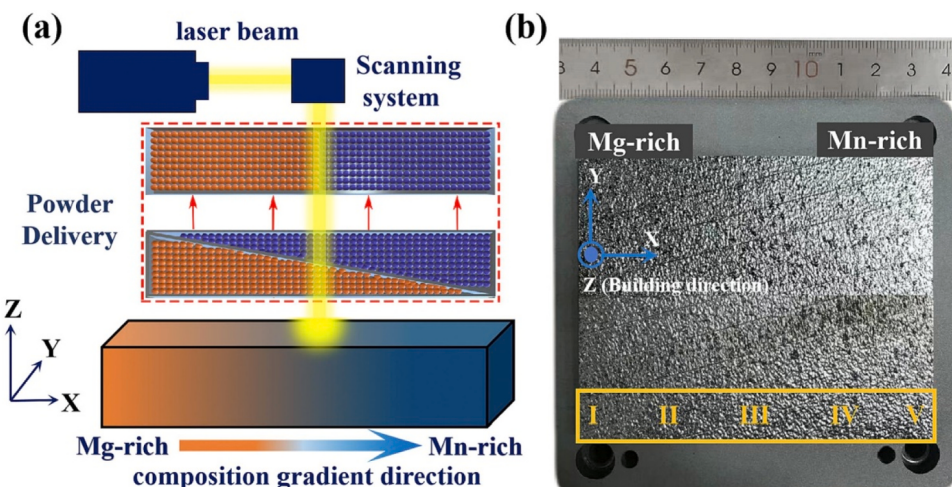


**Fig. 29.** (a) Schematic diagram of compositional gradient sample fabrication via LPBF technology, and (b) the image of printed aluminum alloy sample [247].

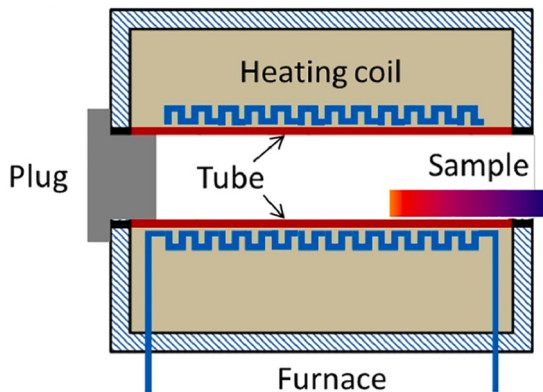


**Fig. 30.** Schematic diagram of gradient temperature heat treatment technology [249].

beam melting to create the compositional gradient alloy.

##### 5.1.5. Gradient heat treatment technologies

Heat treatment processes influence the microstructure and properties of alloys [248]. Gradient heat treatment technologies, as a high-throughput experimental approach, enable the formation of

temperature or cooling rate gradients within a single sample, thereby allowing multiple heat treatment parameters to be investigated in a single experiment. This significantly enhances experimental efficiency and shortens the overall research cycle. Wei et al. [249] developed an easily implementable gradient temperature heat treatment technique. The thermocouples are placed on the sample at specified intervals. As shown in Fig. 30, the sample is positioned at the open end of a tube furnace to generate a temperature gradient, and the temperature variations at different locations on the sample are monitored by the thermocouples.

Additionally, Wu et al. [250] generated specimens with cooling rate gradients using the end-quenching method, i.e., quenching only the bottom of the specimen, thereby introducing cooling rate gradients within a single specimen. Wang et al. [251] performed laser heat treatment on the surface of cold-rolled specimens, as shown in Fig. 31, successfully creating a stable gradient temperature field on the cross-section of the cold-rolled specimens. Xu et al. [252] applied direct current heating to a truncated conical specimen and, based on the principle that different cross-sectional areas lead to varying current thermal effects, successfully produced a temperature gradient on the surface of the specimen.

In addition to the high-throughput preparation methods discussed above, high-gravity technology [253,254], wedge-shaped rolling technology [255], directional solidification technology [256], cyclic torsion technology [257], and surface mechanical attrition treatment

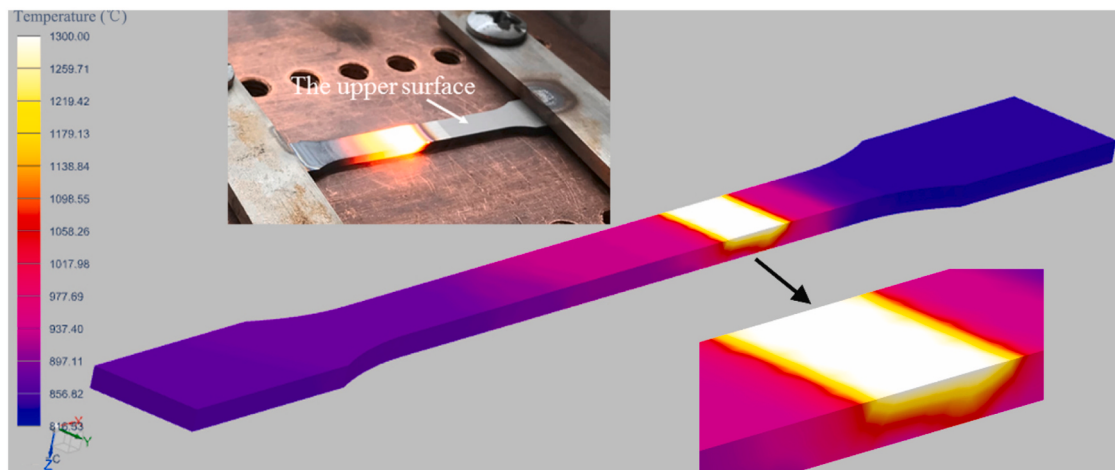


**Fig. 31.** Qualitative analysis of the gradient temperature field during laser heat treatment [251].

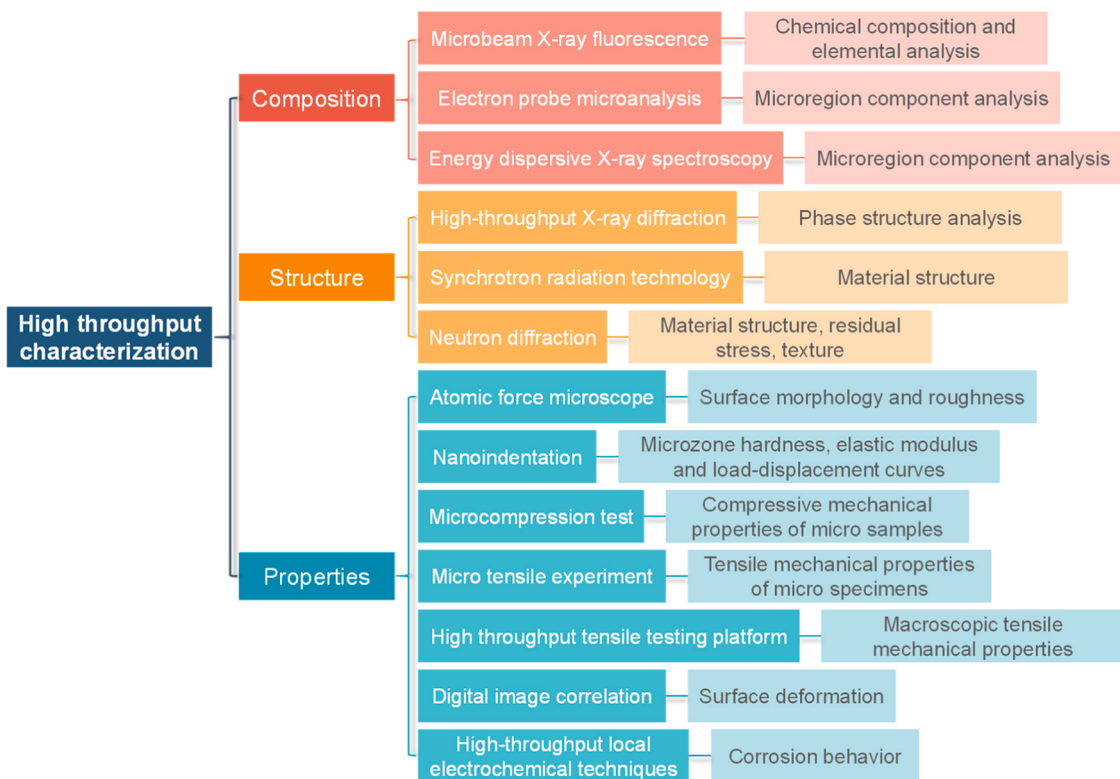


Fig. 32. High-throughput characterization techniques in the field of metallic materials.

technology [258] have promising applications in the field of HEAs. The choice of high-throughput preparation methods should be made rationally based on the specific design requirements of HEAs.

### 5.2. High-throughput characterization

High-throughput preparation techniques enable the synthesis or processing of a large number of samples in a single batch, thus imposing higher demands on characterization techniques. There is an urgent need to develop characterization methods tailored for high-throughput samples, known as high-throughput characterization techniques. High-throughput characterization refers to the acquisition of compositional, structural, and performance data for a large number of samples through a single experiment or a few tests, thereby enabling rapid evaluation and screening of materials.

For high-throughput samples with continuous composition gradients, high-resolution material characterization techniques are required to characterize the micro-regions of the samples, such as nano-indentation experiments, micro-tensile experiments, microcompression experiments, electron probe microanalysis, energy dispersive X-ray spectroscopy, and high-throughput local electrochemical techniques. For example, Fan et al. [259] employed high-throughput nano-indentation to measure the nano-hardness of the  $(\text{FeMnCoCr-Ni})_{98.6}\text{Co}_{0.6}\text{N}_{0.8}$  HEA and revealed the creep behavior of HEAs with different microstructures. Tong et al. [260] characterized the Young's modulus and hardness of  $\text{CoCrNiMo}_x$  HEAs with varying Mo content using high-throughput nanoindentation, and in conjunction with SEM, EDS, and XRD results, established the relationship between composition, microstructure, and mechanical properties of FCC phase, Laves phase, and lamellar structures. Zhang et al. [261] investigated the strengthening mechanism of  $\text{CoCrNiTa}_x$  multi-principal-element alloy based on high-throughput nanoindentation techniques. The results indicated that as the Ta content increased, the volume fraction of the Laves phase gradually increased, and the hardness of the Laves phase was higher than that of the FCC phase and lamellar structures.

High-throughput characterization techniques are also applicable to continuous composition gradient samples prepared by additive manufacturing and magnetron sputtering. For example, Nie et al. [262] employed high-throughput local electrochemical techniques to characterize the corrosion behavior of composition gradient materials produced by additive manufacturing, enabling rapid investigation of corrosion characteristics such as pitting, Volta potential, and local corrosion susceptibility. Nguyen et al. [263] prepared a  $\text{Ba}(\text{Ti},\text{Zr},\text{Ta},\text{Hf},\text{Mo})\text{O}_3$  high-entropy thin film library using magnetron sputtering and utilized high-throughput X-ray fluorescence to perform elemental analysis at 576 locations on the thin film library, thereby studying the elemental distribution of the film library.

For large-scale sample arrays with discrete compositions, high-efficiency characterization techniques are necessary for precise and rapid testing of the arrays, such as high-throughput tensile testing platforms and high-throughput X-ray diffraction. For example, Huang et al. [264] designed a high-throughput tensile testing platform that efficiently tests the tensile properties of a batch of samples, obtaining stress-strain curves in a short time. Zhao et al. [228] utilized high-throughput X-ray diffraction to quickly characterize the phase structures of 106 powder metallurgy samples, establishing the relationship between alloy phase structures and compositions. Ohtani et al. [265] developed an X-ray diffractometer equipped with a curved monochromator and a two-dimensional detector, achieving high-throughput characterization of the crystal structure of epitaxial film samples.

Moreover, the integration of large-scale scientific facilities such as neutron diffraction and synchrotron radiation can significantly enhance characterization capabilities, enabling the development of comprehensive databases on alloy composition, structure, and properties, thus guiding alloy design. For instance, Li et al. [266] employed *in situ* synchrotron radiation X-ray diffraction to determine the phase structure of the  $\text{Al}_{0.1}\text{CoCrFeNi}$  HEA under various pressures, investigating the pressure-induced phase transition process. Zhou et al. [267] utilized *in situ* neutron diffraction to explore the deformation mechanisms of the

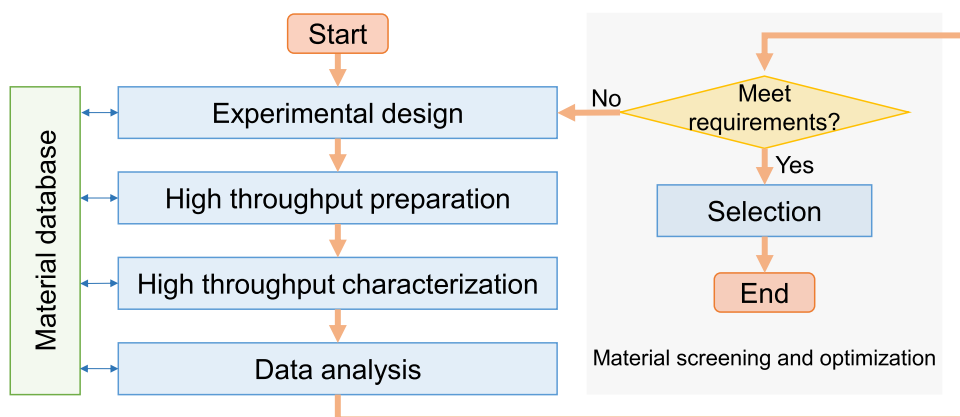


Fig. 33. Flowchart of HEA design based on high-throughput experiments.

**Table 1**  
Advantages, limitations, and application areas of four design methods for HEAs.

Design methods	Advantages	Limitations	Application areas
Materials science	Low usage cost. Computationally convenient.	Simplified model. Difficult to address the complex requirements of alloy design.	Preliminary compositional screening. Early-stage alloy design.
Computational materials science	Computational simulations at different scales. High-accuracy prediction.	High computational cost. The coupling of multiscale computational methods is challenging.	Investigation of material mechanisms.
Machine learning	Powerful nonlinear modeling capability.	Strong data dependence. Insufficient interpretability.	Suitable for multi-objective optimization problems.
High-throughput experiments	Efficient preparation and characterization. Abundant experimental data.	High equipment cost. Processing experimental data is challenging.	Fast screening of alloy compositions or processes. Construction of high-quality materials databases.

(TiZrHfNb)<sub>98</sub>N<sub>2</sub> refractory HEA under tensile loading. Fig. 32 summarizes the high-throughput characterization methods commonly used for the composition, structure, and properties of metallic materials.

### 5.3. Section summary

The key to high-throughput experiments lies in the high-throughput preparation and characterization of materials. As shown in Fig. 33, the flowchart for HEA design based on high-throughput experiments illustrates that by obtaining extensive data on alloy composition, structure, and properties through high-throughput preparation and characterization, a high-quality materials database can be established. This database is then utilized for alloy screening and optimization, enabling the efficient design of HEAs.

The HEA design method based on high-throughput experiments offers significant advantages and potential. It enables the rapid preparation and characterization of a large number of HEAs with different compositions or processes, thereby facilitating the swift screening and optimization of these alloys and accelerating their research and development. Additionally, high-throughput experimental methods can quickly construct databases of HEA compositions, processes, and properties, providing reliable data for methods such as CALPHAD and machine learning, as demonstrated by the studies of Garel [268] and Sun [269]. However, high-throughput experimental methods necessitate highly precise experimental equipment to ensure accuracy, as well as

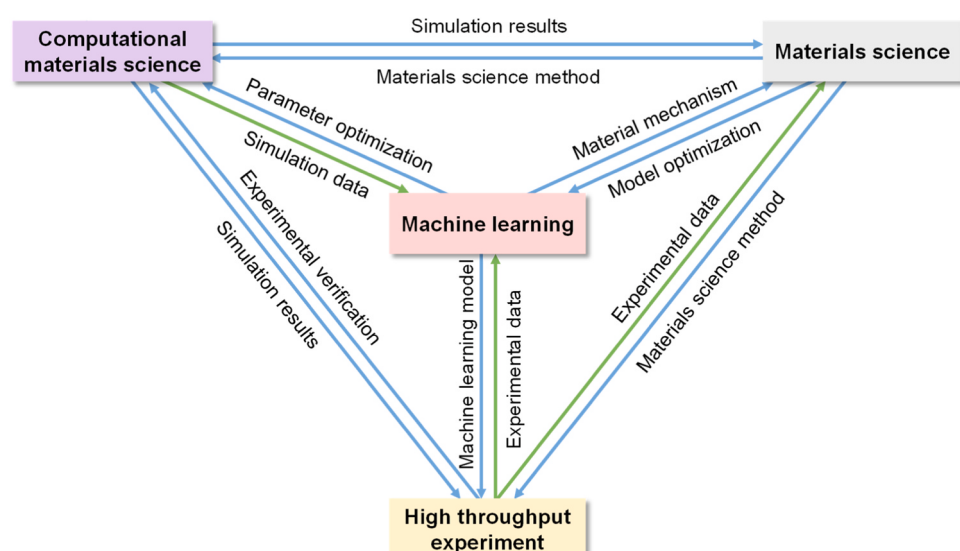
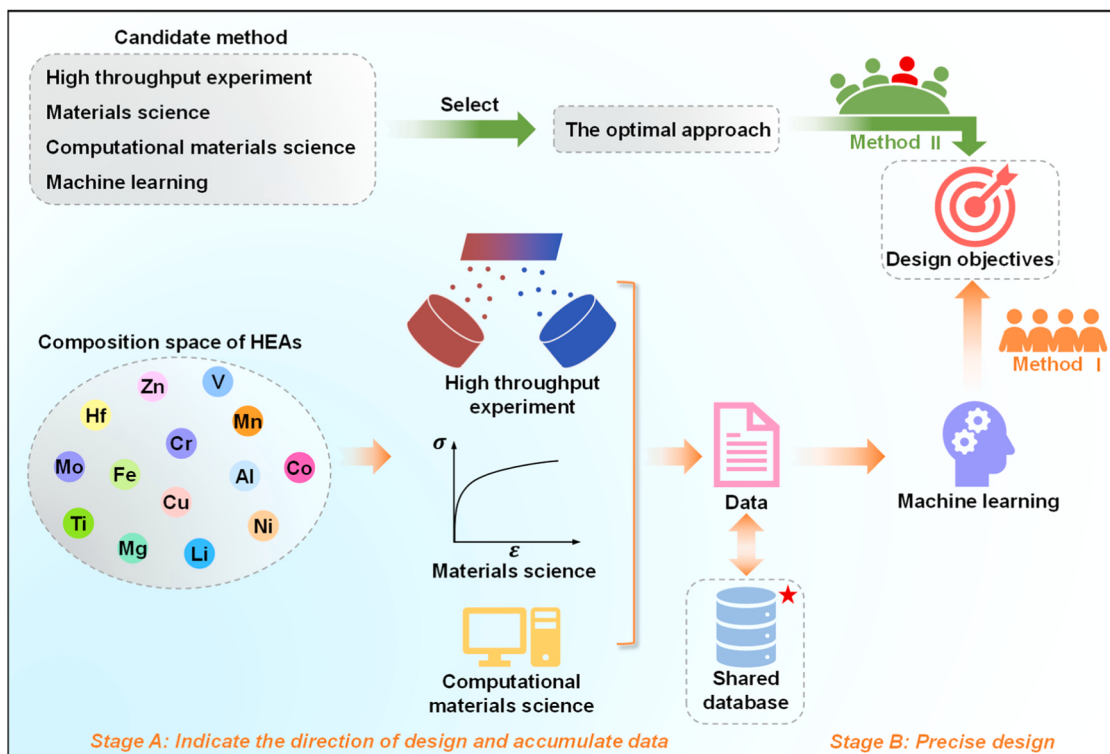


Fig. 34. The relationships among HEA design methods.



**Fig. 35.** Development directions for HEA design methods.

sophisticated data analysis tools capable of managing and interpreting the vast volumes of data generated. Finally, Table 1 summarizes the advantages, limitations, and application areas of the four design methods for HEAs.

## 6. Conclusions and outlook

The introduction of the HEA concept has revolutionized traditional alloying strategies, paving a new way for overcoming the strength-ductility trade-off. The vast compositional space of HEAs imposes higher demands on alloy design methods. This paper systematically discusses the design methodologies for HEAs, including high-throughput experiments, machine learning, computational materials science, and materials science, while also summarizing the advantages and disadvantages of each method. As shown in Fig. 34, the relationships among the four HEA design methods reveal that they are not isolated but interconnected. However, certain limitations still exist within the design methodologies for HEAs. To address these, future efforts can focus on the following five aspects to achieve the efficient design and development of HEAs.

### (1) Construction and development of databases.

Data quality significantly impacts the accuracy of models. Experimental data, literature data, and computational simulation data for HEAs often face issues such as scattered distribution and complex experimental conditions. Despite the establishment of numerous material databases under the Materials Genome Initiative, challenges remain in the field of HEAs, including small data volumes and inconsistent standards across different databases. Therefore, there is an urgent need to integrate the concept of material genome engineering to develop efficient automated data acquisition technologies and further establish high-quality, standardized, and large-scale databases for HEAs.

### (2) Encouragement of interdisciplinary exchange and resource sharing.

The design of HEAs is a complex, multidisciplinary challenge that requires broad collaboration among researchers from different fields to achieve the synergistic development of various design methodologies. To ensure the robust development of HEA design, data sharing and open-source software are encouraged, along with efforts to enhance the extensibility and user-friendliness of programs. Additionally, while published data typically emphasize positive outcomes, negative and unsuccessful experimental results are equally important for the completeness of the sample space and should also be shared.

### (3) Development and construction of experimental equipment

With the increasing application of high-throughput experiments in the design of HEAs, there is an urgent need to develop efficient and precise experimental preparation and characterization equipment, as well as to enhance the use of large-scale scientific facilities such as synchrotron radiation and neutron diffraction. Simultaneously, experimental data acquisition and analysis technologies must be advanced in tandem. Computational simulations require extensive computing resources, particularly for HEAs with vast compositional space. Therefore, the development of supercomputers with formidable computational capabilities is essential.

### (4) Cost-effectiveness and life cycle assessment.

The current design objectives of HEAs are focused on properties such as strength, ductility, and corrosion resistance. However, for alloys intended for industrial applications, greater emphasis should be placed on environmental friendliness, taking into account the environmental impact of HEAs throughout their entire life cycle, including waste recycling, service life, energy consumption, and emissions. Additionally, cost-effectiveness should be considered to provide a competitive advantage for the industrial application of HEAs.

### (5) Development directions for HEA design methods.

This paper proposes two design methodologies for HEAs that hold

potential for future development. As shown in Fig. 35, the first approach involves the integration of high-throughput experiments, computational materials science, materials science, and machine learning. The crux of this approach lies in the effective transmission of data, which interlinks the various design methods. A multi-scale, multi-method model for HEA design is thus established, addressing the limitations of individual methods while maximizing their strengths, thereby enabling more precise and efficient alloy design. The second approach advocates for the strategic selection and application of design methods based on their respective advantages and disadvantages. For instance, when the need arises to rapidly ascertain the quantitative relationships between composition, processing, and performance, the use of machine learning is recommended. Conversely, for the design of HEAs with specific microstructures, methods such as molecular dynamics, first-principles calculations, and phase-field modeling are suggested to facilitate a deeper understanding and design from a microstructural perspective.

HEAs possess vast application potential, yet there remains a long path ahead in the development of efficient design methods for these materials. The alloy design methodologies discussed in this paper are not only applicable to HEAs but also offer valuable insights for the design of other materials.

#### CRediT authorship contribution statement

**Lingxin Li:** Writing – original draft, Visualization, Methodology, Investigation, Formal analysis, Conceptualization. **Zhengdi Liu:** Validation, Investigation. **Xulong An:** Validation, Formal analysis. **Wenwen Sun:** Validation, Supervision, Methodology, Investigation, Funding acquisition, Formal analysis, Conceptualization.

#### Declaration of Competing Interest

The authors declare that they have no known competing financial interests or personal relationships that could have appeared to influence the work reported in this paper.

#### Acknowledgments

The authors sincerely appreciate the financial support of Natural Science Foundation for Young Scholars of Jiangsu Province (Grant No. BK20220628), the National Natural Science Foundation for Young Scholars of China (No. 52301130), the National Natural Science Foundation of China (Grant No. 52371103).

#### References

- [1] L.A. Dobrzański, Significance of materials science for the future development of societies, *J. Mater. Process. Technol.* 175 (2006) 133–148.
- [2] R.O. Ritchie, The conflicts between strength and toughness, *Nat. Mater.* 10 (2011) 817–822.
- [3] J.-W. Yeh, S.-K. Chen, S.-J. Lin, J.-Y. Gan, T.-S. Chin, T.-T. Shun, et al., Nanostructured high-entropy alloys with multiple principal elements: novel alloy design concepts and outcomes, *Adv. Eng. Mater.* 6 (2004) 299–303.
- [4] B. Cantor, I.T.H. Chang, P. Knight, A.J.B. Vincent, Microstructural development in equiatomic multicomponent alloys, *Mater. Sci. Eng.: A* 375–377 (2004) 213–218.
- [5] X. Gao, W. Jiang, Y. Lu, Z. Ding, J. Liu, W. Liu, et al., Excellent strength-ductility combination of Cr26Mn20Fe20Co20Ni14 high-entropy alloy at cryogenic temperatures, *J. Mater. Sci. Technol.* 154 (2023) 166–177.
- [6] J. Yi, L. Wang, L. Zeng, M. Xu, L. Yang, S. Tang, Excellent strength-ductility synergy in a novel single-phase equiatomic CoFeNiTiV high entropy alloy, *Int. J. Refract. Met. Hard Mater.* 95 (2021) 105416.
- [7] F. Jiang, J. Wang, Q. Jiang, G. Yang, M. Xu, W. Xu, et al., An excellent synergy in yield strength and plasticity of NbTiZrTa0.25Cr0.4 refractory high entropy alloy through the regulation of cooling rates, *Int. J. Refract. Met. Hard Mater.* 117 (2023) 106409.
- [8] P.X. Yan, J. Chang, W.L. Wang, X.N. Zhu, M.J. Lin, B. Wei, Eutectic growth kinetics and microscopic mechanical properties of rapidly solidified CoCrFeNiMo0.8 high entropy alloy, *Acta Mater.* 237 (2022) 118149.
- [9] Y. Li, X. Jin, A. Lan, J. Qiao, Superior strength-ductility synergy of FeMnCrNiAlSi high entropy alloy with heterogeneous structures, *J. Alloy. Compd.* 1025 (2025) 180279.
- [10] M. Mugale, S. Karki, A. Choudhari, S. Digole, M. Garg, V.A.S. Kandadai, et al., High strength-ductility combination in low-density dual phase high entropy alloys, *J. Alloy. Compd.* 1010 (2025) 177762.
- [11] N. Ali, M. Wang, T. He, A. Amar, Y. Lu, I. Shahid, et al., Exceptional strength-ductility synergy in hyper-eutectic Al19Fe20Co20Ni37.5Mo3Ta0.5 high entropy alloy with heterogeneous structure, *J. Alloy. Compd.* 1022 (2025) 179751.
- [12] S. Wang, Z. Chen, R. Chen, Z. Wu, Y. Jia, W. Zhang, et al., Superior strength-ductility synergy in additively manufactured CoCrFeNi high-entropy alloys with multi-scale hierarchical microstructure, *J. Alloy. Compd.* 1006 (2024) 176268.
- [13] Q. Wei, A. Zhang, J. Han, B. Xin, B. Su, X. Wang, et al., Development of a Ti30Hf20Nb20Ta10V10Mo7W3 refractory high entropy alloy with excellent mechanical properties and wear resistance, *J. Alloy. Compd.* 966 (2023) 171571.
- [14] H. Li, X. Li, C. Jin, Q. Li, Q. Ma, K. Hua, et al., Mechanical and tribological performance of AlCr0.5NbTaxTi4-x (x = 0, 0.5, 1) refractory high-entropy alloys, *J. Mater. Sci. Technol.* 156 (2023) 241–253.
- [15] Q. Gao, S. Guo, Z. Hu, Q. Guan, J. Guan, S. Guo, et al., Al content regulation of microstructure, wear resistance, and corrosion behavior in Mo0.5NbTiZrAlx high-entropy alloys, *J. Alloy. Compd.* 1017 (2025) 179037.
- [16] Y. Yuan, J.J. Wang, J. Wei, W.Y. Chen, H.L. Yan, N. Jia, Cu alloying enables superior strength-ductility combination and high corrosion resistance of FeMnCoCr high entropy alloy, *J. Alloy. Compd.* 970 (2024) 172543.
- [17] H. Cheng, H. Luo, X. Wang, X. Li, Microstructure and corrosion resistance properties of (FeCoNi)86Al7Ti7 high-entropy alloy via different aging time, *Corros. Sci.* 226 (2024) 111670.
- [18] H. Yao, X. Yang, W. Zhao, S. Zhang, Y. Yang, Y. Zhao, et al., Regulating corrosion resistance of precipitation strengthened FeCoNiCrMn high-entropy alloy using boron doping, *J. Alloy. Compd.* 1022 (2025) 179899.
- [19] L. Li, Y. Chen, A. Huang, X. Liu, H. Zhang, H. Zhang, et al., A novel NiCoCrAlPt high-entropy alloy with superb oxidation resistance at 1200 °C, *Corros. Sci.* 228 (2024) 111819.
- [20] D. Wu, B. Li, Y. Shi, X. Hou, C. Li, Y. Gao, et al., Effects of different Al contents on mechanical properties and high temperature oxidation resistance of AlxCuCr0.6NiV0.6 high entropy alloy, *J. Alloy. Compd.* 1025 (2025) 180348.
- [21] B. Su, Y. Zhu, F. Cheng, Y. Zhang, Z. Li, Achieving exceptional high-temperature strength and oxidation resistance in an additively manufactured refractory high-entropy alloy via strategic elemental substitutions, *J. Alloy. Compd.* 1010 (2025) 177079.
- [22] Y. Zhang, M. Liu, J. Sun, G. Li, R. Zheng, W. Xiao, et al., Excellent thermal stability and mechanical properties of bulk nanostructured FeCoNiCu high entropy alloy, *Mater. Sci. Eng.: A* 835 (2022) 142670.
- [23] Q. Liu, X. Li, G. Wang, Y. Liu, H. Liang, L. Cui, et al., Exceptional thermal stability and hot deformation behavior of a powder metallurgy ultra-fine-grained MoNbTaTiV refractory high-entropy alloy, *J. Alloy. Compd.* 1004 (2024) 175977.
- [24] G. Liu, Y. Jiang, C. Ma, Z. Yuan, B. Sun, T. Shen, Ultrastrong nanocrystalline FeCoNiCr high entropy alloy with outstanding thermal stability, *Mater. Sci. Eng.: A* 933 (2025) 148282.
- [25] L. Chen, The materials genome initiative and advanced materials, *Engineering* 1 (2015) 169.
- [26] A. Jain, S.P. Ong, G. Hautier, W. Chen, W.D. Richards, S. Dacek, et al., Commentary: the materials project: a materials genome approach to accelerating materials innovation, *APL Mater.* 1 (2013).
- [27] S.A. Krishna, N. Noble, N. Radhika, B. Saleh, A comprehensive review on advances in high entropy alloys: Fabrication and surface modification methods, properties, applications, and future prospects, *J. Manuf. Process.* 109 (2024) 583–606.
- [28] S. Ragunath, N. Radhika, B. Saleh, Advancements and future prospects of additive manufacturing in high-entropy alloy applications, *J. Alloy. Compd.* 997 (2024) 174859.
- [29] Y.-F. Yang, F. Hu, T. Xia, R.-H. Li, J.-Y. Bai, J.-Q. Zhu, et al., High entropy alloys: A review of preparation techniques, properties and industry applications, *J. Alloy. Compd.* 1010 (2025) 177691.
- [30] A. Ghasemi, A.R. Eivani, S.M. Abbasi, H.R. Jafarian, M. Ghosh, S.H.M. Anjidan, Al-Co-Cr-Fe-Ni-Ti high entropy alloys: A review of microstructural and mechanical properties at elevated temperatures, *J. Alloy. Compd.* 1010 (2025) 178216.
- [31] K.K. Alaneme, J.U. Anaele, S.A. Kareem, Hot deformability, microstructural evolution and processing map assessment of high entropy alloys: A systematic review, *J. Mater. Res. Technol.* 26 (2023) 1754–1784.
- [32] J. Liu, Z. Lv, Z. Wu, J. Zhang, C. Zheng, C. Chen, et al., Research progress on the influence of alloying elements on the corrosion resistance of high-entropy alloys, *J. Alloy. Compd.* 1002 (2024) 175394.
- [33] T. Qureshi, M.M. Khan, H.S. Pali, The future of hydrogen economy: Role of high entropy alloys in hydrogen storage, *J. Alloy. Compd.* 1004 (2024) 175668.
- [34] A. Kalhor, M.J. Sohrabi, H. Mirzadeh, M.Z. Aghdam, M.S. Mehranpour, K. Rodak, et al., Improving the mechanical properties of high-entropy alloys via germanium addition: a focused review, *J. Alloy. Compd.* 1010 (2025) 177527.
- [35] L. Zhang, Y.-k Dou, B. Bai, B.-t Yu, X.-f He, W. Yang, Research progress on creep resistance of high entropy alloys, *J. Alloy. Compd.* 1011 (2025) 178280.
- [36] E.P. George, W.A. Curtin, C.C. Tasan, High entropy alloys: a focused review of mechanical properties and deformation mechanisms, *Acta Mater.* 188 (2020) 435–474.
- [37] Y. Zhang, Y.J. Zhou, J.P. Lin, G.L. Chen, P.K. Liaw, Solid-solution phase formation rules for multi-component alloys, *Adv. Eng. Mater.* 10 (2008) 534–538.
- [38] S. Guo, C. Ng, J. Lu, C.T. Liu, Effect of valence electron concentration on stability of fcc or bcc phase in high entropy alloys, *J. Appl. Phys.* 109 (2011).

- [39] L. Jiang, Y.P. Lu, H. Jiang, T.M. Wang, B.N. Wei, Z.Q. Cao, et al., Formation rules of single phase solid solution in high entropy alloys, *Mater. Sci. Technol.* 32 (2016) 588–592.
- [40] B. Chanda, J. Das, An assessment on the stability of the eutectic phases in high entropy alloys, *J. Alloy. Compd.* 798 (2019) 167–173.
- [41] Y. Lu, X. Gao, L. Jiang, Z. Chen, T. Wang, J. Jie, et al., Directly cast bulk eutectic and near-eutectic high entropy alloys with balanced strength and ductility in a wide temperature range, *Acta Mater.* 124 (2017) 143–150.
- [42] Y. Lu, Y. Dong, S. Guo, L. Jiang, H. Kang, T. Wang, et al., A promising new class of high-temperature alloys: eutectic high-entropy alloys, *Sci. Rep.* 4 (2014) 6200.
- [43] L. Jiang, Y. Lu, Y. Dong, T. Wang, Z. Cao, T. Li, Effects of Nb addition on structural evolution and properties of the CoFeNi2V0.5 high-entropy alloy, *Appl. Phys. A* 119 (2015) 291–297.
- [44] H. Jiang, H. Zhang, T. Huang, Y. Lu, T. Wang, T. Li, Microstructures and mechanical properties of Co<sub>2</sub>MoxNi<sub>2</sub>VWx eutectic high entropy alloys, *Mater. Des.* 109 (2016) 539–546.
- [45] X. Chen, J.Q. Qi, Y.W. Sui, Y.Z. He, F.X. Wei, Q.K. Meng, et al., Effects of aluminum on microstructure and compressive properties of Al-Cr-Fe-Ni eutectic multi-component alloys, *Mater. Sci. Eng.: A* 681 (2017) 25–31.
- [46] S.G. Ma, Y. Zhang, Effect of Nb addition on the microstructure and properties of AlCoCrFeNi high-entropy alloy, *Mater. Sci. Eng.: A* 532 (2012) 480–486.
- [47] Y. Tan, J. Li, J. Wang, H. Kou, Seaweed eutectic-dendritic solidification pattern in a CoCrFeNiMnPd eutectic high-entropy alloy, *Intermetallics* 85 (2017) 74–79.
- [48] S. Vrnik, S. Guo, S. Sheikh, A. Jelen, P. Koželj, J. Luzar, et al., Magnetism of CoCrFeNi<sub>2</sub>x eutectic high-entropy alloys, *Intermetallics* 93 (2018) 122–133.
- [49] Y. Lu, H. Jiang, S. Guo, T. Wang, Z. Cao, T. Li, A new strategy to design eutectic high-entropy alloys using mixing enthalpy, *Intermetallics* 91 (2017) 124–128.
- [50] X. Jin, Y. Zhou, L. Zhang, X. Du, B. Li, A novel Fe<sub>20</sub>Co<sub>20</sub>Ni<sub>41</sub>Al<sub>19</sub> eutectic high entropy alloy with excellent tensile properties, *Mater. Lett.* 216 (2018) 144–146.
- [51] L. Jiang, Z.Q. Cao, J.C. Jie, J.J. Zhang, Y.P. Lu, T.M. Wang, et al., Effect of Mo and Ni elements on microstructure evolution and mechanical properties of the CoFeNixVMoy high entropy alloys, *J. Alloy. Compd.* 649 (2015) 585–590.
- [52] A.K. Mishra, S. Samal, K. Biswas, Solidification Behaviour of Ti-Cu-Fe-Co-Ni High Entropy Alloys, *Trans. Indian Inst. Met.* 65 (2012) 725–730.
- [53] S. Guo, N. Chun, C.T. Liu, Sunflower-like solidification microstructure in a near-eutectic high-entropy alloy, *Mater. Res. Lett.* 1 (2013) 228–232.
- [54] O.N. Senkov, G.B. Wilks, J.M. Scott, D.B. Miracle, Mechanical properties of Nb<sub>25</sub>Mo<sub>25</sub>Ta<sub>25</sub>W<sub>25</sub> and V<sub>20</sub>Nb<sub>20</sub>Mo<sub>20</sub>Ta<sub>20</sub>W<sub>20</sub> refractory high entropy alloys, *Intermetallics* 19 (2011) 698–706.
- [55] W.H. Liu, J.Y. He, H.L. Huang, H. Wang, Z.P. Lu, C.T. Liu, Effects of Nb additions on the microstructure and mechanical property of CoCrFeNi high-entropy alloys, *Intermetallics* 60 (2015) 1–8.
- [56] O.N. Senkov, C. Woodward, D.B. Miracle, Microstructure and properties of aluminum-containing refractory high-entropy alloys, *JOM* 66 (2014) 2030–2042.
- [57] M.-H. Tsai, K.-Y. Tsai, C.-W. Tsai, C. Lee, C.-C. Juan, J.-W. Yeh, Criterion for sigma phase formation in Cr- and V-containing high-entropy alloys, *Mater. Res. Lett.* 1 (2013) 207–212.
- [58] F. Otto, Y. Yang, H. Bei, E.P. George, Relative effects of enthalpy and entropy on the phase stability of equiatomic high-entropy alloys, *Acta Mater.* 61 (2013) 2628–2638.
- [59] C.-M. Lin, H.-L. Tsai, H.-Y. Bor, Effect of aging treatment on microstructure and properties of high-entropy Cu<sub>0.5</sub>CoCrFeNi alloy, *Intermetallics* 18 (2010) 1244–1250.
- [60] Y.-J. Hsu, W.-C. Chiang, J.-K. Wu, Corrosion behavior of FeCoNiCrCuX high-entropy alloys in 3.5% sodium chloride solution, *Mater. Chem. Phys.* 92 (2005) 112–117.
- [61] O.N. Senkov, J.M. Scott, S.V. Senkova, D.B. Miracle, C.F. Woodward, Microstructure and room temperature properties of a high-entropy TaNbHfZrTi alloy, *J. Alloy. Compd.* 509 (2011) 6043–6048.
- [62] N.D. Stepanov, N.Y. Yurchenko, D.V. Skibin, M.A. Tikhonovsky, G.A. Salishchev, Structure and mechanical properties of the AlCr<sub>x</sub>NbTiV ( $x = 0, 0.5, 1, 1.5$ ) high entropy alloys, *J. Alloy. Compd.* 652 (2015) 266–280.
- [63] X. Yang, Y. Zhang, Prediction of high-entropy stabilized solid-solution in multi-component alloys, *Mater. Chem. Phys.* 132 (2012) 233–238.
- [64] Y.F. Ye, Q. Wang, J. Lu, C.T. Liu, Y. Yang, Design of high entropy alloys: A single-parameter thermodynamic rule, *Scri. Mater.* 104 (2015) 53–55.
- [65] Z. Wang, Y. Huang, Y. Yang, J. Wang, C.T. Liu, Atomic-size effect and solid solubility of multicomponent alloys, *Scri. Mater.* 94 (2015) 28–31.
- [66] Y. Dong, Y. Lu, L. Jiang, T. Wang, T. Li, Effects of electro-negativity on the stability of topologically close-packed phase in high entropy alloys, *Intermetallics* 52 (2014) 105–109.
- [67] N. Yurchenko, N. Stepanov, G. Salishchev, Laves-phase formation criterion for high-entropy alloys, *Mater. Sci. Technol.* 33 (2017) 17–22.
- [68] A.K. Singh, N. Kumar, A. Dwivedi, A. Subramaniam, A geometrical parameter for the formation of disordered solid solutions in multi-component alloys, *Intermetallics* 53 (2014) 112–119.
- [69] Y. Lu, Y. Dong, L. Jiang, T. Wang, T. Li, Y. Zhang, A criterion for topological close-packed phase formation in high entropy alloys, *Entropy* 17 (2015) 2355–2366.
- [70] M.G. Poletti, L. Battezzati, Electronic and thermodynamic criteria for the occurrence of high entropy alloys in metallic systems, *Acta Mater.* 75 (2014) 297–306.
- [71] S. Guo, C.T. Liu, Phase stability in high entropy alloys: Formation of solid-solution phase or amorphous phase, *Prog. Nat. Sci.: Mater. Int.* 21 (2011) 433–446.
- [72] O.N. Senkov, D.B. Miracle, A new thermodynamic parameter to predict formation of solid solution or intermetallic phases in high entropy alloys, *J. Alloy. Compd.* 658 (2016) 603–607.
- [73] M.-H. Tsai, K.-C. Chang, J.-H. Li, R.-C. Tsai, A.-H. Cheng, A second criterion for sigma phase formation in high-entropy alloys, *Mater. Res. Lett.* 4 (2016) 90–95.
- [74] O.N. Senkov, G.B. Wilks, D.B. Miracle, C.P. Chuang, P.K. Liaw, Refractory high-entropy alloys, *Intermetallics* 18 (2010) 1758–1765.
- [75] V.N. Khiratkar, K. Mishra, P. Srinivasulu, A. Singh, Effect of inter-lamellar spacing and test temperature on the Charpy impact energy of extremely fine pearlite, *Mater. Sci. Eng.: A* 754 (2019) 622–627.
- [76] S.-H. Yu, S.-M. Lee, S. Lee, J.-H. Nam, J.-S. Lee, C.-M. Bae, et al., Effects of lamellar structure on tensile properties and resistance to hydrogen embrittlement of pearlitic steel, *Acta Mater.* 172 (2019) 92–101.
- [77] Y. Koyanagi, S. Ueta, T. Kawasaki, S. Harjo, K. Cho, H.Y. Yasuda, Investigation of strengthening mechanism in Ni-38Cr-3.8Al alloy with fine lamellar structure by in situ neutron diffraction analysis, *Mater. Sci. Eng.: A* 773 (2020) 138822.
- [78] L. Fan, T. Yang, Y. Zhao, J. Luan, G. Zhou, H. Wang, et al., Ultrahigh strength and ductility in newly developed materials with coherent nanolamellar architectures, *Nat. Commun.* 11 (2020) 6240.
- [79] P. Shi, R. Li, Y. Li, Y. Wen, Y. Zhong, W. Ren, et al., Hierarchical crack buffering triples ductility in eutectic herringbone high-entropy alloys, *Science* 373 (2021) 912–918.
- [80] X.L. An, Z.D. Liu, L.T. Zhang, Y. Zou, X.J. Xu, C.L. Chu, et al., A new strong pearlitic multi-principal element alloy to withstand wear at elevated temperatures, *Acta Mater.* 227 (2022) 117700.
- [81] Q. Lu, K. Li, H. Chen, M. Yang, X. Lan, T. Yang, et al., Simultaneously enhanced strength and ductility of 6xxx Al alloys via manipulating meso-scale and nano-scale structures guided with phase equilibrium, *J. Mater. Sci. Technol.* 41 (2020) 139–148.
- [82] W. Sun, Y. Zhu, R. Marceau, L. Wang, Q. Zhang, X. Gao, et al., Precipitation strengthening of aluminum alloys by room-temperature cyclic plasticity, *Science* 363 (2019) 972–975.
- [83] Z.M. Li, X.N. Li, Y.L. Hu, Y.H. Zheng, M. Yang, N.J. Li, et al., Cuboidal  $\gamma'$  phase coherent precipitation-strengthened Cu-Ni-Al alloys with high softening temperature, *Acta Mater.* 203 (2021) 116458.
- [84] Z. Hao, G. Xie, X. Liu, Q. Tan, R. Wang, The precipitation behaviours and strengthening mechanism of a Cu-0.4 wt% Sc alloy, *J. Mater. Sci. Technol.* 98 (2022) 1–13.
- [85] J.Y. He, H. Wang, H.L. Huang, X.D. Xu, M.W. Chen, Y. Wu, et al., A precipitation-hardened high-entropy alloy with outstanding tensile properties, *Acta Mater.* 102 (2016) 187–196.
- [86] T. Yang, Y.L. Zhao, Y. Tong, Z.B. Jiao, J. Wei, J.X. Cai, et al., Multicomponent intermetallic nanoparticles and superb mechanical behaviors of complex alloys, *Science* 362 (2018) 933–937.
- [87] Z. Lei, X. Liu, Y. Wu, H. Wang, S. Jiang, S. Wang, et al., Enhanced strength and ductility in a high-entropy alloy via ordered oxygen complexes, *Nature* 563 (2018) 546–550.
- [88] T.H. Fang, W.L. Li, N.R. Tao, K. Lu, Revealing Extraordinary Intrinsic Tensile Plasticity in Gradient Nano-Grained Copper, *Science* 331 (2011) 1587–1590.
- [89] Y. Lin, J. Pan, H.F. Zhou, H.J. Gao, Y. Li, Mechanical properties and optimal grain size distribution profile of gradient grained nickel, *Acta Mater.* 153 (2018) 279–289.
- [90] Q. Pan, L. Zhang, R. Feng, Q. Lu, K. An, A.C. Chuang, et al., Gradient cell-structured high-entropy alloy with exceptional strength and ductility, *Science* 374 (2021) 984–989.
- [91] S. Qin, M. Yang, P. Jiang, J. Wang, X. Wu, H. Zhou, et al., Designing structures with combined gradients of grain size and precipitation in high entropy alloys for simultaneous improvement of strength and ductility, *Acta Mater.* 230 (2022) 117847.
- [92] I.A. Ovid'ko, 14-Enhanced ductility and its mechanisms in nanocrystalline metallic materials, in: S.H. Whang (Ed.), *Nanostructured Metals and Alloys*, Woodhead Publishing, 2011, pp. 430–458.
- [93] Z. Fu, W. Chen, H. Wen, D. Zhang, Z. Chen, B. Zheng, et al., Microstructure and strengthening mechanisms in an FCC structured single-phase nanocrystalline Co<sub>25</sub>Ni<sub>12</sub>Fe<sub>25</sub>Al<sub>7.5</sub>Cu<sub>17.5</sub> high-entropy alloy, *Acta Mater.* 107 (2016) 59–71.
- [94] Y. Wang, M. Chen, F. Zhou, E. Ma, High tensile ductility in a nanostructured metal, *Nature* 419 (2002) 912–915.
- [95] Z. Wang, J. Li, Y. Yang, L. Pang, M. Liu, H. Li, et al., A novel high-entropy alloy with exceptional strength and elongation via bimodal grains and lamellar nanoprecipitates, *Mater. Sci. Eng.: A* 870 (2023) 144851.
- [96] C. Herrera, D. Ponge, D. Raabe, Design of a novel Mn-based 1GPa duplex stainless TRIP steel with 60% ductility by a reduction of austenite stability, *Acta Mater.* 59 (2011) 4653–4664.
- [97] D.R. Steinmetz, T. Jäpel, B. Wietbrock, P. Eisenlohr, I. Gutierrez-Urrutia, A. Saeed-Akbari, et al., Revealing the strain-hardening behavior of twinning-induced plasticity steels: theory, simulations, experiments, *Acta Mater.* 61 (2013) 494–510.
- [98] T. Watanabe, S. Tsurekawa, The control of brittleness and development of desirable mechanical properties in polycrystalline systems by grain boundary engineering, *Acta Mater.* 47 (1999) 4171–4185.
- [99] Y. Deng, C.C. Tasan, K.G. Pradeep, H. Springer, A. Kostka, D. Raabe, Design of a twinning-induced plasticity high entropy alloy, *Acta Mater.* 94 (2015) 124–133.
- [100] Z. Li, K.G. Pradeep, Y. Deng, D. Raabe, C.C. Tasan, Metastable high-entropy dual-phase alloys overcome the strength-ductility trade-off, *Nature* 534 (2016) 227–230.

- [101] J.B. Seol, J.W. Bae, Z. Li, J. Chan Han, J.G. Kim, D. Raabe, et al., Boron doped ultrastrong and ductile high-entropy alloys, *Acta Mater.* 151 (2018) 366–376.
- [102] Y. Zhu, X. Wu, Heterostructured materials, *Prog. Mater. Sci.* 131 (2023) 101019.
- [103] Y. Zhu, A. Kei, M. AP, J. Bl, G. Huajian, K.H. Seop, et al., Heterostructured materials: superior properties from hetero-zone interaction, *Mater. Res. Lett.* 9 (2021) 1–31.
- [104] Y. Zhu, Introduction to Heterostructured Materials: A Fast Emerging Field, *Metall. Mater. Trans. A* 52 (2021) 4715–4726.
- [105] D. Xu, X. Wang, Y. Lu, Heterogeneous-Structured Refractory High-Entropy Alloys: A Review of State-of-the-Art Developments and Trends, *Adv. Funct. Mater.* 34 (2024) 2408941.
- [106] Y. Zhang, H. Wang, J. Yang, Y. Zhu, J. Li, Z. Li, et al., Enhancing the strain-hardening rate and uniform tensile ductility of lightweight refractory high-entropy alloys by tailoring multi-scale heterostructure strategy, *Int. J. Plast.* 185 (2025) 104237.
- [107] W. Li, J. Zhang, D. Cui, X. Wang, P. Zhang, H. Wang, et al., Enhanced strength-ductility synergy by high density heterogeneous precipitation microstructure in high-entropy alloys, *Mater. Sci. Eng.: A* 928 (2025) 147983.
- [108] X. Pei, Y. Du, H. Wang, T. Li, M. Hu, H. Wang, et al., Effects of Al/Si on the oxidation behavior of a TiZrV0.5Nb0.5 refractory high entropy alloy at 1000 °C, *Corros. Sci.* 224 (2023) 111527.
- [109] X. Pei, Y. Du, H. Wang, M. Hu, Y. Li, W. Zhou, et al., Attaining exceptional wear resistance in an in-situ ceramic phase reinforced NbMoTa refractory high entropy alloy composite by Spark plasma sintering, *Wear* 558–559 (2024) 205572.
- [110] Y. Du, T. Li, Q. Zhou, X. Pei, H. Wang, T. Feng, et al., Achieving excellent mechanical and robust lubrication behavior in the CoCrNi medium-entropy alloy via in-situ graphite, *Carbon* 229 (2024) 119503.
- [111] T. Li, M. Hu, X. Pei, Y. Du, W. Zhou, H. Wang, Effect of SiC ceramic nano-particles on microstructure and tribological performance of the AlTiVNbNi refractory high entropy alloy in a wide temperature range, *Tribology Int.* 198 (2024) 109850.
- [112] W.H. Liu, Y. Wu, J.Y. He, T.G. Nieh, Z.P. Lu, Grain growth and the Hall-Petch relationship in a high-entropy FeCrNiCoMn alloy, *Scri. Mater.* 68 (2013) 526–529.
- [113] B. Gwaliani, V. Soni, M. Lee, S.A. Mantri, Y. Ren, R. Banerjee, Optimizing the coupled effects of Hall-Petch and precipitation strengthening in a Al0.3CoCrFeNi high entropy alloy, *Mater. Des.* 121 (2017) 254–260.
- [114] M. Guo, L. Xu, L. Qi, Y. Zhao, Z. Li, S. Wei, Effect of sintering temperature on microstructure and mechanical properties of MoNbVTa0.5Cr high-entropy alloys fabricated by powder metallurgy method, *J. Alloy. Compd.* 1002 (2024) 175310.
- [115] R. Song, L. Wei, C. Yang, S. Wu, Phase formation and strengthening mechanisms in a dual-phase nanocrystalline CrMnFeVti high-entropy alloy with ultrahigh hardness, *J. Alloy. Compd.* 744 (2018) 552–560.
- [116] S.H. Shim, H. Pouraliakbar, B.J. Lee, Y.K. Kim, M.S. Rizi, S.I. Hong, Strengthening and deformation behavior of as-cast CoCrCu1.5MnNi high entropy alloy with micro-/nanoscale precipitation, *Mater. Sci. Eng.: A* 853 (2022) 143729.
- [117] J.M. Guo, B.C. Zhou, S. Qiu, H.J. Kong, M.C. Niu, J.H. Luan, et al., Achieving ultrahigh strength and ductility in high-entropy alloys via dual precipitation, *J. Mater. Sci. Technol.* 166 (2023) 67–77.
- [118] W.-C. Lin, Y.-J. Chang, T.-H. Hsu, S. Gorsse, F. Sun, T. Furuhara, et al., Microstructure and tensile property of a precipitation strengthened high entropy alloy processed by selective laser melting and post heat treatment, *Addit. Manuf.* 36 (2020) 101601.
- [119] X. Fan, R. Qu, Z. Zhang, Relation Between Strength and Hardness of High-Entropy Alloys, *Acta Metall. Sin. (Engl. Lett.)* 34 (2021) 1461–1482.
- [120] Y. Shi, W. Wang, Q. Zhou, Q. Xia, D. Hua, Z. Huang, et al., A molecular dynamics study on the defect formation and mechanical behavior of molybdenum disulfide under irradiation, *ACS Appl. Mater. Interfaces* 16 (2024) 29453–29465.
- [121] Q. Jia, W. He, D. Hua, Q. Zhou, Y. Du, Y. Ren, et al., Effects of structure relaxation and surface oxidation on nanoscopic wear behaviors of metallic glass, *Acta Mater.* 232 (2022) 117934.
- [122] D. Hua, Q. Xia, J. Li, Q. Zhou, M. Xie, S. Liu, et al., Atomistic insights into the role of graphene sheets in CoCrNi/graphene composites, *Acta Mater.* 287 (2025) 120809.
- [123] J. Pokluda, M. Černý, M. Šob, Y. Umeno, Ab initio calculations of mechanical properties: methods and applications, *Prog. Mater. Sci.* 73 (2015) 127–158.
- [124] Y. Qiu, Y.J. Hu, A. Taylor, M.J. Styles, R.K.W. Marceau, A.V. Ceguera, et al., A lightweight single-phase AlTiVCr compositionally complex alloy, *Acta Mater.* 123 (2017) 115–124.
- [125] D. Ma, B. Grabowski, F. Körmann, J. Neugebauer, D. Raabe, Ab initio thermodynamics of the CoCrFeMnNi high entropy alloy: Importance of entropy contributions beyond the configurational one, *Acta Mater.* 100 (2015) 90–97.
- [126] S.-M. Chen, Z.-J. Ma, S. Qiu, L.-J. Zhang, S.-Z. Zhang, R. Yang, et al., Phase decomposition and strengthening in HfNbTaTiZr high entropy alloy from first-principles calculations, *Acta Mater.* 225 (2022) 117582.
- [127] I. Avula, A. Chavan, S. Mukherjee, M. Roy, Phase stability and mechanical properties of Ta enriched TiTaNbZrMo refractory high entropy alloys, *J. Alloy. Compd.* 989 (2024) 174408.
- [128] Y. Hong, M. Beyramali Kivy, M. Asle Zaeem, Competition between formation of Al<sub>2</sub>O<sub>3</sub> and Cr<sub>2</sub>O<sub>3</sub> in oxidation of Al0.3CoCrCuFeNi high entropy alloy: A first-principles study, *Scr. Mater.* 168 (2019) 139–143.
- [129] I. Roy, C. Ekuma, G. Balasubramanian, Examining the thermodynamic stability of mixed principal element oxides in AlCoCrFeNi high-entropy alloy by first-principles, *Comput. Mater. Sci.* 213 (2022) 111619.
- [130] Y. Wu, D.L. Irving, Finite temperature elastic properties of equiatomic CoCrFeNi from first principles, *Scr. Mater.* 162 (2019) 176–180.
- [131] Y.L. Hu, L.H. Bai, Y.G. Tong, D.Y. Deng, X.B. Liang, J. Zhang, et al., First-principle calculation investigation of NbMoTaW based refractory high entropy alloys, *J. Alloy. Compd.* 827 (2020) 153963.
- [132] R. Chang, W. Fang, J. Yan, H. Yu, X. Bai, J. Li, et al., Microstructure and mechanical properties of CoCrNi-Mo medium entropy alloys: Experiments and first-principle calculations, *J. Mater. Sci. Technol.* 62 (2021) 25–33.
- [133] F. Kies, Y. Ikeda, S. Ewald, J.H. Schleifenbaum, B. Hallstedt, F. Körmann, et al., Combined Al and C alloying enables mechanism-oriented design of multi-principal element alloys: Ab initio calculations and experiments, *Scr. Mater.* 178 (2020) 366–371.
- [134] H.L. Zhang, D.D. Cai, X. Sun, H. Huang, S. Lu, Y.Z. Wang, et al., Solid solution strengthening of high-entropy alloys from first-principles study, *J. Mater. Sci. Technol.* 121 (2022) 105–116.
- [135] J. Kumar, A. Linda, M. Sadhasivam, K.G. Pradeep, N.P. Gurao, K. Biswas, The effect of Al addition on solid solution strengthening in CoCrFeMnNi: experiment and modelling, *Acta Mater.* 238 (2022) 118208.
- [136] S. Zhang, G. Wang, Predicting mechanical properties of high entropy alloys with face centered cubic structure from first principles calculations, *Mater. Today Commun.* 32 (2022) 104059.
- [137] J.X. Yan, J.Y. Qin, J.H. Liu, H. Chen, Y.H. Huang, M. Liu, et al., Composition design study of strong and ductile Mo-alloyed CoCrNi medium-entropy alloys, *J. Mater. Sci. Technol.* 186 (2024) 37–47.
- [138] A. Mohammadi, Y. Ikeda, P. Edalati, M. Mito, B. Grabowski, H.-W. Li, et al., High-entropy hydrides for fast and reversible hydrogen storage at room temperature: Binding-energy engineering via first-principles calculations and experiments, *Acta Mater.* 236 (2022) 118117.
- [139] J. Gong, Y. Li, X. Song, Y. Wang, Z. Chen, Hydrogen storage of high entropy alloy NbTiVZr and its effect on mechanical properties: a first-principles study, *Vacuum* 219 (2024) 112754.
- [140] C.-C. Yen, H.-N. Lu, M.-H. Tsai, B.-W. Wu, Y.-C. Lo, C.-C. Wang, et al., Corrosion mechanism of annealed equiatomic AlCoCrFeNi tri-phase high-entropy alloy in 0.5 M H<sub>2</sub>SO<sub>4</sub> aqueous solution, *Corros. Sci.* 157 (2019) 462–471.
- [141] L. Kaufman, H. Bernstein, Computer Calculation of Phase Diagrams with Special Reference to Refractory Metals, Academic Press Inc, United States, 1970.
- [142] F. Zhang, C. Zhang, S.L. Chen, J. Zhu, W.S. Cao, U.R. Kattner, An understanding of high entropy alloys from phase diagram calculations, *Calphad* 45 (2014) 1–10.
- [143] J.E. Saal, I.S. Berglund, J.T. Sebastian, P.K. Liaw, G.B. Olson, Equilibrium high entropy alloy phase stability from experiments and thermodynamic modeling, *Scr. Mater.* 146 (2018) 5–8.
- [144] J.O. Andersson, T. Helander, L. Höglund, P. Shi, Sundman B. Thermo-Calc & DICTRA, computational tools for materials science, *Calphad* 26 (2002) 273–312.
- [145] W. Cao, S.L. Chen, F. Zhang, K. Wu, Y. Yang, Y.A. Chang, et al., PANDAT software with PanEngine, PanOptimizer and PanPrecipitation for multi-component phase diagram calculation and materials property simulation, *Calphad* 33 (2009) 328–342.
- [146] Kozeschnik E. MATCALC-a simulation tool for multicomponent thermodynamics, diffusion and phase transformations. Mathematical Modelling of Weld Phenomena52001.
- [147] K. Shobu, CaTCalc: New thermodynamic equilibrium calculation software, *Calphad* 33 (2009) 279–287.
- [148] R.H. Davies, A.T. Dinsdale, J.A. Gisby, J.A.J. Robinson, S.M. Martin, MTDATA - thermodynamic and phase equilibrium software from the national physical laboratory, *Calphad* 26 (2002) 229–271.
- [149] C.W. Bale, E. Béline, P. Chartrand, S.A. Deiterov, G. Eriksson, K. Hack, et al., FactSage thermochemical software and databases — recent developments, *Calphad* 33 (2009) 295–311.
- [150] B. Sundman, U.R. Kattner, M. Palumbo, S.G. Fries, OpenCalphad - a free thermodynamic software, *Integr. Mater. Manuf. Innov.* 4 (2015) 1–15.
- [151] R. Otis, Z.-K. Liu, pycalphad: CALPHAD-based Computational Thermodynamics in Python, *J. Open Res. Softw.* (2017).
- [152] T. Li, S. Wang, W. Fan, Y. Lu, T. Wang, T. Li, et al., CALPHAD-aided design for superior thermal stability and mechanical behavior in a TiZrHfNb refractory high-entropy alloy, *Acta Mater.* 246 (2023) 118728.
- [153] J. Gan, J. Hou, T. Chou, X. Luo, J. Ju, J. Luan, et al., A novel D022-strengthened medium entropy alloy with outstanding strength-ductility synergies over ambient and intermediate temperatures, *J. Mater. Sci. Technol.* (2024).
- [154] H.-S. Do, T.J. Jang, K.J. Kim, S.S. Sohn, B.-J. Lee, A novel high-entropy alloy with multi-strengthening mechanisms: activation of TRIP effect in C-doped high-entropy alloy, *Mater. Sci. Eng.: A* 859 (2022) 144220.
- [155] Y. Lu, Y. Dong, H. Jiang, Z. Wang, Z. Cao, S. Guo, et al., Promising properties and future trend of eutectic high entropy alloys, *Scr. Mater.* 187 (2020) 202–209.
- [156] F. He, Z. Wang, P. Cheng, Q. Wang, J. Li, Y. Dang, et al., Designing eutectic high entropy alloys of CoCrFeNiNb, *J. Alloy. Compd.* 656 (2016) 284–289.
- [157] M. Wu, S. Wang, H. Huang, D. Shu, B. Sun, CALPHAD aided eutectic high-entropy alloy design, *Mater. Lett.* 262 (2020) 127175.
- [158] H. Gasan, A. Ozcan, New eutectic high-entropy alloys based on Co–Cr–Fe–Mo–Ni–Al: design, characterization and mechanical properties, *Met. Mater. Int.* 26 (2020) 1152–1167.
- [159] F. Wang, Y. Guo, Q. Liu, X. Shang, Nanoparticle-strengthened Ni<sub>2</sub>CoCrNb<sub>0.2</sub> medium-entropy alloy with an ultrastrong cryogenic yield strength fabricated by additive manufacturing, *J. Mater. Sci. Technol.* 163 (2023) 17–31.
- [160] S.-K. Chen, P.-H. Lee, H. Lee, H.-T. Su, Hydrogen storage of C14-CuFeV<sub>2</sub>Mn<sub>2</sub>Ti<sub>2</sub>V<sub>2</sub>Zr<sub>2</sub> alloys, *Mater. Chem. Phys.* 210 (2018) 336–347.
- [161] P. Edalati, R. Floriano, A. Mohammadi, Y. Li, G. Zepon, H.-W. Li, et al., Reversible room temperature hydrogen storage in high-entropy alloy TiZrCrMnFeNi, *Scr. Mater.* 178 (2020) 387–390.

- [162] J.B. Ponsoni, V. Aranda, Td.S. Nascimento, R.B. Strozi, W.J. Botta, G. Zepon, Design of multicomponent alloys with C14 laves phase structure for hydrogen storage assisted by computational thermodynamic, *Acta Mater.* 240 (2022) 118317.
- [163] P. Lu, J.E. Saal, G.B. Olson, T. Li, O.J. Swanson, G.S. Frankel, et al., Computational materials design of a corrosion resistant high entropy alloy for harsh environments, *Scr. Mater.* 153 (2018) 19–22.
- [164] Tazuddin, N.P. Gurao, K. Biswas, In the quest of single phase multi-component multiprincipal high entropy alloys, *J. Alloy. Compd.* 697 (2017) 434–442.
- [165] E. Ghassemali, P.L.J. Conway, High-Throughput CALPHAD: a powerful tool towards accelerated metallurgy, *Front. Mater.* 9 (2022).
- [166] S.-y. Yen, H. Murakami, S.-k Lin, Low-density CoAlTi-B2 strengthened Al-Co-Cr-Mo-Ti bcc refractory high-entropy superalloy designed with the assistance of high-throughput CALPHAD method, *J. Alloy. Compd.* 952 (2023) 170027.
- [167] K. Wu, Y.A. Chang, Y. Wang, Simulating interdiffusion microstructures in Ni-Al-Cr diffusion couples: a phase field approach coupled with CALPHAD database, *Scr. Mater.* 50 (2004) 1145–1150.
- [168] J. Gao, J. Zhong, G. Liu, S. Yang, B. Song, L. Zhang, et al., A machine learning accelerated distributed task management system (Malac-Distmas) and its application in high-throughput CALPHAD computation aiming at efficient alloy design, *Adv. Powder Mater.* 1 (2022) 100005.
- [169] X.-S. Yang, Chapter Eight - Finite element methods, in: X.-S. Yang (Ed.), *Engineering simulation and its applications*, Academic Press, 2024, pp. 99–115.
- [170] M.R. Rahul, S. Samal, S. Venugopal, G. Phanikumar, Experimental and finite element simulation studies on hot deformation behaviour of AlCoCrFeNi2.1 eutectic high entropy alloy, *J. Alloy. Compd.* 749 (2018) 1115–1127.
- [171] S. Sinha, M. Komarasamy, T. Wang, R.S. Haridas, P. Agrawal, S. Shukla, et al., Notch-tensile behavior of Al0.1CrFeCoNi high entropy alloy, *Mater. Sci. Eng.: A* 774 (2020) 138918.
- [172] Y. Kim, P. Asghari-Rad, J. Lee, G.H. Gu, M. Jang, O. Bouaziz, et al., Solid solution induced back-stress in multi-principal element alloys: Experiment and modeling, *Mater. Sci. Eng.: A* 835 (2022) 142621.
- [173] Z. Gao, L. Wang, Y. Wang, F. Lyu, X. Zhan, Crack defects and formation mechanism of FeCoCrNi high entropy alloy coating on TC4 titanium alloy prepared by laser cladding, *J. Alloy. Compd.* 903 (2022) 163905.
- [174] H.G. Li, T.L. Lee, W. Zheng, Y.Z. Lu, H.B.C. Yin, J.X. Yang, et al., Characterization of residual stress in laser melting deposited CoCrFeMnNi high entropy alloy by neutron diffraction, *Mater. Lett.* 263 (2020) 127247.
- [175] X. Song, P.K. Liaw, Z. Wei, Z. Liu, Y. Zhang, Evolution of the microstructures, magnetic and mechanical behaviors of Co47.5Fe28.5Ni19Si3.4Al1.6 high-entropy alloy fabricated by laser powder bed fusion, *Addit. Manuf.* 71 (2023) 103593.
- [176] H. Li, Y. Huang, S. Jiang, Y. Lu, X. Gao, X. Lu, et al., Columnar to equiaxed transition in additively manufactured CoCrFeMnNi high entropy alloy, *Mater. Des.* 197 (2021) 109262.
- [177] H. Rui, W. Meiping, C. Chen, J. Dadong, G. Yuling, M. Xiaojin, Microstructure evolution, mechanical properties of FeCrNiMnAl high entropy alloy coatings fabricated by laser cladding, *Surf. Coat. Technol.* 447 (2022) 128851.
- [178] D. Frenkel, B. Smit, Chapter 4 - Molecular Dynamics simulations, in: D. Frenkel, B. Smit (Eds.), *Understanding molecular simulation*, Third ed., Academic Press, 2023, pp. 97–124.
- [179] L. Zhang, Y. Shibata, Inverse Hall-Petch relationship of high-entropy alloy by atomistic simulation, *Mater. Lett.* 274 (2020) 128024.
- [180] K.-T. Hsieh, Y.-Y. Lin, C.-H. Lu, J.-R. Yang, P.K. Liaw, C.-L. Kuo, Atomistic simulations of the face-centered-cubic-to-hexagonal-close-packed phase transformation in the equiatomic CoCrFeMnNi high entropy alloy under high compression, *Comput. Mater. Sci.* 184 (2020) 109864.
- [181] J.-C. Huang, Evaluation of tribological behavior of Al-Co-Cr-Fe-Ni high entropy alloy using molecular dynamics simulation, *Scanning* 34 (2012) 325–331.
- [182] Z. Wang, J. Li, Q. Fang, B. Liu, L. Zhang, Investigation into nanoscratching mechanical response of AlCrCuFeNi high-entropy alloys using atomic simulations, *Appl. Surf. Sci.* 416 (2017) 470–481.
- [183] H. Xie, Z. Ma, W. Zhang, H. Zhao, L. Ren, Amorphization transformation in high-entropy alloy FeNiCrCoCu under shock compression, *J. Mater. Sci. Technol.* 175 (2024) 72–79.
- [184] D. Hua, Q. Xia, W. Wang, Q. Zhou, S. Li, D. Qian, et al., Atomistic insights into the deformation mechanism of a CoCrNi medium entropy alloy under nanoindentation, *Int. J. Plast.* 142 (2021) 102997.
- [185] Q. Guo, H. Hou, Y. Pan, X. Pei, Z. Song, P.K. Liaw, et al., Hardening-softening of Al0.3CoCrFeNi high-entropy alloy under nanoindentation, *Mater. Des.* 231 (2023) 112050.
- [186] L. Xie, G. Wu, P.K. Liaw, W. Wang, D. Li, Q. Peng, et al., Temperature gradient enhances the solidification process and properties of a CoCrFeNi high-entropy alloy: atomic insights from molecular dynamics simulations, *Comput. Mater. Sci.* 231 (2024) 112538.
- [187] Y. He, W. Shi, C. Han, K. He, C. Liu, Z. Chen, et al., Molecular dynamics simulations of primary cascade damage in FeCoCrNiCu high-entropy alloys, *J. Alloy. Compd.* 983 (2024) 173972.
- [188] J.L. Li, Z. Li, Q. Wang, C. Dong, P.K. Liaw, Phase-field simulation of coherent BCC/B2 microstructures in high entropy alloys, *Acta Mater.* 197 (2020) 10–19.
- [189] I. Roy, P.K. Ray, G. Balasubramanian, Modeling oxidation of AlCoCrFeNi high-entropy alloy using stochastic cellular automata, *Entropy* 24 (2022) 1263.
- [190] P. Lu, T.W. Zhang, D. Zhao, S.G. Ma, Q. Li, T. Wang, et al., Effects of stress states and strain rates on mechanical behavior and texture evolution of the CoCrFeNi high-entropy alloy: Experiment and simulation, *J. Alloy. Compd.* 851 (2021) 156779.
- [191] Q. Ye, B. Yang, G. Yang, J. Zhao, Z. Gong, Stability prediction of AlCoCrFeMo0.05Ni2 high entropy alloy by Kinetic Monte Carlo method, *Mater. Lett.* 306 (2022) 130907.
- [192] Y. Chen, S. Wang, H. Feng, W. Li, B. Liu, J. Li, et al., Irradiation hardening behavior of high entropy alloys using random field theory informed discrete dislocation dynamics simulation, *Int. J. Plast.* 162 (2023) 103497.
- [193] Y.Z. Liu, J. Wang, S.H. Oh, S.P. Hu, W. Fu, X.G. Song, et al., Multiscale computational model of TWIP and TRIP in medium/high entropy alloys, *J. Alloy. Compd.* 1022 (2025) 179770.
- [194] B.S. Murty, J.W. Yeh, S. Ranganathan, P.P. Bhattacharjee, 7 - Solid Solution Phases and Their Microstructures in HEAs, in: B.S. Murty, J.W. Yeh, S. Ranganathan, P.P. Bhattacharjee (Eds.), *High-entropy alloys*, Second Ed., Elsevier, 2019, pp. 119–144.
- [195] Y. Zhang, C. Wen, C. Wang, S. Antonov, D. Xue, Y. Bai, et al., Phase prediction in high entropy alloys with a rational selection of materials descriptors and machine learning models, *Acta Mater.* 185 (2020) 528–539.
- [196] W. Huang, P. Martin, H.L. Zhuang, Machine-learning phase prediction of high-entropy alloys, *Acta Mater.* 169 (2019) 225–236.
- [197] N. Qu, Y. Chen, Z. Lai, Y. Liu, J. Zhu, The phase selection via machine learning in high entropy alloys, *Procedia Manuf.* 37 (2019) 299–305.
- [198] K. Kaufmann, K.S. Vecchio, Searching for high entropy alloys: a machine learning approach, *Acta Mater.* 198 (2020) 178–222.
- [199] Z. He, H. Zhang, H. Cheng, M. Ge, T. Si, L. Che, et al., Machine learning guided BCC or FCC phase prediction in high entropy alloys, *J. Mater. Res. Technol.* 29 (2024) 3477–3486.
- [200] Y. Yan, D. Lu, K. Wang, Accelerated discovery of single-phase refractory high entropy alloys assisted by machine learning, *Comput. Mater. Sci.* 199 (2021) 110723.
- [201] W. Zhu, W. Huo, S. Wang, X. Wang, K. Ren, S. Tan, et al., Phase formation prediction of high-entropy alloys: a deep learning study, *J. Mater. Res. Technol.* 18 (2022) 800–809.
- [202] T. Nazir, N. Shaukat, Nu.H. Tariq, R.N. Shahid, M.H. Bhatti, A comprehensive strategy for phase detection of high entropy alloys: machine learning and deep learning approaches, *Mater. Today Commun.* 37 (2023) 107525.
- [203] S. Hou, M. Sun, M. Bai, D. Lin, Y. Li, W. Liu, A hybrid prediction frame for HEAs based on empirical knowledge and machine learning, *Acta Mater.* 228 (2022) 117742.
- [204] Q. Wu, Z. Wang, X. Hu, T. Zheng, Z. Yang, F. He, et al., Uncovering the eutectics design by machine learning in the Al-Co-Cr-Fe-Ni high entropy system, *Acta Mater.* 182 (2020) 278–286.
- [205] F. Liu, X. Xiao, L. Huang, L. Tan, Y. Liu, Design of NiCoCrAl eutectic high entropy alloys by combining machine learning with CALPHAD method, *Mater. Today Commun.* 30 (2022) 103172.
- [206] G. Vazquez, P. Singh, D. Sauceda, R. Couperthwaite, N. Britt, K. Youssef, et al., Efficient machine-learning model for fast assessment of elastic properties of high-entropy alloys, *Acta Mater.* 232 (2022) 117924.
- [207] Z. Gao, F. Zhao, S. Gao, T. Xia, Machine learning prediction of hardness in solid solution high entropy alloys, *Mater. Today Commun.* 37 (2023) 107102.
- [208] I. Toda-Caraballo, P.E.J. Rivera-Díaz-del-Castillo, Modelling solid solution hardening in high entropy alloys, *Acta Mater.* 85 (2015) 14–23.
- [209] X. Zhang, R. Dong, Q. Guo, H. Hou, Y. Zhao, Predicting the stacking fault energy in FCC high-entropy alloys based on data-driven machine learning, *J. Mater. Res. Technol.* 26 (2023) 4813–4824.
- [210] C. Wen, Y. Zhang, C. Wang, D. Xue, Y. Bai, S. Antonov, et al., Machine learning assisted design of high entropy alloys with desired property, *Acta Mater.* 170 (2019) 109–117.
- [211] C. Chen, L. Ma, Y. Zhang, P.K. Liaw, J. Ren, Accelerating the design of high-entropy alloys with high hardness by machine learning based on particle swarm optimization, *Intermetallics* 154 (2023) 107819.
- [212] Q. Guo, Y. Pan, H. Hou, Y. Zhao, Predicting the hardness of high-entropy alloys based on compositions, *Int. J. Refract. Met. Hard Mater.* 112 (2023) 106116.
- [213] C. Yang, C. Ren, Y. Jia, G. Wang, M. Li, W. Lu, A machine learning-based alloy design system to facilitate the rational design of high entropy alloys with enhanced hardness, *Acta Mater.* 222 (2022) 117431.
- [214] Z. Dong, A. Sun, S. Yang, X. Yu, H. Yuan, Z. Wang, et al., Machine learning-assisted discovery of Cr, Al-containing high-entropy alloys for high oxidation resistance, *Corros. Sci.* 220 (2023) 111222.
- [215] H.C. Ozdemir, A. Nazaraha, B. Yilmaz, D. Canadinc, E. Bedir, R. Yilmaz, et al., Machine learning – informed development of high entropy alloys with enhanced corrosion resistance, *Electrochim. Acta* 476 (2024) 143722.
- [216] W. Liu, C. Wang, C. Liang, J. Chen, H. Tan, J. Yang, et al., Optimal design of γ-strengthened high-entropy alloys via machine learning multilayer structural model, *Mater. Sci. Eng.: A* 871 (2023) 144852.
- [217] X. Li, M. Zheng, C. Li, H. Pan, W. Ding, J. Yu, Accelerated design of low-activation high entropy alloys with desired phase and property by machine learning, *Appl. Mater. Today* 36 (2024) 102000.
- [218] T.Z. Khan, T. Kirk, G. Vazquez, P. Singh, A.V. Smirnov, D.D. Johnson, et al., Towards stacking fault energy engineering in FCC high entropy alloys, *Acta Mater.* 224 (2022) 117472.
- [219] S. Curtarolo, W. Setyawan, S. Wang, J. Xue, K. Yang, R.H. Taylor, et al., AFLOWLIB.ORG: a distributed materials properties repository from high-throughput ab initio calculations, *Comput. Mater. Sci.* 58 (2012) 227–235.
- [220] M. Singh, E. Barr, D. Aidhy, Consolidated database of high entropy materials (COD'HEM): An open online database of high entropy materials, *Comput. Mater. Sci.* 248 (2025) 113588.

- [221] J.J. Hanak, The “multiple-sample concept” in materials research: Synthesis, compositional analysis and testing of entire multicomponent systems, *J. Mater. Sci.* 5 (1970) 964–971.
- [222] P.J. Kelly, R.D. Arnell, Magnetron sputtering: a review of recent developments and applications, *Vacuum* 56 (2000) 159–172.
- [223] Y. Zhang, X. Yan, J. Ma, Z. Lu, Y. Zhao, Compositional gradient films constructed by sputtering in a multicomponent Ti-Al-(Cr, Fe, Ni) system, *J. Mater. Res.* 33 (2018) 3330–3338.
- [224] Y. Shi, B. Yang, P.D. Rack, S. Guo, P.K. Liaw, Y. Zhao, High-throughput synthesis and corrosion behavior of sputter-deposited nanocrystalline Alx(CoCrFeNi)100-x combinatorial high-entropy alloys, *Mater. Des.* 195 (2020) 109018.
- [225] Y. Li, J. Ma, P.K. Liaw, Y. Zhang, Exploring the amorphous phase formation and properties of W-Ta-(Cr, Fe, Ni) high-entropy alloy gradient films via a high-throughput technique, *J. Alloy. Compd.* 913 (2022) 165294.
- [226] J. Beddoes, M.J. Bibby, 6 - Powder metallurgy, in: J. Beddoes, M.J. Bibby (Eds.), *Principles of Metal Manufacturing Processes*, Butterworth-Heinemann, Oxford, 1999, pp. 173–189.
- [227] L. Zhao, L. Jiang, L.X. Yang, H. Wang, W.Y. Zhang, G.Y. Ji, et al., High throughput synthesis enabled exploration of CoCrFeNi-based high entropy alloys, *J. Mater. Sci. Technol.* 110 (2022) 269–282.
- [228] L. Zhao, S.-R. Liu, L. Jiang, L.-X. Yang, L.-L. Zhu, H. Wang, et al., A high-throughput strategy for rapid synthesis and characterization of Ni-based superalloys, *Rare Met.* 41 (2022) 2693–2700.
- [229] L. Zhao, Y. Zhou, H. Wang, X. Chen, L. Yang, L. Zhang, et al., High-Throughput Synthesis and Characterization of a Combinatorial Materials Library in Bulk Alloys, *Metall. Mater. Trans. A* 52 (2021) 1159–1168.
- [230] J.C. Zhao, X. Zheng, D.G. Cahill, High-throughput diffusion multiples, *Mater. Today* 8 (2005) 28–37.
- [231] A. Hilhorst, P.J. Jacques, Diffusion Multiples as a Tool to Efficiently Explore the Composition Space of High Entropy Alloys, *J. Phase Equilibr. Diffus.* 42 (2021) 708–719.
- [232] F.G. Coury, P. Wilson, K.D. Clarke, M.J. Kaufman, A.J. Clarke, High-throughput solid solution strengthening characterization in high entropy alloys, *Acta Mater.* 167 (2019) 1–11.
- [233] P. Wilson, R. Field, M. Kaufman, The use of diffusion multiples to examine the compositional dependence of phase stability and hardness of the Co-Cr-Fe-Mn-Ni high entropy alloy system, *Intermetallics* 75 (2016) 15–24.
- [234] J.C. Zhao, M.R. Jackson, L.A. Peluso, Determination of the Nb–Cr–Si phase diagram using diffusion multiples, *Acta Mater.* 51 (2003) 6395–6405.
- [235] J.C. Zhao, M.R. Jackson, L.A. Peluso, Mapping of the Nb–Ti–Si phase diagram using diffusion multiples, *Mater. Sci. Eng.: A* 372 (2004) 21–27.
- [236] Q. Li, W. Chen, J. Zhong, L. Zhang, Q. Chen, Z.-K. Liu, On sluggish diffusion in Fcc Al–Co–Cr–Fe–Ni high-entropy alloys: an experimental and numerical study, *Metals* 8 (2018) 16.
- [237] D.L. Bourell, Perspectives on additive manufacturing, *Annu. Rev. Mater. Res.* 46 (2016) 1–18.
- [238] M. Moorehead, K. Bertsch, M. Niegzoda, C. Parkin, M. Elbakhshwan, K. Sridharan, et al., High-throughput synthesis of Mo–Nb–Ta–W high-entropy alloys via additive manufacturing, *Mater. Des.* 187 (2020) 108358.
- [239] M. Moorehead, P. Nelaturu, M. Elbakhshwan, C. Parkin, C. Zhang, K. Sridharan, et al., High-throughput ion irradiation of additively manufactured compositionally complex alloys, *J. Nucl. Mater.* 547 (2021) 152782.
- [240] T. Borkar, B. Gwalani, D. Choudhuri, C.V. Mikler, C.J. Yannetta, X. Chen, et al., A combinatorial assessment of AlxCrCuFeNi2 ( $0 < x < 1.5$ ) complex concentrated alloys: microstructure, microhardness, and magnetic properties, *Acta Mater.* 116 (2016) 63–76.
- [241] M. Zheng, C. Li, X. Zhang, Z. Ye, Y. Liao, J. Gu, Design of a novel (CoGrNi) 84.5Al15.5 eutectic medium-entropy alloy with hierarchically nano-lamellar microstructure through additively manufactured compositionally graded materials, *Mater. Sci. Eng.: A* 878 (2023) 145209.
- [242] J.W. Pegues, M.A. Melia, R. Puckett, S.R. Whetten, N. Argibay, A.B. Kustas, Exploring additive manufacturing as a high-throughput screening tool for multiphase high entropy alloys, *Addit. Manuf.* 37 (2021) 101598.
- [243] J. Yang, L. Hawkins, M. Song, L. He, M. Bachhav, Q. Pan, et al., Compositionally graded specimen made by laser additive manufacturing as a high-throughput method to study radiation damages and irradiation-assisted stress corrosion cracking, *J. Nucl. Mater.* 560 (2022) 153493.
- [244] B. Gwalani, V. Soni, O.A. Waseem, S.A. Mantri, R. Banerjee, Laser additive manufacturing of compositionally graded AlCrFeMoV ( $x = 0$  to 1) high-entropy alloy system, *Opt. Laser Technol.* 113 (2019) 330–337.
- [245] B. Gwalani, S. Gangireddy, S. Shukla, C.J. Yannetta, S.G. Valentin, R.S. Mishra, et al., Compositinally graded high entropy alloy with a strong front and ductile back, *Mater. Today Commun.* 20 (2019) 100602.
- [246] C. Guo, S. Wei, Z. Wu, P. Wang, B. Zhang, U. Ramamurty, et al., Effect of dual phase structure induced by chemical segregation on hot tearing reduction in additive manufacturing, *Mater. Des.* 228 (2023) 111847.
- [247] Je Sun, Y. Wen, Z. Wang, J. Zhang, L. Wang, X. Qu, et al., Understanding effect of Mg and Mn equivalents on columnar-to-equiaxed transition of high-strength Al alloy fabricated by laser powder bed fusion, *Mater. Charact.* 203 (2023) 113100.
- [248] M. Ashby, H. Shercliff, D. Cebon, Chapter 19 - Processing, Microstructure and Properties, in: M. Ashby, H. Shercliff, D. Cebon (Eds.), *Materials*, Fourth ed., Butterworth-Heinemann, 2019, pp. 551–598.
- [249] C. Wei, J.-C. Zhao, Gradient temperature heat treatment for efficient study of phase precipitation in a high-temperature Fe–Cr–Mo ferritic steel, *Materialia* 3 (2018) 31–40.
- [250] H. Wu, J. Li, F. Liu, L. Huang, X. Zeng, Q. Fang, et al., A high-throughput methodology search for the optimum cooling rate in an advanced polycrystalline nickel base superalloy, *Mater. Des.* 128 (2017) 176–181.
- [251] K. Wang, A. Wei, Z. Shi, X. Chen, J. Lin, X. Tong, et al., The preparation and performance of grain size gradient TWIP steel fabricated by laser heat treatment, *Mater. Sci. Eng.: A* 743 (2019) 294–300.
- [252] S.-h Xu, Y. Liu, B. Liu, X. Wang, Z.-x Chen, Microstructural evolution and mechanical properties of Ti-5Al-5Mo-5V-3Cr alloy by heat treatment with continuous temperature gradient, *Trans. Nonferrous Met. Soc. China* 28 (2018) 273–281.
- [253] R.X. Li, P.K. Liaw, Y. Zhang, Synthesis of AlxCrFeNi high-entropy alloys by high-gravity combustion from oxides, *Mater. Sci. Eng.: A* 707 (2017) 668–673.
- [254] R. Li, Z. Wang, Z. Guo, P.K. Liaw, T. Zhang, L. Li, et al., Graded microstructures of Al–Li–Mg–Zn–Cu entropic alloys under supergravity, *Sci. China Mater.* 62 (2019) 736–744.
- [255] M. Berahmand, M. Ketabchi, M. Jamshidian, S. Tsurekawa, Investigation of microstructure evolution and martensite transformation developed in austenitic stainless steel subjected to a plastic strain gradient: A combination study of Mirco-XRD, EBSD, and ECCT techniques, *Micron* 143 (2021) 103014.
- [256] J. Zhou, X. Zhang, W. Li, Directional solidification induced compositional gradient for a quick evaluation of transport properties in p-PbTe thermoelectrics, *J. Alloy. Compd.* 997 (2024) 174972.
- [257] L.X. Zhang, L. Liu, S. Guo, Q.S. Pan, L. Lu, Microstructure and evolution of gradient dislocation cells in multi-principal element alloy subjected to cyclic torsion, *Acta Mater.* 275 (2024) 120059.
- [258] Z. Yin, X. Yang, X. Ma, J. Moering, J. Yang, Y. Gong, et al., Strength and ductility of gradient structured copper obtained by surface mechanical attrition treatment, *Mater. Des.* 105 (2016) 89–95.
- [259] Q. Fan, K. Gan, D. Yan, Z. Li, Nanoindentation creep behavior of diverse microstructures in a pre-strained interstitial high-entropy alloy by high-throughput mapping, *Mater. Sci. Eng.: A* 856 (2022) 143988.
- [260] Y. Tong, H. Zhang, H. Huang, L. Yang, Y. Hu, X. Liang, et al., Strengthening mechanism of CoCrNiMox high entropy alloys by high-throughput nanoindentation mapping technique, *Intermetallics* 135 (2021) 107209.
- [261] H. Zhang, Y. Tong, X. Ji, H. Huang, L. Yang, Y. Hu, et al., Effect of Tantalum content on microstructure and mechanical properties of CoCrNiTax medium entropy alloys, *Mater. Sci. Eng.: A* 847 (2022) 143322.
- [262] J. Nie, L. Wei, D.-I. Li, L. Zhao, Y. Jiang, Q. Li, High-throughput characterization of microstructure and corrosion behavior of additively manufactured SS316L-SS431 graded material, *Addit. Manuf.* 35 (2020) 101295.
- [263] V.D. Nguyen, T. Nagata, K.S. Chang, High-throughput methodology for the realization of high-entropy sub-nm equivalent-oxide-thickness high-dielectric-constant Ba(Ti,Zr,Ta,Hf,Mo)O<sub>3</sub> film-based metal-oxide-semiconductor-related devices, *Mater. Today Phys.* 37 (2023) 101202.
- [264] K. Huang, C. Kain, N. Diaz-Vallejo, Y. Sohn, L. Zhou, High throughput mechanical testing platform and application in metal additive manufacturing and process optimization, *J. Manuf. Process.* 66 (2021) 494–505.
- [265] M. Ohtani, M. Lippmaa, T. Ohnishi, M. Kawasaki, High throughput oxide lattice engineering by parallel laser molecular-beam epitaxy and concurrent x-ray diffraction, *Rev. Sci. Instrum.* 76 (2005).
- [266] R. Li, Y. Ma, X. Liu, Y. Lu, Y. Zhang, P. Yu, et al., Effect of defects on the phase transition of Al0.1CoCrFeNi high-entropy alloy under high pressure, *Intermetallics* 140 (2022) 107388.
- [267] Y. Zhou, W. Song, F. Zhang, Y. Wu, Z. Lei, M. Jiao, et al., Probing deformation behavior of a refractory high-entropy alloy using in situ neutron diffraction, *J. Alloy. Compd.* 971 (2024) 172635.
- [268] E. Garel, J.-L. Parouty, H. Van Landeghem, M. Verdier, F. Robaut, S. Coindeau, et al., Coupling mixture designs, high-throughput experiments and machine learning for accelerated exploration of multinary systems, *Mater. Des.* 231 (2023) 112055.
- [269] H. Sun, C. Wang, S.-L. Shang, A.M. Beese, J.-C. Zhao, Z.-K. Liu, Thermodynamic modeling of Fe–Nb and Fe–Nb–Ni systems supported by first-principles calculations and diffusion-multiple measurements, *Acta Mater.* 268 (2024) 119747.